# Organisational and signalling cues in membranes

Dissertation

To fulfil the Requirements for the Degree of

"*doctor rerum naturalium*" (Dr. rer. nat.)



Submitted to the Council of the Medical Faculty of the Jena

University Hospital/Friedrich-Schiller-University Jena

by M.Sc Astha Jain

born on 05 Nov 1986 in Mumbai, India

Dissertation Friedrich Schiller University [2022]

**Gutachter**

**1. Professor Dr. Britta Qualmann**

**Institut für Biochemie I, Universitätsklinikum Jena**

**2. Professor Dr. Christian A. Hübner**

**Institut für Humangenetik, Universitätsklinikum Jena**

**3. Professor Britta Eickholt**

**Cluster of Excellence NeuroCure and Institute of Biochemistry,**

**Charité – Universitätsmedizin Berlin**

**Tag der öffentlichen Verteidigung:  06 Dec, 2022**

# TABLE OF CONTENTS

## 3    RESULTS .........................................................................................................36

# Abbreviations

| | |
|---|---|
| °C | Degree Celsius |
| aa | Amino Acid (s) |
| ANKHD1 | Ankyrin Repeat and K Homology Domain-Containing Protein 1 |
| Ankrd | Ankyrin repeat domain-containing protein |
| ANOVA | Analysis Of Variance |
| ARD | Ankyrin Repeat Domain |
| BAR | Bin-Amphiphysin-Rvs |
| BCA | Bicinchoninic Acid |
| BCI | Institute of Biochemistry I |
| bp | Base Pair (s) |
| BSA | Bovine Serum Albumin |
| C- terminal | Carboxy terminal |
| cDNA | Complementary DNA |
| Cobl | Cordon-bleu |
| DAPI | 4′,6-Diamidino-2-phenylindole |
| ddH$_2$O | Double distilled water |
| DIV | Days *in vitro* |
| DMEM | Dulbecco's Modified Eagle's Medium |
| DMSO | Dimethylsuphoxide |
| DNA | Deoxyribonucleic Acid |
| DNase | Deoxyribonuclease |
| dNTPs | Deoxyribonucleotides |
| DTT | Dithiothreitol |
| E.*coli* | Escherichia coli |
| e.g., | For Example |
| EDC | 1-Ethyl-3-(3-dimethylaminopropyl)carbodiimide hydrochloride |
| EDTA | Ethylenediamine-n,n,n',n'-tetraacetic acid |
| EGFP | Enhanced Green Fluorescent Protein |
| EGTA | Ethylene glycol-bis (2-aminoetylether)-n,n,n',n'-tetraacetic acid |
| et al. | Et alia: and others |
| F | Farnesyl |
| F-BAR | Fes/CIP4-Homology - BAR |
| FCS | Foetal Calf Serum |
| FRIL | Freeze-Fracture Replica Immunolabelling |
| Fw | Forward Primer |

| | |
|---|---|
| g | Gram (s) |
| GFP | Green Fluorescent Protein |
| GST | Glutathione-S-Transferase |
| h | Hour (s) |
| HBSS | Hanks' Balanced Salt Solution |
| HCl | Hydrogen chloride |
| HEK | Human Embryonic Kidney |
| HeLa | Henrietta Lacks |
| HEPES | 4-(2-hydroxyethyl)-1-piperazineethanesulfonic acid |
| HN | HEPES/NaCl |
| IF | Immunofluorescence |
| IP | Immunoprecipitation |
| kb | Kilobase |
| kDa | Kilodalton |
| l | Litre(s) |
| LB | Lysogenic Broth |
| LBB | Labelling Blocking Buffer |
| LUVs | Large Unilaminar Vesicles |
| M | Molar |
| m | Meter |
| MAP2 | Microtubule-Associated Protein 2 |
| mg | Milligram |
| min | Minute (s) |
| ml | Millilitre (s) |
| mM | Millimolar |
| mm | Millimetre |
| mRNA | Messenger RNA |
| n | Sample Size Number |
| N-terminal | Amino-terminal |
| NaCl | Sodium Chloride |
| NF-κB | Nuclear Factor Kappa Light Chain Enhancer Of Activated B Cells |
| ng | Nanogram |
| nM | Nanomolar |
| nm | Nanometre |
| P | Pellet |
| PAGE | Polyacrylamide Gel Electrophoresis |
| PBS | Phosphate Buffered Saline |

| | |
|---|---|
| PBS-PIC | Phosphate Buffered Saline With Protease Inhibitor Cocktail |
| PBS-T | PBS-Tween |
| PCR | Polymerase Chain Reaction |
| PI | Protease Inhibitor |
| PIC | Protease Inhibitor Cocktail |
| PSI-BLAST | Position-Specific Iterative Basic Local Alignment Search Tool |
| PVDF | Polyvinylidene Fluoride |
| RIPA | Radioimmunoprecipitation Assay |
| RNA | Ribonucleic Acid |
| RNAi | RNA interference |
| RNase | Ribonuclease |
| ROCK | Rho-Associated Coiled Coil Kinase |
| rpm | Revolutions Per Minute |
| RS | Restriction Sites |
| RT | Room Temperature |
| Rv | Reverse Primer |
| s | Second (s) |
| S | Supernatant |
| Sdp | Syndapin |
| SDS | Sodium Dodecyl Sulphate |
| SEM | Standard Error of Means |
| sh | Short Hairpin |
| SH3 | Src Homology 3 |
| SOC | Super Optimal Broth with Catabolite Repression |
| Src. | Scrambled |
| SUVs | Small Unilaminar Vesicles |
| $T_a$ | Annealing Temperature |
| TAE | Tris/Acetate/EDTA |
| TB | Terrific Broth |
| TD | Touchdown |
| $t_E$ | Extension Time |
| TEM | Transmission Electron Microscopy |
| U | Unit (s) |
| UACA | Uveal Autoantigen with Coiled Coil Domains and Ankyrin Repeats |
| UKJ | Universitätsklinikum Jena |
| v | Volume |
| v/v | Volume per Volume |

| | |
|---|---|
| w/v | Weight per Volume |
| WB | Western Blot |
| x g | Times Gravity |
| x6 | Isoform 6 |
| Δ | Delta, Deletion |
| μg | Microgram |
| μl | Microlitre |
| μM | Micromolar |

## Abstract

Recently, a new class of membrane-shapers termed N-Ank proteins (Wolf et al., 2019) were defined by their ability to bind, sense, and shape the membrane via their N-Ank module, which consists of an amino(N)-terminal amphipathic helix and ankyrin repeats. N-Ank family of membrane-shapers is phylogenetically classified into two sub-families and Ankyrin repeat domain-containing protein (Ankrd) 24, an uncharacterised protein, was suggested to be in their smaller sub-family. Thus, this study unveiled that Ankrd24 isoform 6 (Ankrd24x6) is one of the expressed isoforms in brains of 8-week-old mice. Investigation of the N-Ank properties of Ankrd24x6 using *in vitro* reconstitution assays with liposomes showed that it is an N-Ank protein but with distinct characteristics. The N-Ank module of Ankrd24x6 binds and shape the membrane and displayed that the presence of the putative amphipathic helix is quintessential for its binding. The predicted seven ankyrin repeats in Ankrd24x6 displayed lack of binding to the liposomes irrespective of their curvature. This property of Ankrd24x6 is distinct compared to the other members of the N-Ank superfamily which showed that the ankyrin repeats alone preferred higher curvature liposomes. Ankrd24x6 is also capable of oligomerising as it demonstrated self-association, which was mediated by the predicted coiled coil domains. Another interesting feature of Ankrd24x6 is the presence of a proline-rich motif via which it showed binding to the syndapin I protein. Syndapin I is involved in diverse crucial biological processes like synaptic vesicle recycling, cytoskeletal remodelling, dendritogenesis and ciliogenesis because it is capable of binding and shaping the membranes and can additionally interact with various proteins.

Functionally, Ankrd24 demonstrated to be essential for the early development of dendritic arbor in primary rat hippocampal neurons as it induced the formation of primary dendrites whereas its loss-of-function caused reduced dendritogenesis and dendritic arborization. Taken together, the investigation highlights two most important features of Ankrd24, one that it is a N-Ank protein, belonging to the smaller sub-family of the N-Ank superfamily and second, that it plays an important role in neuromorphogenesis.

## Zusammenfassung

Kürzlich wurde eine neue Klasse von Membranformenden Proteine, die sogenannten N-Ank-Proteine (Wolf et al., 2019), beschrieben, deren Fähigkeit ist, die Membran über ihr N-Ank-Modul zu erkennen, zu binden und zu formen. Das N-Ank-Modul besteht aus einer N-terminalen amphipathischen Helix und Ankyrin-Wiederholungen. Die N-Ank-Familie der membranformenden Proteine wird phylogenetisch in zwei Unterfamilien eingeteilt, und es wurde vermutet, dass Ankyrin Repeat Domain-containing Protein (Ankrd) 24, ein bisher nicht charakterisiertes Protein, zu ihrer kleineren Unterfamilie gehört. In dieser Studie konnte gezeigt werden, dass die Ankrd24-Isoform 6 (Ankrd24x6) in Gehirnen von 8 Wochen alten Mäusen exprimiert wird. Die Untersuchung der N-Ank-Eigenschaften von Ankrd24x6 anhand von *In vitro* Rekonstitutionsversuchen mit Liposomen zeigte, dass es sich um ein N-Ank-Protein handelt, das jedoch im Vergleich zu den in Wolf et al. beschriebenen andere Merkmale aufweist. Das N-Ank-Modul von Ankrd24x6 bindet und formt die Membran, und es zeigte sich, dass das Vorhandensein der mutmaßlichen amphipathischen Helix für seine Bindung von entscheidender Bedeutung ist. Die vorhergesagten sieben Ankyrin-Wiederholungen in Ankrd24x6 zeigten jedoch keine Bindung an die Liposomen, unabhängig von ihrer Krümmung. Diese Eigenschaft von Ankrd24x6 unterscheidet sich von den anderen Mitgliedern der N-Ank-Superfamilie, die zeigten, dass die Ankyrin-Wiederholungen allein Liposomen mit höherer Krümmung bevorzugten. Ankrd24x6 ist auch zur Oligomerisierung fähig, da es Selbstassoziation veranschaulichte, die durch die vorhergesagten Coiled Coil Domänen vermittelt wurde. Ein weiteres interessantes Merkmal von Ankrd24x6 ist das Vorhandensein eines prolinreichen Motivs, über das es eine Bindung an das Syndapin-I-Protein zeigte. Syndapin I ist an verschiedenen wichtigen biologischen Prozessen wie dem Recycling synaptischer Vesikel, dem Umbau des Zytoskeletts, der Dendritogenese und der Zilienbildung beteiligt, da es in der Lage ist, die Membranen zu binden und zu formen, und außerdem mit verschiedenen Proteinen interagieren kann. Funktionell erwies sich Ankrd24 als essentiell für die frühe Entwicklung des dendritischen Arbors in primären Hippocampus-Neuronen der Ratte, da es die Bildung von primären Dendriten induzierte, während sein

Funktionsverlust zu einer reduzierten Dendritogenese und dendritischen Arborisierung führte.

Insgesamt hebt diese Arbeit zwei wichtige Eigenschaften von Ankrd24 hervor: erstens, dass es ein N-Ank-Protein ist, das zur kleineren Unterfamilie der N-Ank-Superfamilie gehört, und zweitens, dass es eine wichtige Rolle bei der Neuromorphogenese spielt.

# 1 Introduction

## 1.1 Membrane remodelling

Structure remodelling of cells including their organelles is the basis of vital biological processes such as cell growth, division, movement, organelle biogenesis, vesicle transportation or membrane trafficking. Striking example of one such cell, which is involved in most of the above processes except division, is a neuronal cell, which actively restructures its exon and dendritic arbor in response to variety of signals (Bradke & Dotti, 2000; Horton & Ehlers, 2003), and displays both functional and structural plasticity (Hofbruker-Mackenzie et al., 2019.; Leuner & Gould, 2010; Tavosanis, 2011).

Morphological changes during dendritogenesis of dissociated primary rat hippocampal neurons in cell culture have been well characterized. It has been demonstrated *in vitro* that within half day, a neuronal cell develops lamellipodia-like structures, followed by the establishment of polarity of the neuron, axonal guidance and growth in another day. At day 4, neurons commence outgrowing their dendrites and in another 3 days, they mature by developing pre- and postsynapses (synaptogenesis) and thus, networking with neighbouring cells (Dotti et al., 1988; Kessels et al., 2011).

Such an elaborate remodelling of the cells is accomplished by dynamic and flexible structure of the membrane, defined by the 'fluid mosaic' model, which allows the cell to change and adapt its morphology, depending on the type and strength of a signal (Singer & Nicolson, 1972). Biomembranes surrounding the cell, e.g., plasma membrane, or the intracellular organelles like mitochondria, the endoplasmic reticulum, or the Golgi complex acts like a physical barrier in not only protecting its internal content from the outside environment but by also maintaining the required isolated conditions within, for performing various biochemical reactions (Engelman, 2005; Goñi, 2014). The membranes are also semipermeable, which allows the cell and/or organelle to maintain the dynamic activities and vital functions by the uptake of nutrients, excretion of waste and communication with its surrounding environment. The basic structural element of the biomembranes are lipids to which proteins are associated. Lipids such as

phospholipids, glycolipids, cholesterol, consist of a hydrophilic head group and a non-polar hydrophobic hydrocarbon tail. The hydrophilic groups face and interact with the aqueous, ionic phase, and the non-polar hydrophobic hydrocarbon chains face each other, self-associating to avoid water interactions, thus, the non-covalent interactions between the lipids forms an amphipathic semi-permeable bilayer (Goñi, 2014; Simunovic et al., 2015; Suetsugu et al., 2014). Such non-covalent interactions also modify the formation of liposomes during hydration of dry lipids like phosphatidylcholines (Akbarzadeh et al., 2013) under pH, temperature, and ionic strength similar to physiological conditions (Goñi, 2014). Liposomes are artificially prepared vesicles which are spherical in shape and are composed of one or more lipid bilayers (Daraee et al., 2016).

The interplay between the lipids and the proteins allows the membrane to either form concave (positive) or convex (negative) curvatures which result in invaginations and protrusions, respectively (McMahon & Gallop, 2005; Suetsugu et al., 2014). Invaginations give rise to vesicles like clathrin-coated which mediate endocytosis, a well described membrane-shaping process (Kaksonen & Roux, 2018; Qualmann et al., 2011) while protrusions result in membrane processes such as filopodia, which are involved in several dynamic processes of the cell like migration or adhesion (Mattila & Lappalainen, 2008; Suetsugu et al., 2014).

## 1.2   Membrane-shaping proteins

### 1.2.1   Membrane-shaping proteins of the Bin-Amphiphysin-Rvs (BAR) domain superfamily

BAR domain containing proteins are shaped-like bananas (Peter et al., 2004) and use mechanisms of hydrophobic insertion and scaffolding to bend and shape the membranes (McMahon & Gallop, 2005; Qualmann et al., 2011; Zimmerberg & Kozlov, 2006). BAR domain is conserved from yeast to human (David et al., 1994) and a BAR module is defined by its ability to not only bind to the membrane but to also sense the membrane-curvature and form dimers (Peter et al., 2004). The positively charged amino acid residues on the structural surface of the BAR domain interacts with the cellular

membranes which are negatively charged due to the presence of phospholipids like phosphatidylserine and phosphorylated phosphatidylinositols (Frost et al., 2009; Qualmann et al., 2011; Suetsugu, 2016; Suetsugu et al., 2010). The x-ray crystallography of amphiphysin, an N-BAR containing protein elucidated that BAR domains are dimers, forming a six-helix bundle by three long monomers and because amphiphysin also has an N-terminal amphipathic helix, which strengthens the interaction between the BAR domain and the membrane, it is classified as having an N-BAR domain (Peter et al., 2004). Amphiphysin is a brain enriched protein which is involved in clathrin-mediated endocytosis (Yoshida et al., 2004).

**Amphipathic α helices**

Lipid bilayer-interactive amphipathic α helices are secondary structure motifs, defined by the spatial rearrangement of amino acids residues such that it forms polar and a non-polar (hydrophobic) face. Such helices are reflected by the reoccurrence of polar (e.g., lysine, arginine) or apolar amino acids (e.g., phenylalanine, tryptophan) and are formed when the unfolded peptide sequences come in close vicinity to the phospholipid bilayer membrane by the electrostatic interaction between positively charged amino acid residues of the peptide and the negatively charged phosphate group of the lipids. Next, the hydrophobic amino acid residues of the peptide insert themselves between the hydrophobic hydrocarbon tails of the lipids because of the hydrophobic effect, resulting into adsorption and a change in the conformation to an α helix (Anantharamaiah, 1986; Drin et al., 2007; Drin & Antonny, 2009; Seelig, 2004; Segrest et al., 1990). This mechanism of the formation of an amphipathic α helix is energy driven and proteins use either sensing or hydrophobic interactions or a combination of both to bind to the membrane (Chen et al., 2016). Ankycorbin, a protein containing an N-terminal amphipathic helix was recently characterised for its membrane-binding and shaping abilities and it was suggested that the amphipathic helix inserts itself into one leaflet of the bilayer membrane via both electrostatic and hydrophobic interactions (Wolf et al., 2019). Such interactions enable the amphipathic helix to sense and bend the lipid bilayer membranes, which may lead to fusion, fission or in stabilizing protein-lipid complexes (Giménez-Andrés et al., 2018). As an example, α-Synuclein, a protein

associated with Parkinson's disease, has an amphipathic helix, which stabilizes curved structures of membrane, and, at high concentrations, can also induce vesiculation and tubulation of the membrane (Braun et al., 2017; Choi et al., 2013).

**Fer/CIP4 Homology-BAR (F-BAR)**

Based on the similarity of the amino acid sequences, the difference in the degree of the intrinsic curvature formed by the dimers of the BAR domain and the presence of additional domains, this superfamily of BAR domain-containing membrane-shapers has been divided into the classical BAR, N-BAR, F-BAR, Inverse-BAR, BAR- Pleckstrin Homology and PhoX-BAR (Frost et al., 2009; Suetsugu et al., 2010). The F-BAR domain have been shown to bend the membranes in the form of tubules which are ~3-fold wider in diameter than the N-BAR domain (Frost et al., 2008). Thus, the F-BAR domain form a shallow degree of invagination (Henne et al., 2007; Shimada et al., 2007; Wang et al., 2009). Most of the the F-BAR containing-proteins, also have an additional Src homology 3 (SH3) domain (Peter et al., 2004; Qualmann et al., 2011) and latter are amongst the most abundant and conserved protein-protein interaction modules, which comprise of ~60 amino acid residues. The amino acids fold into two antiparallel β sheets at right angles to one another, consisting of two variable loops. Most SH3 domains prefer polyproline peptides with a consensus PxxP, where P is proline and x any amino acid and when bound, the SH3 ligands, adapt an all-trans left-handed helical conformation, called polyproline type II, which resembles a triangular prism (Macarthur & Thornton, 1991). Depending on the location of basic residues, whether at N- or C-terminus with respect to PxxP, the proline-rich motifs are classified as class I, or class II, respectively (Feng et al., 1994; Mayer, 2001). Proline offers a sequence-specific recognition with low affinity as it is the only proteinogenic amino acid with a secondary amine and is stable as a cis isomer over the peptide bond (Macarthur & Thornton, 1991; Williamson, 1994; Zarrinpar et al., 2003). In short, SH3 domains act as lock and polyproline peptide sequences as helical keys (Meirson et al., 2019; Musacchio, 2002).

**1.2.1.1 Syndapin, F-BAR domain-containing membrane-shaping proteins**

Family of proteins called syndapin (also known as pascin) belong to F-BAR domain-containing proteins of membrane-shapers which also have a carboxy (C)-terminal SH3 domain. The F-BAR domain of syndapin proteins can induce membrane invaginations and form lipid tubules ranging from 10 nanometer (nm) to more than 150 nm in diameter (Bai et al., 2012; Wang et al., 2009). There are three isoforms of syndapin found in mammals, which show tissue specific expression with syndapin I being brain-enriched, syndapin II-s (small) and syndapin II-l (long) being ubiquitously expressed (Qualmann & Kelly, 2000; Ritter et al., 1999) and syndapin III being highly expressed in muscle (Kessels & Qualmann, 2004; Qualmann et al., 2011).

The SH3 domain of syndapin I and II proteins have been known to interact with synaptojanin, dynamin I, synapsin I, and N-WASP, a stimulator of Arp2/3 induced actin filament nucleation. Receptor-mediated internalization of transferrin was also inhibited by the SH3 domain of both syndapin I and II proteins. Thus, both the isoforms of syndapin regulate clathrin-mediated endocytosis but as syndapin I is highly expressed in mammalian brain, it is involved in synaptic vesicle endocytosis (Anggono & Robinson, 2007; Kessels & Qualmann, 2002; Koch et al., 2011; Qualmann et al., 1999; Qualmann & Kelly, 2000; Rao et al., 2010). Furthermore, transient accumulation of actin, the Arp2/3 complex and N-WASP were observed at the site endocytosis, which is coordinated by dynamin-mediated vesicle fission (Merrifield et al., 2002, 2004). Syndapin proteins demonstrated the ability to shape the plasma membrane (Dharmalingam et al., 2009) and self-associate via their F-BAR domain. The feature of oligomerisation has been shown to be essential for both syndapin-mediated endocytosis and actin cytoskeletal remodelling. Thus, syndapin proteins acted like a link between the two processes (Kessels & Qualmann, 2006). Full-length syndapin proteins were shown to be vital for inducing filopodia (Qualmann & Kelly, 2000), additionally both syndapin I and II have been reported to be crucial in the process of ciliogenesis (Insinna et al., 2019; Schüler et al., 2013). Functional studies of syndapin I in primary rat hippocampal neurons unveiled that syndapin I is essential for neuromorphogenesis as it induced dendrite formation and branching, while loss-of-function of syndapin I resulted

in increased axon length and branching (Dharmalingam et al., 2009). SH3 domain of syndapin I interacts with the proline-rich motif of ProSAP1/SHANK2 in the postsynaptic density and thus, syndapin I regulates the formation of excitatory synapses. The loss-of-function of syndapin I resulted in a significant reduction of both synapses and dendritic spine densities of primary rat hippocampal neurons (Schneider et al., 2014) and also caused seizures and schizophrenia-like symptoms in mice (Koch et al., 2020). Syndapin I was also shown to recruit the novel actin nucleator, cordon-bleu (Cobl) (Ahuja et al., 2007) to the membrane and physically link Cobl's relative Cobl-like (Izadi et al., 2017) by the F-BAR domain of syndapin I protein and further demonstrated that all the three proteins coordinated spatially in a controlled fashion at the dendritic branch induction sites (Izadi et al., 2021; Schwintzer et al., 2011). Nanoclusters of syndapin I at the protrusion sites of the dendrites of hippocampal neurons were also observed by the high-resolution technique of freeze-fracture replica immunolabelling (FRIL) and transmission electron microscopy (TEM) (Izadi et al., 2021). These findings indicated the vital role of syndapin I protein as a scaffold, where it interacts with various diverse proteins and brings them together on a signalling cue. In short, syndapin proteins might be acting like a bridge because of their important functional feature of self-association (Kessels & Qualmann, 2004).

Other isoforms like syndapin II and syndapin III have been shown to be important for the formation of uniform plasma membrane invaginations called caveolae which are ~70 nm in diameter and have been suggested to be important for maintaining muscle cell integrity (Hansen et al., 2011; Seemann et al., 2017; Senju et al., 2011).

SH3 domain of syndapin I interacts with the proline-rich motif RRQAPPPP in dynamin I (Anggono & Robinson, 2007), RKKAPPPPKR in ProSAP1/Shank2 (Schneider et al., 2014), proline-rich consensus 'KrRAPpPP' in Cobl (Schwintzer et al., 2011) and 'Kr+APxpP' in Cobl-like (Izadi et al., 2021). These interactions between Syndapin I and its proline-rich motif-containing binding partners has been shown to be crucial in the development of neurons, thus, suggesting that the investigation of the potential

syndapin I-interacting partners might have paramount relevance in the development of brain.

### 1.2.2 N-Ank superfamily of membrane-shaping proteins

Interesting, the prototype of N-Ank proteins (Wolf et al., 2019), ankycorbin, which was recognized as a putative interacting partner of syndapin I protein during an *in silico* analysis (Schwintzer, 2012), was reported to be crucial in the early development of the neuronal dendritic arbor (Wolf et al., 2019). N-Ank proteins were characterized by their ability to bind and bend the lipid bilayer via their N-Ank module, which comprised of an N-terminal amphipathic helix followed by ankyrin repeat domain (ARD) (Wolf et al., 2019).

Takahashi et al. (2014) and Kim et al. (2014) had reported for the first time that ARD, which is famous for protein-protein interactions, is also capable of binding lipids. ARD consists of tandem repeat arrays of ~33 amino acids and two to more of such repeats forms a curved secondary structure. The number of repeats in an ARD varies from protein to protein, which results in structural and functional versatility. It has been reported earlier that for an ankyrin repeat to fold, it at least needs two of them (Mosavi et al., 2004) and the increase in number of repeats makes the structure more compact and concave (Islam et al., 2018; Li et al., 2006; Sedgwick & Smerdon, 1999).

Interestingly, the transient receptor potential cation channel subfamily vanilloid member 4, was shown to bind to phosphatidylinositol 4,5-bisphosphate via its ARD, resulting in reduced activity of the channel (Takahashi et al., 2014). The ARD of *Arabidopsis* ankyrin repeat domain-containing protein 2A was shown to specifically bind to phosphatidylglycerol and monogalactosyldiacylglycerol; two lipids, which are enriched in the chloroplast outer membrane (Kim et al., 2014).

Functionally, ARD are well documented to be involved in intra- and intermolecular protein-protein, protein-sugar, and protein-lipid interactions (Islam et al., 2018; Mosavi et al., 2004; Sedgwick & Smerdon, 1999). Thus, proteins comprising of ARD are

involved in diverse physiological processes such as cell-cell signalling and it is further important to note that dysfunction in ankyrin repeats can have pathological implications like in cancer (Islam et al., 2018; Li et al., 2006). Ankyrin repeats in IκBα, inhibitor of nuclear factor kappa-light-chain-enhancer of activated B cells (NF-κB) interact with the transcriptional activator NF-κB, thus regulating its transcriptional activity (Sue et al., 2008). p85 has 6 ankyrin repeats at its N-terminus and its direct association with protein phosphatase 1 isoform δ was reported to be critical for actin depolymerization (Tan et al., 2001). Two proteins, Shank and Sharpin, highly enriched in the postsynaptic density of excitatory synapses in brain, interact with each other via the ankyrin repeats of Shank (Lim et al., 2001). It is fascinating to know that ankyrin repeat-containing protein are reported to be highly expressed in vertebrate brain (Kunimoto et al., 1991).

Amphipathic helix in the N-Ank module of ankycorbin was demonstrated to be essential for binding to the membrane while ankyrin repeats displayed the property of sensing the curvature of liposomes membrane and binding higher curvature liposomes. Like N-Ank proteins, another protein called ANK and KH domain-containing protein 1 (ANKHD1), uses a combination of amphipathic helix and ARD to bend and shape the membranes. ANKHD1 is involved in early endosome enlargement and unlike N-Ank proteins has an N-terminal ARD and a C-terminal amphipathic helix. N-terminal ARD comprises of 25 ankyrin repeats, out of which, the former 15 mediate dimerization and the latter 10 tubulate and vesiculate the membrane along with the C-terminal amphipathic helix. Along with ANKHD1, there are 18 other proteins suggested in this category of membrane-shaping proteins (Kitamata et al., 2019).

Ankycorbin also displayed the property of self-association mediated via its additional putative domain called coiled coil. Coiled coil domains are widely known for their protein-protein interaction capability and are mostly characterised by the formation of α helical supersecondary structures comprising of the periodic appearance of seven residue 'heptap repeat, abcdefg', such that a and d are hydrophobic amino acids. Such repeats in a protein can range from 2-200 (Mason & Arndt, 2004). Additionally, they are known to oligomerise within the same or different polypeptide chains, enabling structural

formation of scaffolds in the form of long fibers, zippers, tubes, spirals, tubes, or rings (Lupas et al., 2017). Coiled coil domains in proteins are known to regulate vital biological processes like remodelling of the actin cytoskeleton. As an example, Rho-associated coiled coil kinase (ROCK2) exists as a dimer and the length of its coiled coil domain determines its active signalling as truncation in the same resulted in *in vivo* defects of stress fibre formation with no loss of catalytic activity (Truebestein et al., 2015). It was also reported that oligomerisation of coiled coil domain in SNARE proteins, which are membrane-binding proteins, promote membrane fusion (Parry et al., 2008).

Functional analysis of ankycorbin in hippocampal neurons unveiled that ankycorbin was essential for inducing dendritic branches as its gain-of and loss-of-function significantly affected the formation of dendritic branches. The analysis also demonstrated that all domains of ankycorbin (amphipathic helix, ankyrin repeats and coiled coil) and also the proline-rich motif of consensus 'KrRAPpPP' with which it interacts with syndapin proteins were crucial for ankycorbin's function in neuromorphogenesis. Furthermore, high resolution ultrastructure technique of FRIL and TEM, showed that ankycorbin accumulated at the base of dendritic protrusions (Wolf, 2018; Wolf et al., 2019).

Since the function of ankycorbin was domain-dependent, it was postulated that there might be other proteins with similar arrangement of domains, which could illustrate an evolutionarily conserved mechanism behind bending and shaping of lipid bilayers. Thus, domain-based *in silico* analysis was performed and 15 other proteins were identified and phylogenetically classified as N-Ank proteins. This family of 16 proteins was divided into two subfamilies with a smaller subfamily consisting of ankycorbin, uveal autoantigen with coiled-coil domains and ankyrin repeats (UACA), Ankrd35 and Ankrd24 (Wolf, 2018; Wolf et al., 2019). N-Ank properties of UACA from smaller sub-family and Ankrd20A1 from the larger second family were characterized for their N-Ank properties, and the results showed that the N-Ank module of both UACA and Ankrd20A1 behaved similarly as ankycorbin's N-Ank module. The N-terminal amphipathic helix of UACA and Ankrd20A1 showed binding to the membrane, while the

ankyrin repeats sensed the curvature of liposomes mediated via electrostatic interactions and the combination of amphipathic helix and ankyrin repeats, the N-Ank module, thus shaped the membrane.

**1.2.2.1 Ankrd24**

In the newly classified superfamily of membrane-shaping proteins called N-Ank, ankycorbin, UACA, Ankrd35 and Ankrd24 were phylogenetically classified into the smaller sub-family of N-Ank proteins (Wolf et al., 2019). Ankrd24 was additionally identified as the potential syndapin I-interacting partner (Schwintzer, 2012). Ankrd24 (UniProtKB Q80VM7) is an uncharacterised protein which shares 50.63% percent identity ("BLAST: Basic Local Alignment Search Tool", 2021) with the syndapin-binding partner, ankycorbin (UniProtKB Q9EP71), 37.69% with Ankrd35 (UniProtKB E9Q9D8) and 37.22% with UACA (UniProtKB Q8CGB3), respectively. The sequences were aligned using alignment feature of BLAST and percent identity is defined the number of the same amino acid residues present at the same positions in an alignment, expressed as a percentage (Fassler & Cooper, 2021). The amino acid sequence similarity is at N-terminal and C-terminal of Ankrd24 and all proteins of this smaller family have been predicted to contain the N-Ank module and also the coiled coil domain (Wolf et al., 2019).

No experimental preliminary data except from the ribonucleic acid (RNA) sequencing at 'the human protein atlas' (Uhlén et al., 2015, Sjöstedt et al., 2020) is available, where it was suggested that Ankrd24 is highly expressed in human and mouse brain. RNA transcriptomics studies have associated *Ankrd24* in several diseases like progeria (Sola-Carvajal et al., 2019), ovarian cancer (Dausinas et al., 2020), pituitary adenoma (Wang et al., 2019), glioma (Liu et al., 2021), congenital heart disease (Matos-Nieves et al., 2021) and *Ankrd24* is also one of the ER stress-dependent genes (Bartoszewski et al., 2020). *Ankrd24* was also reported to be one of the upregulated genes in human adrenocorticotropin-secreting pituitary adenomas from female patients with Cushing's disease (Giraldi et al., 2020).

## 1.3  Aims of the study

Therefore, the aim of this study was to test the hypothesis that Ankrd24 as well has N-Ank properties of membrane sensing, binding, and shaping, which would further strengthen the N-Ank hypothesis, and to reveal potential overlapping but also distinct properties related to the other members of the N-Ank superfamily. Biochemical analysis for evaluating the N-Ank module of Ankrd24 for its interacting and shaping behaviour with lipid bilayer include liposome assays and freeze-fracture experiments, respectively. *In vivo* membrane-association of Ankrd24 can be studied by subcellular fractionation and colocalisation experiments. The characterisation of coiled coil domain in Ankrd24 for oligomerisation ability shall reveal a potential molecular mechanism for the formation of larger membrane interacting Ankrd24 scaffolds. Additionally, this study aimed at identifying putative functions of Ankrd24 in neuromorphogenesis in primary rat hippocampal neurons by overexpression and RNA interference (RNAi) experiments.

As Ankrd24 was already predicted to be a putative interacting partner of syndapin I and former was also identified to have a proline-rich motif of consensus 'KrrAPpPP', the investigation aimed to learn if Ankrd24 binds to syndapin proteins by performing protein interaction studies and if so, then whether this interaction would play any role in Ankrd24's biological function. The latter will be analysed by *in vivo* rescue experiments with mutants in primary rat hippocampal neurons. Syndapin proteins are known for their membrane binding and shaping abilities, as well as their function as a scaffold, which has been demonstrated to be crucial in neuromorphogenesis by the isoform, syndapin I.

Overall, this study aimed at further establishing and defining the properties of the N-Ank superfamily of membrane-shapers by characterising another protein, Ankrd24, which will facilitate the understanding of the different role of domains in a protein for membrane-shaping.

## 2   Materials and Methods

### 2.1   Materials

#### 2.1.1   Commercial reagents and buffers

All other general chemical reagents, if not otherwise specified, were purchased from Carl Roth GmbH & Co. KG, Merck KGaA, Sigma-Aldrich® Co. LLC or SERVA Electrophoresis GmbH. Double distilled water (ddH$_2$O) was used as the solvent for the chemical reagents except where otherwise notified.

**Commercial Reagents and Buffers**

| | |
|---|---|
| 0.5% Trypsin- Ethylenediamine-n,n,n',n'-tetraacetic acid (EDTA) (10x) No Phenol Red | Gibco® Invitrogen GmbH |
| 10x T4 Deoxyribonucleic Acid (DNA) Ligase Buffer | Thermo Fisher Scientific Inc. |
| 5x Phusion® GC Buffer | Thermo Fisher Scientific Inc. |
| 5x Phusion® High Fidelity Buffer | Thermo Fisher Scientific Inc. |
| Agarose | Biozym Scientific GmbH |
| Alkaline Phosphatase FastAP™ | Thermo Fisher Scientific Inc. |
| Ampicillin Sodium Salt | Carl Roth GmbH |
| Ampuwa® Water For Injection | Fresenius Kabi |
| B-27® Serum-Free Supplement (50x) | Gibco® Invitrogen GmbH |
| Bovine Serum Albumin (BSA) Fraction V | Carl Roth GmbH |
| Bromophenol Blue | Carl Roth GmbH |
| Coomassie Brilliant Blue G-250 | Carl Roth GmbH |
| 4',6-Diamidin-2'-phenylindol-Dihydrochloride (DAPI) | Roche Diagnostics AG |
| Deoxyribonucleotides (dNTPs), 100 mM | Thermo Fisher Scientific Inc. |
| Dimethyl Sulfoxide (DMSO) | Thermo Fisher Scientific Inc. |
| Dulbecco's Modified Eagle Medium (DMEM) | Gibco® Invitrogen GmbH |
| Deoxyribonuclease (DNase) I | Roche Applied Science |
| DMEM High Glucose | Gibco® Invitrogen GmbH |
| Ethidium Bromide | Carl Roth GmbH |
| Ethyl-3-(3-Dimethylaminopropyl) Carbodiimide Hydrochloride (EDC) | Sigma-Aldrich® Co. LLC |
| Foetal Calf Serum (FCS) | GE Healthcare |
| Folch Fraction I (Brain Extract from Bovine Brain, Type I) | Sigma-Aldrich® Co. LLC |
| Glutamax™ Supplement (100x) | Gibco® Invitrogen GmbH |
| Glutathione Resin | Gene Script |
| Hanks' Balanced Salt Solution (HBSS) No Calcium, No | Gibco® Invitrogen GmbH |

Magnesium, No Phenol Red, L-Glutamine 200 Mm (100x)

| | |
|---|---|
| Horse Serum, Heat Inactivated | Gibco® Invitrogen GmbH |
| Isopropyl-ß-D-Thiogalactopyranoside | Millipore GmbH |
| Kanamycin Sulphate | Carl Roth GmbH |
| Klenow-Fragment | Fermentas GmbH |
| Lysogenic Broth (LB) Agar | Carl Roth GmbH & Co. KG |
| Lipofectamine® 2000 Transfection Reagent | Thermo Fisher Scientific Inc. |
| LB Medium | Carl Roth GmbH & Co. KG |
| Lysozyme | Sigma-Aldrich® Co. LLC |
| Mowiol® 4-88 | Calbiochem |
| Neurobasal™ Medium | Gibco® Invitrogen GmbH |
| Opti-MEM® | Gibco® Invitrogen GmbH |
| Penicillin/Streptomycin (100x) | Gibco® Invitrogen GmbH |
| Phusion® High Fidelity DNA Polymerase | Thermo Fisher Scientific Inc. |
| Poly-D-Lysine Hydrobromide | Sigma-Aldrich® Co. LLC |
| Precission™ Protease | Ge Health Care Life Science |
| Propane Ethane (1:1 Liquid Mix) | Linde AG |
| Protease Inhibitor Complete (PIC) EDTA Free Tablet | Roche Applied Science |
| Proteinase K | Thermo Fisher Scientific Inc. |
| Restriction Endonucleases | Thermo Fisher Scientific Inc. |
| Ribonuclease (RNase) A | QIAGEN GmbH |
| Skimmed Milk Powder | Carl Roth GmbH |
| T4 DNA Ligase | Thermo Fisher Scientific Inc. |
| T4 Polynucleotide Kinase | Fermentas GmbH |
| Triton®X-100 | Sigma-Aldrich® Co. LLC |
| Turbofect™ | Thermo Fisher Scientific Inc. |
| Tween®20 | SERVA Electrophoresis GmbH |
| Yeast Extract | Carl Roth GmbH & Co. KG |

**DNA Markers**

| | |
|---|---|
| Generuler™ 100bp Plus DNA Ladder | Thermo Fisher Scientific Inc. |
| Generuler™ 1kb DNA Ladder | Thermo Fisher Scientific Inc. |

**Protein Markers**

| | |
|---|---|
| Pageruler™ Prestained Protein Ladder 26616 | Thermo Fisher Scientific Inc. |
| Spectra™ Multicolor High Range Protein Ladder 26625 | Thermo Fisher Scientific Inc. |

**Kits**

| | |
|---|---|
| Nucleo Bond® Xtra Midi | Macherey-Nagel GmbH |

| | |
|---|---|
| Nucleo Spin® Gel and Polymerase Chain Reaction (PCR) Clean-Up | Macherey-Nagel GmbH |
| Pierce™ Bicinchoninic Acid (BCA) Protein Assay | Thermo Fisher Scientific Inc. |

### 2.1.2 Bacterial and animal strains and mammalian cell line

Bacterial strains (*E. coli*) BL21-CodonPlus® (DE3)-RIPL was used for protein expression and XL-10 Gold™ for plasmid production, respectively and they were both obtained from Agilent Technologies Inc. More detailed information about the genotype of the bacterial strains is described in table 1.

**Table 1: Bacterial strains (*E. coli*) and genotype**

| Name | Genotype |
|---|---|
| BL21-CodonPlus® (DE3)-RIPL | *E. coli* B F⁻ *ompT hsdS* (r$_B^-$ m$_B^-$) *dcm$^+$* Tet$^r$ *gal* λ*(DE3) endA* Hte [*argU proL* Cam$^r$] [*argU ileY leuW* Strep/Spec$^r$] |
| XL-10 Gold™ | Tet$^r$Δ*(mcrA)183* Δ*(mcrCB-hsdSMR-mrr)173 endA1 supE44 thi-1 recA1 gyrA96 relA1 lac* Hte [F' *proAB lacI qZΔM15* Tn*10* (Tet$^r$) Amy Cam$^r$] |

*Rattus norvegicus* Wistar strain for rat and *Mus musculus* C56/BL6J strain for mice were used, respectively. Both animal strains were purchased from Charles River Laboratories Inc. Human embryonic renal (HEK) 293 cells (Graham et al., 1977) were used for biochemical applications and for testing RNAi constructs. Henrietta Lacks (HeLa) cells, a human cervix carcinoma cell line (Scherer et al., 1953) were used for microscopic analysis of green fluorescent protein (GFP) fused proteins.

### 2.1.3 Laboratory constituted Reagents, Medium and Buffers

**Table 2: Buffers and their composition**

| Buffers | Composition |
|---|---|
| 1x Trypsin Solution | 0.5% ((weight per volume) (w/v)) Trypsin-EDTA (10x) No Phenol Red Stock Solution 1:10 in HBSS |
| 2.5% Sodium Dodecyl Sulphate (SDS) Solution | 2.5% (w/v) SDS, 30 millimolar (mM) Sucrose in 10 mM Tris/Hydrogen Chloride (HCl); pH 8.4 |
| 25x Protease Inhibitor (PI) | 1 Tablet PIC EDTA Free in 2 millilitre (ml) Phosphate Buffered Saline (PBS) |
| 4x SDS Sample Buffer | 4% (w/v) SDS, 40% ((volume per volume) (v/v) |

| | |
|---|---|
| | Glycerol, 250 mM Tris/HCl, 20% (v/v) ß-Mercaptoethanol, 0.004% (w/v) Bromophenol Blue; pH 6.8 |
| 50x Tris/Acetate/EDTA (TAE) Running Buffer | 2 molar (M) Tris/HCl, 5.71% (v/v) Acetic Acid, 0.05 M EDTA; pH 8.5 |
| 6x DNA Loading Buffer | 0.25% (w/v) Bromophenol Blue, 0.25% (w/v) Xylocyanol, 30% (v/v) Glycerol, 50 mM EDTA; pH 8.0 |
| Annealing Buffer | 100 mM Sodium Chloride (NaCl), 50 mM 4-(2-hydroxyethyl)piperazine-1-ethanesulfonic acid (HEPES); pH 7.4 |
| Blocking Solution | 2% (w/v) BSA, 10% (v/v) Horse Serum in PBS; pH 7.4 |
| Bradford Reagent | 100 milligram (mg)/ litre (l) Coomassie Brilliant Blue G-250, 5% (v/v) Ethanol, 10% (v/v) Phosphoric Acid (Filtered) |
| Colloidal Coomassie Staining Solution | 1% (w/v) Coomassie Brilliant Blue G-250, 10% (w/v) Ammonium sulphate,, 23.5% (v/v) Phosphoric Acid |
| DAPI Solution | 0.2% (w/v) DAPI Stock Solution 1:10000 in PBS |
| DMEM Plus Additives (DMEM++) | 2 mM L-Glutamine, 10% (v/v) FCS, Penicillin/ Streptomycin in DMEM |
| Glutathione-S-Transferase (GST) Elution Buffer | 20 mM Glutathione, 50 mM Tris/HCl, 120 mM NaCl; pH 8.0 |
| HEPES NaCl (HN) Buffer | 20 mM HEPES, 150 mM NaCl, 1 mM Dithiothreitol; pH 7.4 |
| Homogenisation Buffer | 5 mM HEPES, 1x PI, 0.32 M Saccharose, 1 mM EDTA; pH 7.4 |
| Immunoprecipitation (IP) Buffer | 10 mM HEPES, 1 mM ethylene glycol bis(2-aminoethyl) tetraacetic acid (EGTA), 0.1 mM Magnesium Chloride, 150 mM NaCl, 1x PI; pH 7.4 |
| Labelling Blocking Buffer (LBB) | 1% (w/v) BSA, 0.5% (w/v) Fish Gelatine, 0.005% (v/v) Tween®20 in PBS; pH 7.4 |
| LB Agar | 15 gram (g) Agar in 1 l LB Medium |
| LB Medium | 10 g Tryptone/Peptone, 5 g NaCl, 5 g Yeast Extract in 1 l ddH$_2$O; pH 7.2 |
| Lysis Buffer | 10 mM HEPES, 1 mM EGTA, 0.1 mM Magnesium Chloride, 150 mM NaCl, 1% (v/v) Triton®X-100; pH 7.4 |
| Mowiol | 10% (w/v) Mowiol® 4-88, 25% (w/v) Glycerol, 100 mM Tris/HCl; pH 8.5 |
| P1 Buffer | 50 mM Tris, 10 mM EDTA, 100 mg/ml RNase A; pH 8.0 |
| P2 Buffer | 200 mM Sodium Hydroxide, 1% (w/v) SDS |
| P3 Buffer | 3 M Potassium Acetate; pH 5.5 |

| | |
|---|---|
| PBS | 2.68 mM Potassium Chloride, 1.47 mM Potassium Phosphate, 136.9 mM NaCl, 7.98 mM Sodium Phosphate Dibasic Dihydrate; pH 7.4 |
| PBS-T | 0.05% (v/v) Tween®20 in PBS |
| Quench Buffer | 25 mM Glycine in PBS |
| Radioimmunoprecipitation (RIPA) Buffer | 50 mM Tris, 150 mM NaCl, 1% (v/v) NP-40, 0.5% (w/v) Na-deoxycholate, 0.1% (w/v) SDS; pH 8.0 |
| SDS Running Buffer | 0.25 M Tris/HCl, 192 mM Glycine, 0.1% (w/v) SDS |
| Separating Gel Buffer | 1.5 M Tris/HCl, 0.4% (w/v) SDS; pH 8.8 |
| Super Optimal Broth with Catabolite Repression (SOC) Medium | 0.5% (w/v) Yeast Extract, 2% (w/v) Tryptone, 10 mM NaCl, 2.5 mM Potassium Chloride, 10 mM Magnesium Chloride, 10 mM Magnesium Sulphate, 20 mM Glucose |
| Terrific Broth (TB) Medium | 12 g Tryptone, 24 g Yeast Extract, 4 ml Glycerol, 2.3 g Potassium Phosphate, 12.5 g Dipotassium Hydrogen Phosphate in 1 l ddH$_2$O |
| Transfer Buffer | 25 mM Tris, 192 mM Glycine, 0.02% (w/v) SDS, 20% (v/v) Methanol |

## 2.1.4  Primers

Biomers.net GmbH Ulm synthesised the primers. Restriction sites (RS) are mentioned in lower case letters and KOZAC sequence (GCCACC) was added for better transfection, wherever necessary.

**Table 3: Primers designed for cloning *Mus musculus* Ankrd24x6 constructs**. The sequence of the primers aligns to the base pairs (bp) of Ankrd24x6 (NCBI Reference Sequence: XM_006514096.5), Fw: forward primer; Rv: reverse primer

| Primer | Sequence 5'-3' | Aligns to bp | RS |
|---|---|---|---|
| BQ2893 | Fw: ATAgaattcGCCACCATGAAGACCCTCCGG | 1-15 | EcoRI |
| BQ2894 | Rv: TATgtcgacTGTGCTGGCTGGAGGCTG | 855-838 | SalI |
| BQ2895 | Rv: TATgtcgacAGTGGCATCCTGGCCCAG | 666-649 | SalI |
| BQ2907 | Rv: TATgtcgacGCGACCCTGAGCCTG | 3123-3109 | SalI |
| BQ2940 | Fw: ATAgaattcGCCACCATGAAGACCCTCCGGGCACGATTCAAGAAAACAGAGGGC | 1-39 | EcoRI |
| BQ2999 | Fw: ATAgaattcGCCACCATGGGAAGGCACCCCAGCCTCCAGCCAGCACACCAGTTCCTGACG | 827-868 | EcoRI |

| BQ3000 | Fw:<br>ATAaagcttGCCACCATGAAGACCCTCCGGGCACGATTC<br>AAGAAAACAGAGGGCCAAGAC | 1-45 | HindIII |
|---|---|---|---|
| BQ3208 | Fw:<br>ATAgaattcGCCACCATGAAAACAGAGGGCCAAGACTGG | 28-48 | EcoRI |

**Table 4: Oligonucleotides used for constructing short hairpin (sh) RNAs**
The bp alignment is in reference to *Rattus norvegicus* Ankrd24x2 isoform (NCBI Reference Sequence XM_039078672.1 as of 19 May 2021). The isoforms which were targeted in respective species has been mentioned (for all information of Ankrd24 isoforms in *Mus musculus* and *Rattus norvegicus, see* Fig. 3 and Fig. 16, respectively). Lower case letters signify HindIII and BamHI RS, which were used to insert the sequence into the pRNAT-H1.1/GFP-N vector.

| Primer | Isoforms targeted | Sequence 5'-3' | Aligns to bp |
|---|---|---|---|
| BQ3130 | *Mus musculus*: All except isoform 21 and 22<br><br>*Rattus norvegicus*: All except isoform 1 | Fw:<br>gatccGCTCAGATGTGTCACACA<br>GATTGATATCCGTCTGTGTGA<br>CACATCTGAGCTTTTTTA | *712-731* |
| BQ3131 | *Mus musculus*: All except isoform 21 and 22<br><br>*Rattus norvegicus*: All except isoform 1 | Rv:<br>agcttAAAAAAGCTCAGATGTGT<br>CACACAGACGGATATCAATCT<br>GTGTGACACATCTGAGCG | 731-712 |
| BQ3132 | *Mus musculus:* All except isoform 21 and 22<br><br>*Rattus norvegicus*: All except isoform 1 | Fw:<br>gatccGCTCATCTTGCAGCTTCT<br>ACATTGATATCCGTGTAGAAG<br>CTGCAAGATGAGCTTTTTTA | 927-947 |
| BQ3133 | *Mus musculus:* All except isoform 21 and 22<br><br>*Rattus norvegicus*: All except isoform 1 | Rv:<br>agcttAAAAAAGCTCATCTTGCA<br>GCTTCTACACGGATATCAATG<br>TAGAAGCTGCAAGATGAGCG | 947-927 |
| BQ3134 | All isoforms in *Mus musculus* and *Rattus norvegicus* | Fw:<br>gatccGAGGAGAAGGAGAGCCT<br>GGGTTGATATCCGCCCAGGCT<br>CTCCTTCTCCTCTTTTTTA | 1291-1310 |
| BQ3135 | All isoforms in *Mus musculus* and *Rattus norvegicus* | Rv:<br>agcttAAAAAAGAGGAGAAGGAG<br>AGCCTGGGCGGATATCAACCC<br>AGGCTCTCCTTCTCCTCG | 1310-1291 |
| BQ3136 | *Mus musculus:* All except isoform 21 and 22<br><br>*Rattus norvegicus*: All except isoform 1 | Fw:<br>gatccGGTTGTTTGTCCTGCTCA<br>AAGTTGATATCCGCTTTGAGC<br>AGGACAAACAACCTTTTTTA | 622-642 |

| BQ3137 | *Mus musculus:* All except isoform 21 and 22<br><br>*Rattus norvegicus:* All except isoform 1 | Rv: agcttAAAAAAGGTTGTTTGTCC TGCTCAAAGCGGATATCAACT TTGAGCAGGACAAACAACCG | 642-622 |

**Table 5: Primers designed for creating insensitive rescue mutant**

To verify that the gene silencing effect was due to shRNA targeting *Ankrd24* and not due to off-target effects, insensitive rescue mutant was designed. It was designed by creating point mutations which will result in silent mutations. The nucleotide with point mutation is shown by bold letters. The bp alignment is in reference to *Rattus norvegicus* Ankrd24x2 isoform.

| Primer | Sequence 5'-3' | Aligns to bp |
|---|---|---|
| BQ3312 | Fw:<br>CTCATCATAGCAGC**A**CA**A**ATGTG**C**CA**T**AC**G**GATCTGTGC CGCCTC | 478-497 |
| BQ3313 | Rv:<br>GAGGCGGCACAGATC**C**GT**A**TG**G**CACAT**T**GT**T**GCTGCTAT GATGAG | 497-478 |

## 2.1.5 Vectors and expression constructs

Clone codes in italics were previously constructed by Institute of Biochemistry I (BCI), Universitätsklinikum Jena (UKJ). Enhanced GFP(EGFP); Farnesyl (F).

**Table 6: Vectors**

| Vector | Source/reference |
|---|---|
| mcherryF | Martin Korte, TU Braunschweig |
| pEGFP-N3 | Clontech Laboratories Inc. |
| pGex-6P-1 | GE Healthcare |
| pGex-2T | GE Healthcare |
| pRNAT-H1.1/GFP-N | GenScript, SD1214 |
| pRNAT-H1.1/GFP-N/mcherry | BCI, UKJ, modified from pRNAT-H1.1/GFP-N by Annemarie Landmark (BCI/UKJ) |

**Table 7: Constructs for mammalian expression**

Ankrd24x6 refers to *Mus musculus* species. Superscript refers to the amino acid number. For RNAi, the superscript refers to the amino acid number it targets. Constructs marked by '*' denote the RNAi insensitive rescue mutants.

| Clone code | Construct | Vector |
|---|---|---|
| *IPT3* | Scrambled RNAi/GFP | pRNAT-H1.1/GFP-N; Wolf, 2018 |
| JYP2 | Ankrd24x6$^{1-285}$-GFP | pEGFP-N3 |
| KCH10 | Ankrd24x6$^{1-222}$-GFP | pEGFP-N3 |
| KEX3 | Ankrd24x6$^{1-1041}$-GFP | pEGFP-N3 |
| KMH1 | Ankrd24x6$^{283-1041}$-GFP | pEGFP-N3 |
| KPH6 | RNAi$^{160-166}$/GFP | pRNAT-H1.1/GFP-N |
| KPK11 | RNAi$^{130-136}$/GFP | pRNAT-H1.1/GFP-N |
| KQF1 | RNAi$^{160-166}$/Ankrd24x6$^{1-1041}$-GFP/mcherry | pRNAT-H1.1/GFP-N/mcherry |
| KQG6 | RNAi$^{231-237}$/Ankrd24x6$^{1-1041}$-GFP/mcherry | pRNAT-H1.1/GFP-N/mcherry |
| KQH7 | RNAi$^{272-277}$/Ankrd24x6$^{1-1041}$-GFP/mcherry | pRNAT-H1.1/GFP-N/mcherry |
| KQI2 | RNAi$^{130-136}$/Ankrd24x6$^{1-1041}$-GFP/mcherry | pRNAT-H1.1/GFP-N/mcherry |
| KSY5 | Scrambled RNAi/Ankrd24x6$^{1-1041}$-GFP/mcherry | pRNAT-H1.1/GFP-N/mcherry |
| LAW11 | Ankrd24x6$^{1-1041}$-GFP* | pRNAT-H1.1/GFP-N |
| LFX10 | Ankrd24x6$^{1-1041\Delta273-286}$-GFP* | pRNAT-H1.1/GFP-N |

**Table 8: Constructs for bacterial expression**

Clone code in *italics* were provided by Michaela Roeder (BCI, UKJ). Superscript refers to its amino acid number

| Clone code | Construct | Species | Vector |
|---|---|---|---|
| *BG2* | GST-SdpI$^{1-441}$ | rat | pGEX-2T; Qualmann et al., 1999 |
| *HXR2* | GST-SdpII-l$^{1-488}$ | rat | pGEX-6P1 |
| *HXS1* | GST-SdpII-s$^{1-447}$ | rat | pGEX-6P1 |
| *HXT1* | GST-SdpIII$^{1-424}$ | rat | pGEX-6P1; Izadi et al., 2021 |
| JYO10 | GST-Ankrd24$^{1-285}$ | mouse | pGEX-6P1 |
| KCI5 | GST-Ankrd24$^{1-222}$ | mouse | pGEX-6P1 |

| *KHX1* | GST-SdpI$^{378-441}$ | rat | pGEX-6P1 |
|---|---|---|---|
| *KHY1* | GST-SdpI$^{P434L}$ | rat | pGEX-6P1 |
| KRW5 | GST-Ankrd24$^{10-285}$ | mouse | pGEX-6P1 |
| KSA10 | GST-Ankrd24$^{10-222}$ | mouse | pGEX-6P1 |
| *HSP2* | GST-SdpI$^{1-441}$ | rat | pGEX-6P1; Izadi et al., 2021 |

## 2.1.6  Antibodies

**Table 9: Primary and Secondary antibodies**
Antibodies applied in Western blot (WB) and immunofluorescence (IF) staining with their respective use of dilution and source.

| Antibodies and species | Dilution | WB/IF | Company/ Reference |
|---|---|---|---|
| anti-β-actin mouse | 1:5000 | WB | Sigma-Aldrich® Co. LLC, A5441 |
| anti-Flag mouse | 1:1000 | WB | Sigma-Aldrich® Co. LLC, F3165 |
| anti-GFP mouse | 1:8000 | WB | Clontech Laboratories Inc., 632381 |
| anti-GST rabbit | 1:500 | WB | Qualmann et al., 1999 |
| anti-Lamin B1 rabbit | 1:5000 | WB | Abcam® plc, ab16048 |
| anti-Microtubule-associated protein 2 (MAP2) mouse | 1:500 | IF | Sigma-Aldrich® Co. LLC, M4403 |
| anti-mCherry rabbit | 1:1000 | WB | Abcam® plc, ab167453 |
| anti-Syndapin I rabbit | 1:1000 | WB | Qualmann et al., 1999 |
| **Secondary Antibodies** | | | |
| Donkey anti-goat AlexaFluor® 680 | 1:10000 | WB | Molecular Probes® Invitrogen GmbH, 1871998 |
| Donkey anti-goat IRDye® 800CW | 1:10000 | WB | LI-COR Biosciences GmbH, 926-32214 |
| Donkey anti-mouse AlexaFluor® 568 | 1:600 | IF | Molecular Probes® Invitrogen GmbH, A10037 |
| Goat anti-mouse AlexaFluor® 680 | 1:10000 | WB | Molecular Probes® Invitrogen GmbH, A21058 |
| Goat anti-mouse DyLight™ 800 conjugated | 1:10000 | WB | Thermo Fisher Scientific Inc., SA5-35521 |
| Goat anti-rabbit AlexaFluor® 680 | 1:10000 | WB | Thermo Fisher Scientific Inc., A32734 |
| Goat anti-rabbit DyLight™ 800 conjugated | 1:10000 | WB | Thermo Fisher Scientific Inc., SA5-35571 |

### 2.1.7 Equipments

**Table 10: Equipment and company**

| Name | Company |
|---|---|
| 5427R Centrifuge | Eppendorf AG |
| Axio Observer.Z1 with ApoTome.2 Module Microscope | Carl Zeiss Microscopy GmbH |
| AxioCam MRm CCD Camera | Carl Zeiss Microscopy GmbH |
| COLIBRI | Carl Zeiss Microscopy GmbH |
| Objectives 40x / 1.3 Oil | Carl Zeiss Microscopy GmbH |
| BioPhotometer | Eppendorf AG |
| C150 Incubator | Binder GmbH |
| Consort EV265 Power Supply | Consort bvba |
| Criterion Tank Blotter | Bio-Rad Laboratories GmbH |
| Desiccator ROTILABO® Glass | Carl Roth GmbH |
| HeraCell 240 (i) $CO_2$ Incubator | Thermo Fisher Scientific Inc. |
| Heraeus multifuge 3 SR+ Centrifuge | Thermo Fisher Scientific Inc. |
| HeraSafe HS/LaminAir® HN2472/ HBR 2448 | Thermo Fisher Scientific Inc. |
| Intas® Gel-Imager | INTAS Science Imaging Instruments GmbH |
| Milli-Q® Gradient Water Purification System | Merck KGaA Millipore |
| Mini-Protean Tetra Cell System SDS- Polyacrylamide Gel Electrophoresis (PAGE) Running Chamber | Bio-Rad Laboratories GmbH |
| Odyssey® Imager | LI-COR Biosciences GmbH |
| Optima MAX-XP Ultracentrifuge | Beckman Coulter |
| Optima™ L70 Ultracentrifuge | Beckman Coulter |
| PowerPac™ HC Power Supply | Bio-Rad Laboratories GmbH |
| RK100 Ultrasonic Tank | Bandelin Sonorex |
| SpectraMax® M2 Multi-Mode Microplate Reader | Molecular Devices LLC |
| T3 Thermocycler PCR Cycler | Biometra® GmbH |
| ThermoMixer® Compact | Eppendorf AG |
| Transmission Electron Microscope EM902A | Carl Zeiss Microscopy GmbH |
| ULTRA-TURRAX® T 10 Basic homogenizer | IKA |
| UP50H Ultrasonicator | Hielscher Ultrasonics GmbH |
| UV star 312 nm UV-light Transilluminator | Biometra® GmbH |

### 2.1.8 Software

Software were used for imaging, processing, and analysing data.

**Table 11: Software and copyright**

| Software name and/or version | Copyright |
|---|---|
| Adobe Photoshop CS2 | Adobe Systems Inc. |
| Ant Renamer | Antoine Potten (www.antp.be/software/renamer) |
| AxioVision SE64 Rel. 4.9, Zen 2011/2012 | Carl Zeiss Microscopy GmbH |
| EM-Menu 4 | TVIPS GmbH |
| GraphPad Prism 5.03 | GraphPad Software Inc. |
| Image Studio Lite System 5.2 | LI-COR Biosciences GmbH |
| ImageJ/FIJI 1.46r | National Institute of Health |
| Imaris 8.4.0 | BITPLANE AG |
| Microsoft Office 365 | Microsoft Corporation |
| Odyssey® Infrared Imaging System Application Software | LI-COR Biosciences GmbH |

## 2.2 Methods

Chemicals like enzymes, proteins, DNA, buffers, etc. were mixed and maintained on ice to avoid any thermal degradation during all experiments unless otherwise stated.

### 2.2.1 Construction of plasmids

### 2.2.1.1 PCR

Ankrd24 encoding plasmids were constructed by performing PCR using complementary DNA (cDNA) of an 8-weeks-old mice brain as a template. cDNA was provided by Annette Kreusch (BCI, UKJ). PCR was performed in a reaction mixture of 50 microlitre (µl) to amplify the region of interest by using specific primers. The product was then cloned in the respective vector, leading to specific plasmid. The reaction mixture constituted of 1x Phusion® GC Buffer, 0.5 micromolar (µM) each of forward and reverse primers, 10% DMSO, 200 µM dNTP, 50-250 nanogram (ng) DNA as template, 1 unit (U) Phusion® high fidelity DNA Polymerase and $ddH_2O$ to make up the volume to 50 µl. The standard conditions for the touchdown (TD) PCR (table 12) were adjusted according to the specific primers used and the size of the product

**Table 12: The TDPCR reaction program**

The annealing temperature ($T_a$) and extension time ($t_E$) were modified according to the specific primers used and the size of the product; °C (degree Celsius); s (second); min (minute)

| Step | Temperature | Time | Cycles |
|------|-------------|------|--------|
| Denaturing | 98°C | 2 min | |
| Denaturing | 98°C | 20 s | 15 |
| Annealing | $T_{a1}$ to $T_{a2}$ | $t_E$ s | |
| Elongation | 72°C | 20 s | |
| Denaturing | 98°C | 20 s | 25 |
| Annealing | $T_a$ | $t_E$ s | |
| Elongation | 72°C | 20 s | |
| Elongation | 72°C | 10 min | |
| Hold on | 4°C | - | |

## 2.2.1.2 DNA agarose gel electrophoresis and DNA extraction from the gel

Depending on the size of the product, DNA was separated on a 0.5-2% (w/v) agarose gel using electrophoresis. Weighed agarose was dissolved in 1x TAE buffer, followed by addition of ethidium bromide to a final concentration of 0.5 µg/ml. DNA was premixed with the 6x orange loading dye before loading onto the gel and running an electrophoresis in 1x TAE buffer at 80-120 volts for 30 min. Next, the DNA bands were visualised under the ultraviolet light and the band of interest was cut out. It was then purified following the Manufactures' manual of NucleoSpin® Gel and PCR clean-up kit.

## 2.2.1.3 DNA restriction digestion and ligation

Both DNA fragment and the vector (each 1-10 µg DNA) were cleaved by restriction enzymes, using the respective buffer and incubation conditions, as per manufactures' instructions. The total reaction mixture was of 30 µl. Cleaved vector was dephosphorylated using 1 µl of fast alkaline phosphatase FastAP™ at 37°C for 30 min and the enzyme was inactivated at 75°C for 10 min. The DNA fragments were then separated by agarose gel electrophoresis and purified according to 2.2.1.2. Ligation

reactions constituted of linearized DNA and vector in the molar ratio of 1:1 to 3:1, 10% v/v 10x T4 DNA ligase buffer and 0.5 U of T4 DNA ligase to make a total volume of 10 µl. The ligation conditions were either 16°C for 18 hours (h) or 4°C for 12 h.

### 2.2.1.4 Transformation

Competent XL-10 Gold$^{TM}$ *E.coli* cells were used for transformation. The cells were prepared by Birgit Schade (BCI/UKJ) according to Inoue et al. (1990). Ligation product containing 0.1-1 µg plasmid DNA was added to 100 µl of competent cells and the mixture was maintained on ice for another 2 min, followed by a heat shock at 42°C for 45 s. The mixture was then cooled on ice for 2 min and later 500 µl SOC medium was added to it, followed by incubation at 37°C for 60 min under 500 revolutions per minute (rpm) shaking. Thereafter, the cells were gently collected by centrifugation at 500 times gravity (x g) for 5 min, resuspended in 40 µl of SOC medium and plated on LB agar plate containing either ampicillin sodium salt or kanamycin sulphate. The plate was then incubated at 37°C for 12 h.

### 2.2.1.5 DNA extraction, test digestion and sequencing

For test digestion, 5-10 colonies were individually inoculated in 2.5 ml of liquid LB medium containing either ampicillin sodium salt or kanamycin sulphate at 37°C for 12 h with 200 rpm shaking. Next day, DNA extraction was performed by using alkaline lysis method. The cells were collected by a centrifugation step at 20817 x g for 1 min, followed by re-suspension of cells in 250 µl of P1 buffer. The cells were then lysed by adding 250 µl of P2 buffer, followed by incubation at room temperature (RT) for 5 min. Next, 250 µl of P3 buffer was added for neutralization and cells were then centrifuged at 20817 x g, RT for 10 min, followed by collecting the supernatant in a new Eppendorf tube containing 650 µl of isopropanol to precipitate the DNA. Next, the precipitated DNA was collected by another centrifugation step at 20817 x g, RT for 10 min and consecutively washed with 750 µl of 70% (v/v) ethanol. The air-dried DNA pellet was then dissolved in 50 µl ddH$_2$O. The DNA was then cleaved by specific restriction enzymes to identify the potential positive clones. The DNA of the positive clones was then sent for sequencing to Microsynth Seqlab GmbH. The constructs used for

transfection of primary hippocampal neurons and HEK293 cells were purified as per user instructions of Nucleo Bond® Xtra Midi kit.

### 2.2.2  RNAi tools

Knockdown of Ankrd24 expression was achieved by RNAi technology, mediated via shRNA. Double stranded oligonucleotide was generated by primer annealing of the two synthesised single stranded oligonucleotides in a 50 µl reaction, supplemented with annealing buffer. The single stranded oligonucleotides were denatured at 90ºC for 4 min, followed by annealing at 70ºC for 10 min to a gradual temperature decrease of 0.3ºC/s to 4ºC. The generated double stranded oligonucleotide was collected by precipitating it in 200 µl isopropanol at RT for 15 min, followed by a centrifugation step at 20817 x g at RT for 3 min. The pellet was then washed with 400 µl 70% (v/v) ethanol and subsequently air dried. Latter was then resuspended in 20 µl 10 mM Tris/HCl (pH 8.0). Double stranded oligonucleotide was phosphorylated by adding 0.5 µl T4 polynucleotide kinase (10 U/µl) and the reaction mixture was supplemented with 5 µl 10x T4-ligase buffer and 24.5 µl ddH$_2$O, followed by incubation at 37°C for 30 min. T4 Polynucleotide kinase was inactivated at 65°C for 20 min. Ligation reaction mixture consisted of 2 µl endonucleases digested dephosphorylated vector, 13 µl of the phosphorylated double stranded oligonucleotide, 2 µl 10x T4 ligase buffer, 1 µl T4 ligase 10 U/ µl and 2 µl polyethylene glycol 4000. The ligation was performed at RT for 2 h before transformation.

### 2.2.3  Cell culture and transfection

### 2.2.3.1  Culture and transfection of HEK293 and HeLa cells

HEK293 and HeLa cells were cultured and passaged by Michaela Roeder and Kristin Gluth (BCI, UKJ). Cells were grown in 75 millimetre (mm) square flask with 80-90% confluency. The cells were washed with 4 ml HBSS, followed by detachment of cells with 1 ml trypsin-EDTA for 3 min at 37°C. The enzyme was inactivated by adding 9 ml of DMEM++ medium and the cells were further seeded to a cell density as per the requirement of the experiment. HEK293 and HeLa cells were grown on poly-D-lysine

coated coverslips (Ø =12 mm) in 24 and 6 well plates with 60-80% confluency, respectively. They were transfected with Turbofect™, following its manual and after 12 h, HeLa cells were fixed for microscopic analysis while HEK293 cells were harvested for lysate preparation.

### 2.2.3.2 Primary hippocampal rat neurons cultivation and transfection

Primary hippocampal rat neurons were isolated and cultured by Annett Kreusch and Kristin Gluth (BCI, UKJ). The procedure for isolation of neurons from embryonic rats (day 17.5 to 18.5) was as per Banker & Cowan (1977) and Brewer et al. (1993). 60000 neurons per well were seeded on poly-D-lysine coated coverslips (Ø =12 mm) in 24 well plates.

Cells were always handled under a laminar flow hood on a 37°C hot plate. At DIV4, primary rat hippocampal neurons were transfected with Lipofectamine® 2000, as per its user guidelines. Before transfection, the medium was changed to antibiotic free neurobasal medium. 50 ml of neurobasal medium consisted of 0.5 mM GlutaMAX™, 1 ml 1x B-27® serum-free supplement, 100 U/ml penicillin and 100 µg/ml streptomycin. The diluted DNA solution with Lipofectamine® 2000 was incubated at RT for 15 min, prior to adding it dropwise to the cells. After 4 h, the medium of the cells was changed back to neurobasal medium, and the cells were further cultured for 26 h (30 h from the start of transfection) and fixed at DIV4+2 (DIV6).

### 2.2.4 Preparation of lysates

### 2.2.4.1 HEK293 cell lysate preparation

Transfected cells were washed with 500 µl RT PBS, followed by scrapping of cells with 500 µl PBS at 4°C and centrifugation at 1000 x g at 4°C for 5 min. The cell pellet was then suspended and lysed in 265 µl of IP buffer, followed by incubation at 4°C for 20 min and a subsequent centrifugation step at 10000 x g at 4°C for 20 min. The supernatant containing soluble proteins was collected in a precooled Eppendorf tube for further experiments.

### 2.2.4.2 Rat brain tissue lysates

Isolated brain from a 21-week-old adult female rat was lysed in lysis buffer (containing PI) using ULTRA-TURRAX® homogenizer at 20000 rpm for 10 s twice. Lysis buffer was added in the ratio of 1:3 (w/v), depending on the weight of the tissue. To the completely homogenized tissue, 20% (v/v) Triton®X-100 was added to a final volume of 1% (v/v). Next, it was incubated at 4°C with constant rotation for 10 min, followed by centrifugation at 12000 x g for 15 min. The supernatant containing soluble proteins was then collected and subjected to endogenous coprecipitation assays after measuring the concentration of soluble proteins as per Bradford (1976).

### 2.2.5 Fixing and staining of cells

While maintaining HeLa cells and primary rat hippocampal neurons on the hot plate at 37°C, the medium was carefully removed, and the cells were fixed with 450 μl 4% (w/v) paraformaldehyde for 3 min. Later, paraformaldehyde was discarded, and the cells were quenched in 500 μl quench buffer at RT for 20 min, followed by storage in 1 ml PBS at 4°C until staining. For immunostaining, fixed cells were permeabilized at RT for 60 min with 450 μl blocking solution to which 20% (v/v) triton®X-100 was added to a final volume of 0.2% (v/v). Primary rat hippocampal neurons were incubated with 35 μl anti-MAP2 for 12 h in a wet chamber at 4°C. On the following day, the neuronal cells were washed 3x with blocking solution at RT for 5 min each and then the cells were incubated with 35 μl fluorescent-dye conjugated secondary antibody at RT for 60 min, preventing the cells from any light exposure. Both primary and secondary antibodies were diluted in blocking solution. Later, the cells were washed once with 200 μl blocking solution, followed by incubation with DAPI for staining DNA and a subsequent wash with PBS at RT for 15 min each. Coverslips were briefly dipped in $ddH_2O$ before mounting them onto slides with 7 μl Mowiol, avoiding air bubbles and subsequently air dried for 12 h at RT and later stored at 4°C. Neither primary nor secondary antibody were used with HeLa cells.

## 2.2.6   Neuromorphologic analysis

IMARIS software 8.4.0 was used to perform neuromorphologic analysis of the fixed and immunostained primary rat hippocampal neurons. The cells were first imaged using an oil objective lens of 40x/1.3 with the apotome feature on Axio Observer Z1. The filament feature of IMARIS software 8.4.0 was used to reconstruct the dendritic tree according to the anti-MAP2 immunostained neuron; the parameter settings of thinnest diameter of 2 µm gap length and a minimum segment length of 10 µm were kept. Data and parameters like the total number of points, total dendritic tree length, dendritic terminal and branch points, dendritic segments, Sholl analysis and dendritic branch depth (Fig. 1) for each cell were obtained from IMARIS software 8.4.0 in the excel sheet format. Total number of points is the sum of dendritic terminal and branch points, and the beginning point of the filament. The total dendritic tree length is the total length of the reconstructed filament. Soma center is the beginning point of the filament (Fig. 1) and Sholl analysis calculates the number of dendritic intersections (Sholl intersections) on a series of concentric spheres from the soma center (Fig. 1). IMARIS software 8.4.0 assigns every segment a dendritic branch depth, depending on the number of bifurcations from the soma center. As an example, a segment with dendritic branch depth '1' has only one bifurcation point i.e., the soma center which is a beginning point. However, a segment with dendritic branch depth '2' has two bifurcations from the soma center, a beginning point and a dendritic branch point (Fig. 1). In other words, dendritic segments with dendritic branch depth '1' are the primary dendrites whereas '2' are the secondary dendrites.
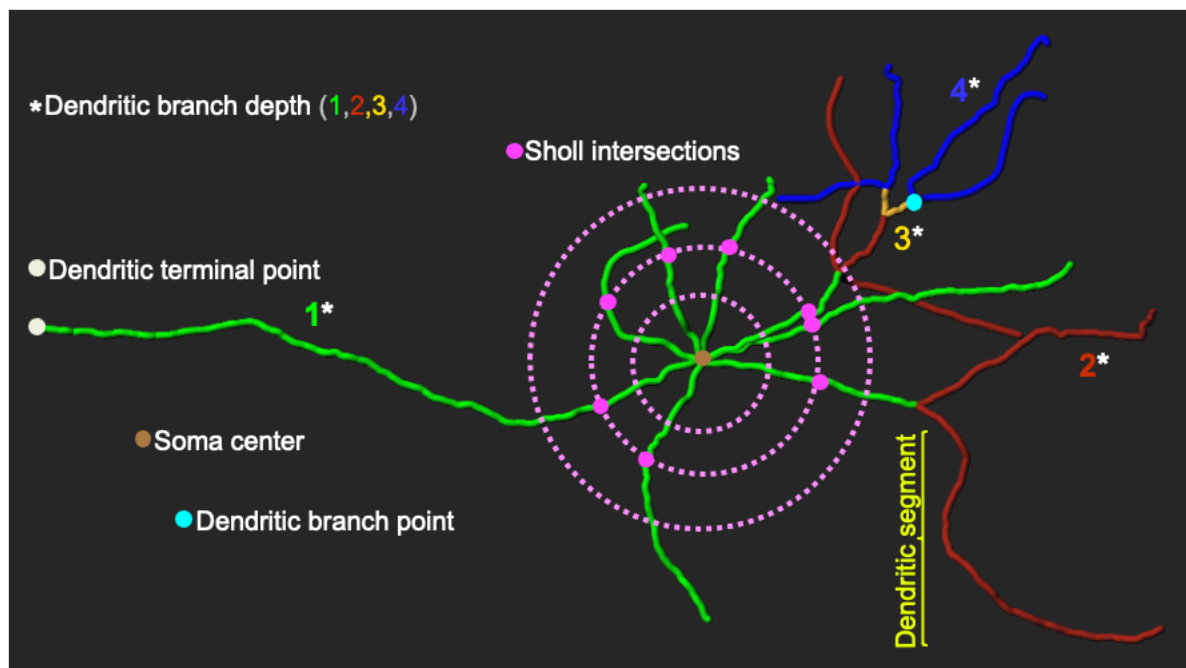
**Fig. 1. Parameters evaluated during neuromorphologic analysis of a reconstructed filament using IMARIS software 8.4.0.** A dendritic tree showing soma center, dendritic terminal and branch point, dendritic segment, Sholl intersections and dendritic branch depth.

### 2.2.7  SDS-PAGE

Samples were mixed with 4x SDS sample buffer and incubated at 100°C for 5 min for denaturing the proteins. The sample was then loaded on the polyacrylamide gels to separate the proteins according to their size. Unless otherwise mentioned, a stacking gel of 5% acrylamide and a separating gel of 9.5% acrylamide were used. The gels were casted by Birgit Schade and Michaela Roeder (BCI, UKJ) as per Wolf (2018). Proteins were separated on the gel by performing electrophoresis with a steady current strength of 8 milliampere per gel in a BIO-RAD Mini-Protein Tetra cell filled with 1x SDS running buffer. Depending on the experiment, the separated proteins were either visualized by Coomassie staining or detected by immunoblotting.

### 2.2.8    Coomassie staining

After separating the proteins by SDS-PAGE, polyacrylamide gels were incubated with colloidal Coomassie staining solution at RT for 12 h with steady shaking for staining the proteins. Protein unbound colloidal Coomassie was removed by washing with ddH$_2$O and

then the stained proteins were visualised at a wavelength of 700 nm, using the Odyssey® imager LI-COR Biosciences GmbH.

### 2.2.9  Immunoblotting

After SDS-PAGE, WB was performed to transfer the proteins from the polyacrylamide gel to a polyvinylidene fluoride (PVDF) membrane using tank blot transfer at 100 V and 3 ampere for 1 h. Next, the PVDF membrane was incubated in 5% (w/v) milk powder in PBS at RT for 1 h, followed by 3x 10 min wash by PBS-T and incubation with primary antibody at 4°C for 12 h. The following day, the blot was washed thrice with 5% (w/v) milk powder in PBS-T for 10 min each and later incubated with fluorescent-dye conjugated secondary antibody (protected from light) diluted in 5% (w/v) milk powder in PBS-T at RT and 10 rpm for 1 h. The membrane was then washed with PBS-T and PBS for 10 min each, before detecting the protein bands at Odyssey® imager LI-COR Biosciences GmbH. Depending on the experiment, the intensity of the protein band was determined using Image Studio Lite System 5.2.

### 2.2.10 Expression and purification of GST-fusion proteins

The selected plasmid was transformed in *E.coli* BL21-CodonPlus® (DE3)-RIPL, followed by inoculating single colony in 100 ml (preculture) and incubating it at 37°C and 200 rpm for 12 h. Following day, the preculture was expanded to 1000 ml TB medium containing the appropriate antibiotics to reach an optical density (OD) 600 of 0.6-0.8 from 0.1 maintaining the temperature of 37°C and 200 rpm. Next, 5.5 ml of 0.1 M isopropyl-ß-D-thiogalactopyranoside was added to the precooled cultures for inducing protein expression at 18°C and 200 rpm for 12 h. The following day, the culture was subjected to a centrifugation step at 4500 x g at 4°C for 15 min to collect the cells, followed by resuspension of the cell pellet in 25 ml PBS containing PI and freezing it in liquid nitrogen. Thereafter, the cells were thawed, and cold PBS-PI was added to a final volume of 37 ml, followed by addition of 100 mg DNase I and lysozyme. The cells were then lysed thrice by sonication for 10 s each and subsequently 2.5 ml 20% (w/v) Triton®X-100, 0.5 ml 1 M MgCl₂ and 50 µl 1M dithiothreitol was added, followed by 30 min incubation at 4°C on a rotor. Centrifugation at 1000 x g at 4°C for 10 min was

carried out to extract the soluble proteins in the supernatant, which was incubated with the PBS-washed 1.5 ml glutathione resin for 45 min, followed by 45 ml PBS wash of 10 min for three times. GST-tagged proteins were eluted through a gravity flow column in 500 μl GST elution buffer in 5 fractions. The protein concentration was measured according to Bradford (1976) and the fractions containing maximum concentration of proteins were pooled together and dialysed against 2 l PBS at 4°C for 2 h.

### 2.2.11 Removal of GST tag

1 mg purified GST-fusion protein and 7 U PreScission™ protease were dialysed against 500 ml HN buffer at 4°C for 12 h. The following day, the dialysed protein in HN buffer was incubated with prewashed 1.5 ml glutathione resin at 4°C for 90 min with constant rotation and the cleaved protein was collected as a flow through sample by centrifugation at 500 x g at 4°C for 5 min in a swing out rotor. An HN buffer prewashed spin column was used.

The success of protein purification, dialysis and GST-tag removal was confirmed by performing SDS-PAGE with analytical samples from each step and visualizing the separated proteins on polyacrylamide gel by staining the proteins with Colloidal Coomassie staining solution.

### 2.2.12  Subcellular Fractionation

Co-transfected HEK293 cells were washed with 500 μl PBS, followed by collection of the cells in 500 μl PBS at 4°C. The cell pellet was collected after a centrifugation step at 500 x g at 4°C for 5 min in the swing out rotor. The cell pellet was resuspended and lysed in 200 μl homogenization buffer using syringe needle Ø = 0.12 mm. 25 μl of the 200 μl was collected as the input (or 'start') and the rest of the sample was subjected to a centrifugation step at 4°C at 1000 x g for 10 min. 25 μl of the supernatant (S) was collected as S1 and the rest of the supernatant was transferred to a new Eppendorf tube, while the pellet (P) was resuspended in 175 μl homogenization buffer and 25 μl of this was removed as P1, discarding the rest. The supernatant which was collected in the new Eppendorf tube was then centrifuged at 4°C, 11700 x g for 20 min. 25 μl of the

supernatant was collected as S2 fraction, while the rest of the supernatant was discarded. The pellet was resuspended in 150 µl homogenization buffer and centrifuged again at 4°C, 11700 x g for 20 min after removing 25 µl as the P2 sample. After the centrifugation step, 25 µl of the supernatant was withdrawn as S2', while discarding the rest of the supernatant. The pellet was resuspended in 125 µl homogenization buffer, out of which 25 µl was removed as P2' and the rest was discarded. All the samples withdrawn were mixed with 8.5 µl 4x SDS sample buffer, followed by protein denaturation at 100°C for 5 min before performing SDS-PAGE and immunoblot analysis.

### 2.2.13 Crosslinking assay by EDC

EDC with concentrations of 4 mM, 10 mM, 30 mM, and 50 mM was added to already prepared HEK293 cell lysates at RT for 20 min, followed by mixing the samples with 4x SDS sample buffer and denaturation of the proteins at 100°C for 5 min before performing SDS-PAGE and immunoblot analysis. Control sample was without EDC.

### 2.2.14 *In vitro* reconstitutions assays with lysates from HEK293 cells and rat brain tissue

Matrix was prepared by washing 1.5 ml glutathione resin twice with 45 ml PBS and centrifugation at 10000 x g, 4°C for 1 min each, followed by incubation of the matrix with 30 µg GST or GST-fusion proteins at 4°C for 1 h with constant rotation. 240 µl prepared HEK293 cell lysates overexpressing GFP, or GFP-fusion proteins were added to the prepared matrix. The matrix was then washed twice with 1 ml PBS and once with IP buffer (without PI), respectively. To this prepared matrix, lysate was added and incubated at 4°C for 2 h with constant rotation, followed by centrifugation at 11000 x g, 4°C for 1 min. 100 µl of the supernatant was collected, discarding the rest. Next, the matrix was washed thrice with 1 ml IP Buffer (without PI) and centrifuged at 11000 x g, 4°C for 1 min to spin down the matrix. Next, 30 µl 4 M Urea was added to the matrix to elute the proteins bound to it. Both samples supernatant and eluates were then mixed with 4x SDS sample buffer, followed by incubation at 100°C for 5 min and analysed by SDS-PAGE and immunoblotting.

When rat brain tissue lysate was used instead of HEK293 cells to check the interaction of a specific protein with immobilized GST (as a control) or GST-tagged fusion proteins, the proteins bound to the matrix were eluted in 30 µl GST elution buffer after 30 min incubation at RT, followed by centrifugation at 16000 x g for 5 min to collect the eluate. Rest of the procedure remained the same.

### 2.2.15  Liposome preparation

The procedure of liposome preparation was adapted from Reeves & Dowben (1969). A Fernbach flask and the glass tube were thoroughly dried prior to use. In a glass tube, 350 µl chloroform and 10 µl methanol were mixed, followed by addition of 80 µl thawed 50 µg/µl Folch fraction I lipids at RT. The solution was spread in a thin layer in Fernbach flask and a steady stream of nitrogen gas was maintained for 1 h to dry the lipid layer. The drying was continued further for 60 min in a desiccator. Lipids were then rehydrated under the steady stream of water saturated nitrogen gas for 30 min and incubated at 42°C in 30 ml 0.3 M sucrose in ddH$_2$O for 12 h. Liposomes were collected by centrifugation with Optima™ L70 ultracentrifuge using swing out rotor (SW 28) at 20000 x g at 28°C for 1 h and the pellet was resuspended in 500 µl 0.3 M sucrose in ddH$_2$O to achieve the final lipid concentration of 8 mg/ml. The liposomes were stored at 4°C and were used within 5 days. Large unilamellar vesicles (LUVs) created by this method had an average diameter of 300-500 nm (Wolf et al., 2019).

Small unilamellar vesicles (SUVs) were obtained after sonification of the LUVs with an UP50H ultrasonicator. LUVs were sonicated thrice for 50 s each with an interval of 1 min in between to avoid any heat-induced degradation. For the latter reason, the liposomes were maintained on ice throughout the procedure. SUVs created by this method had an average diameter of 30-50 nm (Wolf et al., 2019).

### 2.2.16 *In vitro* reconstitutions assays with liposomes

Liposome pelleting assays were performed with LUVs. A pre-spin at 200000 x g, 28°C for 5 min was performed with protein in HN buffer at 0.2 µg/µl to remove aggregation due to protein's self-precipitation. The supernatant was then incubated with the

liposomes at RT for 30 min in a 50 µl reaction containing 4 µM protein, 50 µg liposomes in HN buffer, followed by centrifugation at 200000 x g, 28°C for 20 min. Thereafter, 50 µl supernatant was mixed with 17 µl 4x SDS sample buffer and the pellet was resuspended in 67 µl 1x SDS sample buffer. The samples were then incubated at 100°C for 5 min and analysed by SDS-PAGE and Coomassie staining. Odyssey® imager LI-COR Biosciences GmbH was used to visualise the bands obtained in supernatant and pellet samples, and later the intensity was determined using Image Studio Lite System 5.2.

Liposome sensing assays were performed with both LUVs and SUVs and the above procedure was followed except that instead of 50 µl supernatant, 35 µl was collected. The collecting volume of the supernatant was modified as SUVs being smaller in diameter than LUVs have lower sedimentation efficiency and thus result in lose pellets (Wolf et al., 2019). 12 µl 4x SDS sample buffer was added to 35 µl supernatant and to have a direct volume comparison, the pellet was resuspended in 32 µl 2x SDS sample buffer.

Salt-extraction assays were carried out with LUVs. The procedure remained same as liposome pelleting assay except that the final concentration of NaCl was increased from 150 mM (HN buffer) to 200 and 250 mM, respectively, 5 min prior to centrifugation at 200000 x g, 28°C for 20 min.

## 2.2.17 Freeze-fracture of liposomes for size analysis

Since a concentrated pellet was needed for electron microscopy sample preparation, a 100 µl reaction comprising of 6 µM protein and 100 µg LUVs was incubated at 37°C for 15 min at 800 rpm, followed by removal of unbound protein with 30 µg proteinase K at 45°C for 25 min. Next, liposome pellet was collected by centrifugation at 200000 x g, 28°C for 15 min and subsequently, the pellet was resuspended in 20 µl of the supernatant and this solution was subjected to freeze-fracturing.

0.6 mm high copper profiles were cleaned in a sonicating bath with 4% (w/v) tartaric acid and thereafter, washed in pure acetone before storing in pure methanol at 4°C. A sandwich of two copper profiles with 4 µl liposome solution in between was immediately frozen by plunging it liquid propane ethane (1:1) and then cooled in liquid nitrogen. Dr. Eric Seemann performed the freeze-fracture of prepared liposome samples using Freeze-Etching Device BAF400T machine (Schneider et al., 2014). For analysis, a TEM EM902A at 80 keV and a 1 k FastScan CCD camera and EM-Menu 4 software was used to image, followed by ImageJ/FIJI 1.46r to determine the diameter of the liposomes and excel to further process the data.

## 2.2.18 Statistical analysis and reproducibility

GraphPad Prism 5.03 was used to determine the statistical significance and for determining the distribution of data, Shapiro-Wilk-Test was carried out. For data distributed normally, involving comparison between two conditions, Student's t-test was performed and for minimum three conditions, One-Way analysis of variance (ANOVA) with a subsequent Tukey's multiple comparisons test was performed. For a data distributed non-normally, a Mann-Whitney U test for two conditions and a Kruskal-Wallis test for a minimum of three conditions with a subsequent Dunn's multiple comparison test was conducted, respectively. Two-Way ANOVA was conducted with a subsequent Bonferroni's multiple comparison test for a two-factor analysis.

For *In vitro* reconstitutions assays with liposomes, the results were summarised by examining minimum two independent liposome preparation with two to three technical replicates. For freeze-fracture studies, 500-700 liposomes were analysed for each condition per assay and the analysis was blinded, using Ant Renamer software.

For neuromorphologic analysis, at least 2 independent biological assays with 12-24 cells per condition were used.

# 3 Results

## 3.1 Ankrd24x6 is membrane-associated

Ankrd24 (UniProtKB-Q80VM7) is one of the uncharacterised proteins, belonging to the smaller sub-family of the N-Ank superfamily of membrane shapers (Wolf et al., 2019). Interestingly, 'the human protein atlas' suggested that the messenger RNA (mRNA) expression of Ankrd24 is high in human and mouse brain (Uhlén et al., 2015) and Wolf (2018) was indeed able to obtain partial sequences of *Mus musculus* Ankrd24 isoforms (XM_006514101.3 and XM_006514102.3) from the cDNA of 8-week-old mice brain. These preliminary experiments from Dr. David Wolf suggested that the mRNA of Ankrd24 was expressed in 8-week-old brain mice. But since this project aimed to characterise and obtain full-length Ankrd24 (UniProtKB - Q80VM7; "UniProt: the universal protein knowledgebase", 2016), PCRs were performed using cDNA of 8-week-old mice brain as a template. The sequencing of the PCR products (Fig. 2A) confirmed that the mRNA of the predicted Ankrd24 isoform 6 (XM_006514096.5) is expressed in 8-week-old mice brain.

Next, *in silico* analysis of the secondary structure of Ankrd24x6 was initiated by the protein structure prediction server, (PS)2-v2 as it can efficiently and effectively predict the structure of a given template. (PS)2-v2 can predict and model structure of a protein by essentially integrating Position-Specific Iterative Basic Local Alignment Search Tool (PSI-BLAST) generated position-specific sequence profile from the database and secondary structure propensities of 20 amino acids by using 60 X 60 substitution matrix called S2A2 (Chen et al., 2009). Marcoil is an *in silico* tool which is used for predicting continuous heptad repeats in a protein sequence by securing the probabilities of an amino acid sequence forming heptad by employing algorithm based on reference databases, hidden Markov model and position specific scoring matrix (Delorenzi & Speed, 2002). It was reported to be the best performer for predicting coiled coil domains by being faster and more sensitive than other available tools such as PCOILS (Gruber et al., 2006; Lupas et al., 2017). Therefore, (PS)2-v2 along with Marcoil was used for *in silico* analysis of the secondary structure of Ankrd24x6, furthermore HELIQUEST (Gautier et al., 2008) was used to predict the type of helix. HELIQUEST uses an

algorithm based on the physicochemical behaviour of known helices to predict helices in a given peptide sequence. Altogether, the analysis of the secondary structure of Ankrd24x6[1-285] (Fig. 2B) from the *in silico* tools predicted amphipathic α helix (Fig. 2C) at the N-terminus with amino acid sequence MKTLRARFKKT, followed by 7 ankyrin repeats from amino acid 21-277 (Fig. 2D), thus forming the N-Ank module of Ankrd24x6. Marcoil predicted two putative coiled coil domains in Ankrd24x6[1-1041], from amino acids 289-490 and 746 to 1009, respectively (Fig. 2E). The primary amino acid sequence of Ankrd24x6 also indicated the presence of a proline-rich sequence KKRKAPQPP from amino acid 274-282 (Fig. 2E), which overlapped with the amino acid sequence predicted to form ankyrin repeats.
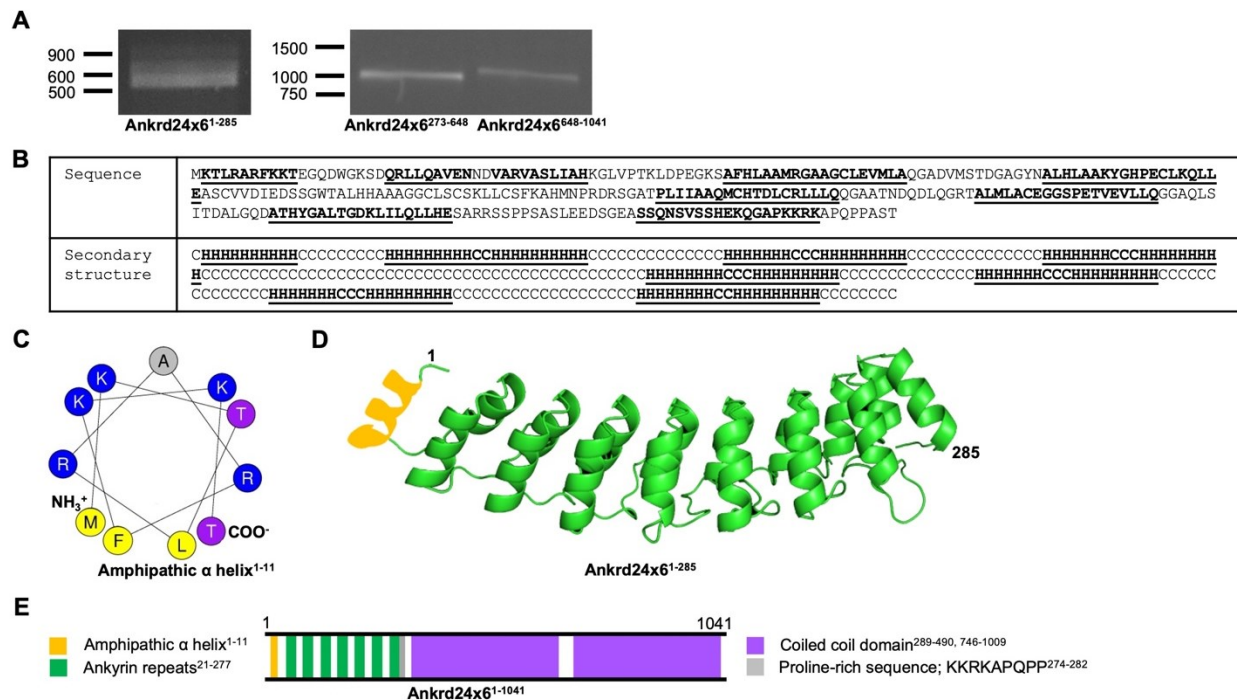


**Fig. 2. Detection of Ankrd24x6 PCR products by agarose gel electrophoresis (A) and Ankrd24x6 secondary structure and domain predictions (B-E).** PCR products for Ankrd24x6[1-285] (855 bp), Ankrd24x6[273-648] (1128 bp), Ankrd24x6[648-1041] (1182 bp) were detected by agarose gel electrophoresis; superscript number indicates the amino acid number of Ankrd24x6 (A), primary amino acid sequence of the N-Ank module of Ankrd24x6, Ankrd24x6[1-285] and its respective secondary structure prediction by (PS)2-v2 (Chen et al., 2009), where H represents α helix (B), helical wheel representation of the putative amphipathic α helix containing hydrophobic and a hydrophilic side; colour coding for amino acids is as follows: yellow, hydrophobic; blue, positively charged; purple, polar uncharged; grey, non-polar; based on the *in silico* tool HeliQuest (Gautier et al., 2008) (C), predicted secondary structure of the putative helices in Ankrd24x6[1-285] by (PS)2-v2 (Chen et al., 2009) (D), schematic representation of the domains and motif in Ankrd24x6 by combining information from the *in silico* tools; (PS)2-

v2 (Chen et al., 2009), HeliQuest (Gautier et al., 2008) and Marcoil (Delorenzi & Speed, 2002) with standard settings, respectively (E).

It was intriguing that Ankrd24x6 was obtained from the primers designed to achieve full-length *Mus musculus* Ankrd24 (UniProtKB-Q80VM7, NCBI Reference Sequence NM_027480.3, NCBI *Mus musculus* gene ID 70615). This observation led to the next step of studying NCBI database of RNA transcriptomics studies in *Mus musculus* on Ankrd24, according to which, 26 isoforms of Ankrd24 were predicted (Fig. 3). The analysis revealed that the majority of the isoforms including Ankrd24x6 (XM_006514096.5) were at initial automatic processing of the NCBI curation of eukaryotic transcript and protein sequences. Except for Ankrd24 isoforms (NM_027480.3 and NM_001374016.1), others were predicted sequences of the isoforms and were the result of the eukaryotic genome annotation pipeline (Pruitt et al., 2002 updated: April 6, 2012). Deeper understanding of the isoforms came by compiling the exon information of different isoforms of Ankrd24 (*Mus musculus* strain C57BL/6J chromosome 10, GRCm39, NCBI Reference Sequence: NC_000076.7; Church et al., 2009, 2011). Ankrd24x3 (XM_006514093.5) was used as a reference to align all other isoforms as it contained all the 23 predicted exons. The first three exons of Ankrd24x3 were also present in Ankrd24x23 (XM_030245274.2), Ankrd24x6, x8 (XM_006514098.5) and x12 (XM_006514102.5). The first 11 amino acids translated from the mRNA transcript of Ankrd24x3 (like x6, x8, x12) and Ankrd24x23 were MKTLRARFKKT and MPKNQSPSAEE, respectively due to alternative transcription and translation start sites. The mRNA transcript of Ankrd24_2 (UniProtKB-Q80VM7, NCBI Reference Sequence NM_027480.3) has an alternative transcription start site and same translation start site as that of Ankrd24x3 and Ankrd24x6 (MKTLRARFKKT). The presence of exon 20 (Ankrd24x3 as a reference) in Ankrd24x6 in the coding sequence explained the additional translated amino acid sequence at the C-terminus, compared to Ankrd24_2 (*see* Appendix 7.1, Fig. 21). Thus, this overview of the exons information in the isoforms of *Ankrd24* in *Mus musculus* indicated that exon 3 (Ankrd24x3 as a reference) has the translation start site for MKTLRARFKKT.

**Fig. 3. Overview of the 26 isoforms of *Ankrd24* with their respective exons in *Mus musculus* according to the NCBI database; gene ID 70615; NCBI Reference Sequence as of 19 May 2021 (*See* Appendix 7.1 for gene locus positions and range of exons of all the isoforms).**

Next, the hypothesis of whether Ankrd24x6 is a membrane-associated protein was investigated by analysing HeLa cells expressing both membrane marker mcherryF and different GFP-fusion proteins of Ankrd24x6. Both full-length Ankrd24x6$^{1-1041}$-GFP (Fig. 4A) and N-terminus amphipathic helix with ankyrin repeats (N-Ank module), Ankrd24x6$^{1-285}$-GFP (Fig. 4B), were colocalised with mcherryF in the filopodia-like membrane structures whereas GFP was expressed ubiquitously in the cell (Fig. 4C).
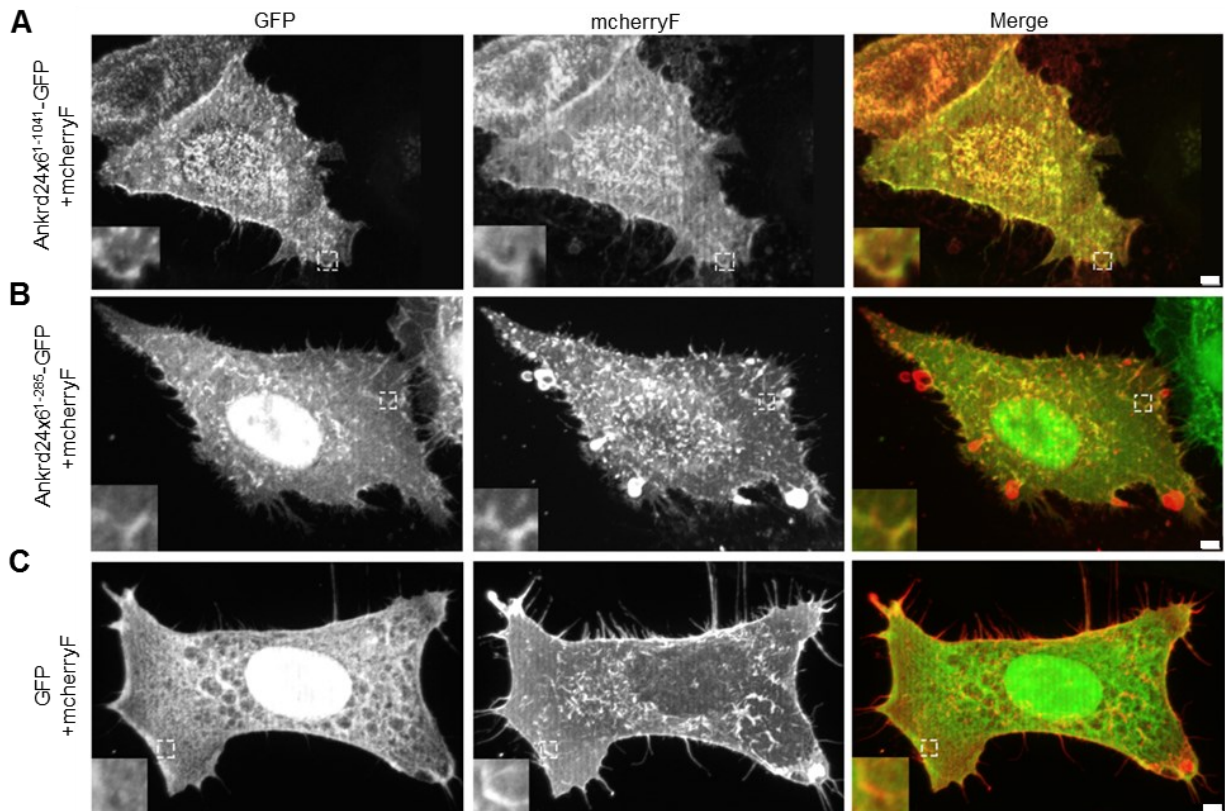


**Fig. 4**. **Colocalisation of Ankrd24x6$^{1-1041}$-GFP and Ankrd24x6$^{1-285}$-GFP with the membrane marker mcherryF at filopodia-like membrane structures in HeLa cells.** Representative maximum intensity projections of mcherryF and Ankrd24x6$^{1-1041}$-GFP (A), Ankrd24x6$^{1-285}$-GFP (B) or GFP (C) in cotransfected HeLa cells for 24 h; mcherryF is depicted in red and GFP-fusion proteins are depicted green in merge. Results showed colocalisation of Ankrd24x6$^{1-1041}$-GFP and Ankrd24x6$^{1-285}$-GFP with mcherryF in filopodia-like membrane structures, additionally shown in enlarged boxes, unlike GFP where no such membrane structure was observed. Scale bars 5 µm.

Furthermore, subcellular fractionation was performed after cotransfecting HEK293 cells with Ankrd24x6 GFP-fusion proteins and mcherryF, and fractions were additionally checked for laminB1, a nuclear membrane protein marker. As a control, cells were

transfected with GFP and mcherryF. The representative immunoblots clearly demonstrated the membrane-association of Ankrd24x6 as the subcellular fractions of the full-length Ankrd24x6$^{1-1041}$-GFP (Fig. 5A) were detected in membrane fractions (P2 and P2') along with mcherryF. Additionally, the subcellular fractions of the N-Ank module Ankrd24x6$^{1-285}$-GFP (Fig. 5B) were also observed in membrane fractions (P2 and P2') along with mcherryF but in much lower amounts compared to its cytoplasmic (S1, S2) and nuclear membrane fraction (P1), thus indicating a weaker membrane-association of the N-Ank module of Ankrd24x6 compared to its full-length. Unlike mcherryF, GFP (Fig. 5C) was detected only in S1 and S2 fractions. Taken together, the results from the immunofluorescence studies in HeLa cells (Fig. 4) and subcellular fractionation of HEK293 cells (Fig. 5) confirmed that Ankrd24x6 is indeed a membrane-associated protein.
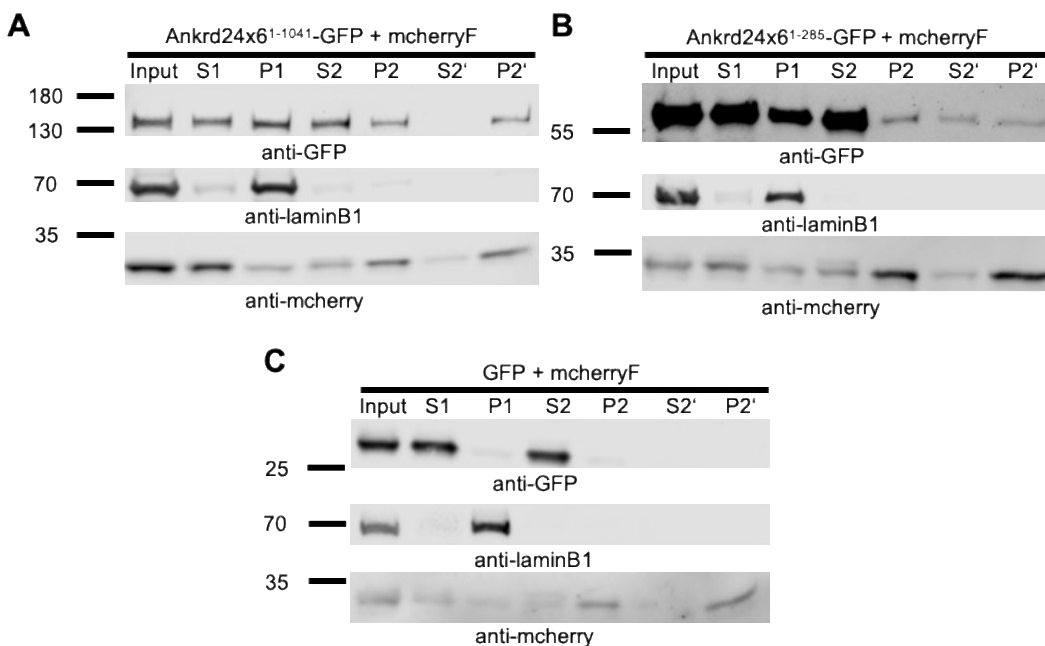


**Fig. 5**. **Cofractionation of Ankrd24x6$^{1-1041}$-GFP and Ankrd24x6$^{1-285}$-GFP with the membrane marker mcherryF in membrane fractions (P2, P2') of HEK293 cells.** Immunoblot analysis of subcellular fractionations (P1, nuclear fraction, P2 and P2', membrane fractions) of HEK293 cells cotransfected for 24 h with mcherryF and full-length Ankrd24x6$^{1-1041}$-GFP (A), N-Ank Ankrd24x6$^{1-285}$-GFP (B) or GFP (C). The results showed coappearance of Ankrd24x6$^{1-1041}$-GFP and Ankrd24x6$^{1-285}$-GFP with the membrane marker mcherryF in the membrane fractions (P2, P2'), unlike GFP. LaminB1 was used as a protein marker for nuclear membrane. Immunoblots represent results from three biological replicates.

## 3.2 The N-Ank module of Ankrd24x6 partially binds to the liposomes via its putative amphipathic $\alpha$ helix

Next, liposome pelleting assays were carried out with purified untagged wildtype and mutant proteins to investigate a putative direct binding of the N-Ank module of Ankrd24x6 to the membrane lipids. It has been reported that ankyrin repeats fold together in a cooperative manner and this coordination tends to decrease as the number of ankyrin repeats increases (Barrick, 2009). Studies also suggest that the increase in number of ankyrin repeats makes the membrane structure more compact and concave (Islam et al., 2018; Li et al., 2006; Sedgwick & Smerdon, 1999) and that the folding of ankyrin repeats is induced at the terminal repeats (Ferreiro et al., 2005). Therefore, to check the influence of the binding ability of fewer and terminal ankyrin repeats to the membrane lipids, two N-Ank wildtype modules were constructed; both consisted of the putative amphipathic $\alpha$ helix but one comprised of all the seven predicted ankyrin repeats (Ankrd24x6$^{1-285}$) and the other comprised of the first five ankyrin repeats, thus lacking the last two terminal repeats (Ankrd24x6$^{1-222}$). Mutants lacking the amphipathic $\alpha$ helix were created to check whether Ankrd24x6 binds to the membrane via amphipathic $\alpha$ helix and if ankyrin repeats alone had affinity to the liposomes.

The quantitative analysis of Coomassie-stained SDS-gels of liposome pelleting assays revealed that the N-Ank module Ankrd24x6$^{1-285}$ (Fig. 6A) partially bound to liposomes as the proteins were found both in the supernatants and the liposome-rich pellets unlike the mutant lacking the putative amphipathic helix, Ankrd24x6$^{10-285}$ (Fig. 6B) which was almost exclusively detected in supernatant fractions. The N-Ank module Ankrd24x6$^{1-285}$ showed ~ 40% binding to liposomes, which was significantly reduced with the mutant, Ankrd24x6$^{10-285}$ (Fig. 6C). Similar behaviour of partial binding to liposomes was also observed with Ankrd24x6$^{1-222}$ (Fig. 6D), which had only the first five ankyrin repeats and its liposome binding ability was also significantly lost from ~40% to none with the mutant lacking the putative amphipathic helix, Ankrd24x6$^{10-222}$ (Fig. 6E-F).

Thus, the liposome pelleting assay confirmed that the putative amphipathic helix is essential for liposome binding of the N-Ank module of Ankrd24x6 and that the mutants

containing only ankyrin repeats (Ankrd24x6$^{10-285}$, Ankrd24x6$^{10-222}$) did not bind to liposomes unlike other members of the N-Ank superfamily, ankycorbin and UACA (Wolf et al., 2019). The assay also indicated that Ankrd24x6$^{1-222}$ which lacked the last two terminal repeats showed similar liposome binding ability as Ankrd24x6$^{1-285}$ with all seven predicted ankyrin repeats.
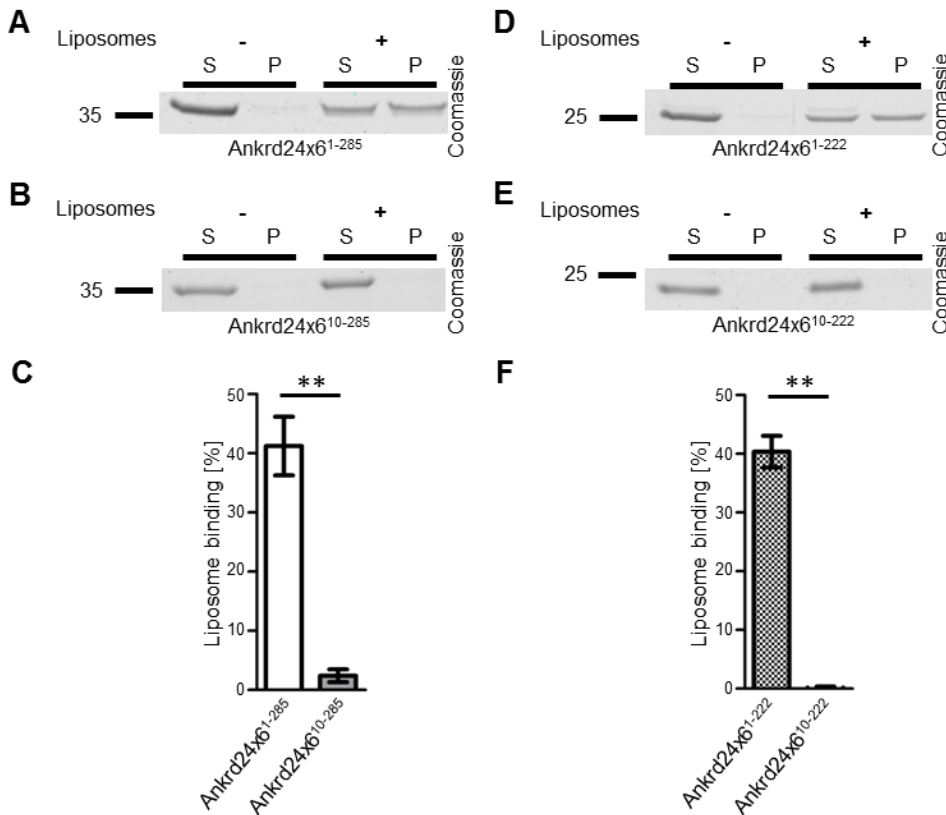


**Fig. 6**. **The N-Ank module of Ankrd24x6 partially bound to liposomes via the putative $\alpha$ amphipathic helix.** Liposome pelleting assays were performed with wildtype and mutant proteins. Coomassie-stained SDS-gels of supernatant (S) and pellet (P) fractions of incubations with (+) or without liposomes (-) Ankrd24x6$^{1-285}$ (A) and Ankrd24x6$^{10-285}$ (B), bar plot representation of quantitative analysis between Ankrd24x6$^{1-285}$ and Ankrd24x6$^{10-285}$ (C), Coomassie-stained SDS-gels of supernatant (S) and pellet (P) fractions of incubations with (+) or without liposomes (-) Ankrd24x6$^{1-222}$ (D) and Ankrd24x6$^{10-222}$ (E), bar plot representation of quantitative analysis between Ankrd24x6$^{1-222}$ and Ankrd24x6$^{10-222}$ (F). The experiment showed that the in the presence of liposomes, wildtype proteins (A, D) were found both in supernatant and pellet whereas mutant proteins were depleted in pellet fractions (B, E). Binding of protein to liposomes was quantified as liposome binding [%]=[((P/(S+P))$_{Sample}$ - (P/(S+P))$_{HN\ buffer\ control}$)x 100], where the sample included the protein and liposomes, while the HN buffer control comprised only of protein. Quantitative analyses included results from two independent liposome preparations with three technical replicates making the sample size (n) = 6 (2*3). Data represent mean ± standard error of means (sem). Unpaired t-test. **p<0.01* (C,F).

## 3.3 The N-Ank module of Ankrd24x6 binds to liposomes, irrespective of their curvature

Since the N-Ank module of Ankrd24x6 showed partial binding to liposomes (Fig. 6) in liposome pelleting assays, which used liposomes with rather lower curvature (LUVs), an investigation regarding a potential preference towards higher membrane curvature was carried out by subjecting wildtype N-Ank modules or their respective mutants to simultaneous incubation with either LUVs or SUVs (higher curvature). The quantitative analysis of Coomassie-stained SDS-gels of liposome sensing assay revealed that Ankrd24x6$^{1-285}$ (Fig. 7A-B) and Ankrd24x6$^{1-222}$ (Fig. 7C-D) bound to LUVs and SUVs similarly with no significant difference.
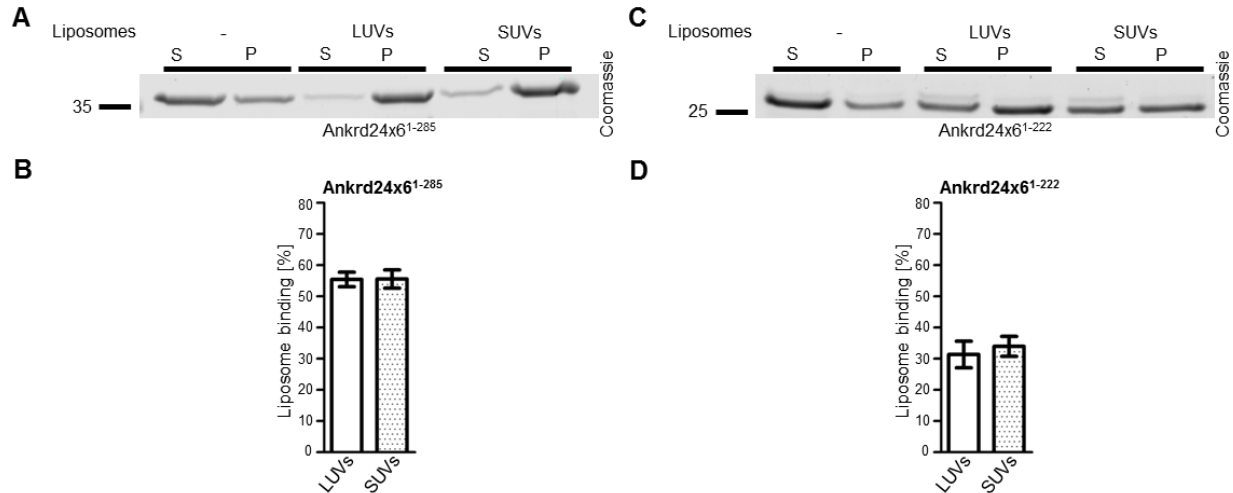


**Fig. 7. The N-Ank modules of Ankrd24x6 were insensitive to different curvatures of the liposome.** Liposome sensing assays were performed with wildtype proteins using LUVs and SUVs, respectively. SUVs were prepared by sonication of liposomes. Coomassie-stained SDS-gels of supernatant (S) and pellet (P) fractions of incubations with liposomes (LUVs, SUVs) or without (-) Ankrd24x6$^{1-285}$ (A) and the bar blot representation of the quantitative analysis of Ankrd24x6$^{1-285}$ protein incubation with LUVs and SUVs (B), Coomassie-stained SDS-gels of supernatant (S) and pellet (P) fractions of incubations with liposomes (LUVs, SUVs) or without (-) Ankrd24x6$^{1-222}$ (C) and the bar blot representation of the quantitative analysis of Ankrd24x6$^{1-222}$ protein incubation with LUVs and SUVs (D). In the presence of LUVs and SUVs, wildtype proteins bound similarly to both (A-D). Binding of protein to liposomes was quantified as liposome binding $[\%]=[((P/(S+P))_{Sample} - (P/(S+P))_{HN\ buffer\ control})x\ 100]$, where the sample included the protein and liposomes, and the HN buffer control comprised only of protein. Quantitative analyses included two independent liposome preparations with three technical replicates: n = 6 (2*3). Data represent mean ± sem. Unpaired t-test (B,D).

However, with the mutants lacking the amphipathic helix, Ankrd24x6$^{10-285}$ (Fig. 8A-B) and Ankrd24x6$^{10-222}$ (Fig. 8C-D), the analysis did not show any binding to either LUVs or SUVs, hence, demonstrating their lack of ability to bind to liposomes irrespective of their curvature and highlighting once again that the amphipathic $\alpha$ helix is crucial for membrane-binding.
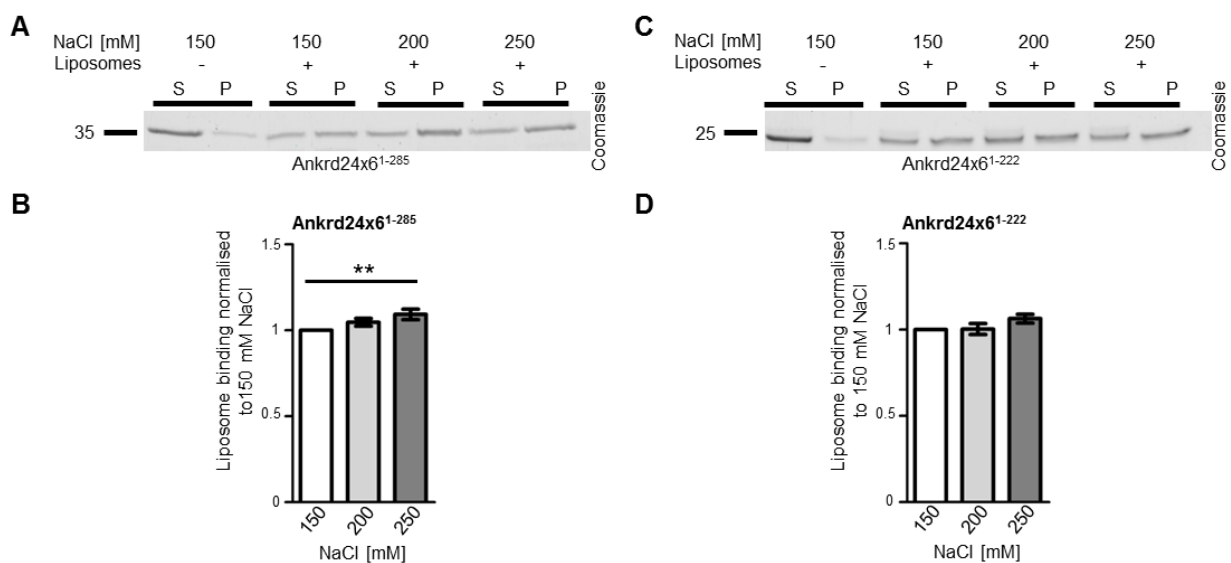
In summary, the N-Ank modules of Ankrd24x6, Ankrd24x6$^{1-285}$ and Ankrd24x6$^{1-222}$ bound equally to LUVs and SUVs, respectively. The mutants containing only the ankyrin repeats bound neither to LUVs nor SUVs, therefore, indicating the lack of binding to the membrane lipids.
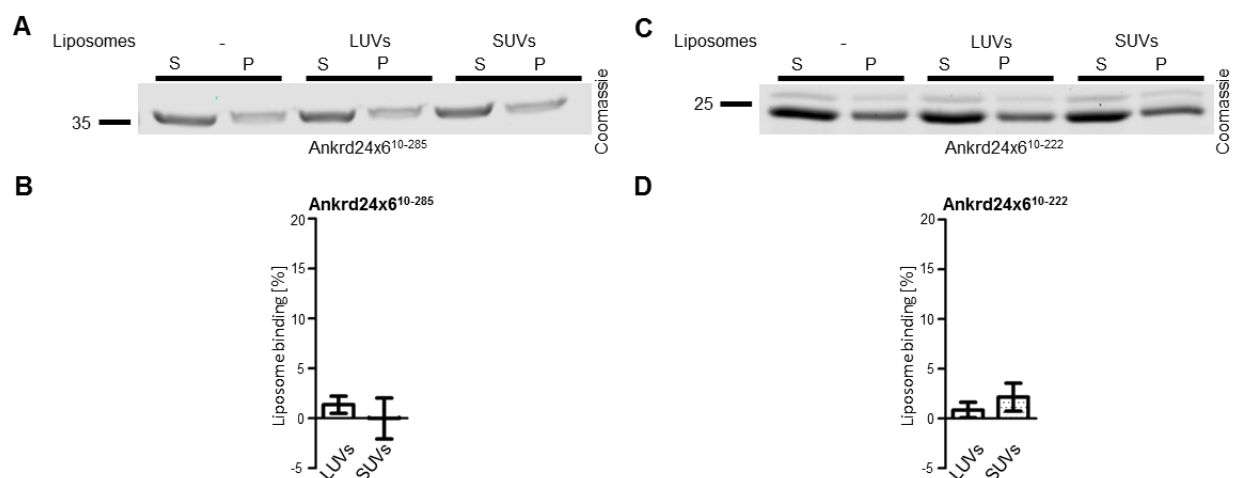


**Fig. 8. Mutants of the N-Ank module lacking the putative amphipathic $\alpha$ helix bound neither to LUVs nor SUVs.** Liposome sensing assays were performed with the mutant proteins using LUVs and SUVs and latter were prepared by liposome sonication. Coomassie-stained SDS-gels of supernatant (S) and pellet (P) fractions of incubations with liposomes (LUVs, SUVs) or without (-) Ankrd24x6$^{10-285}$ (A) and its bar blot representation of quantitative analysis of liposome binding ability to LUVs and SUVs, respectively (B), Coomassie-stained SDS-gels of supernatant (S) and pellet (P) fractions of incubations with liposomes (LUVs, SUVs) or without (-) Ankrd24x6$^{10-222}$ (C) and its bar blot representation of quantitative analysis of liposome binding ability to LUVs and SUVs, respectively (D). In the presence of LUVs and SUVs, mutant proteins were found predominantly in the supernatant than pellet (A,C), which showed their lack of binding or affinity to liposomes, irrespective of their curvature. Binding of protein to liposomes was quantified as liposome binding $[\%]=[((P/(S+P))_{Sample} - (P/(S+P))_{HN\ buffer\ control}) \times 100]$, where the sample included the protein and liposomes, and the HN buffer control comprised only of protein. Quantitative analyses included two independent liposome preparations with three technical replicates, n=6 (2*3). Data represent mean ± sem. Unpaired t-test (B,D).

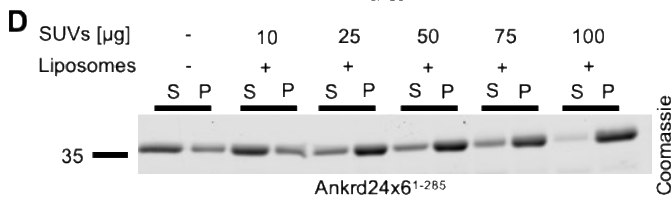## 3.4 The N-Ank module of Ankrd24x6 bound to liposomes in a salt-resistant fashion

Since the results so far showed that the putative amphipathic α helix is necessary for liposome binding of the N-Ank module of Ankrd24x6, the next question to be answered was whether the binding relied mainly on hydrophobic or electrostatic interactions. This hypothesis was tested by carrying out salt-extraction assays with two version of the N-Ank module, Ankrd24x6$^{1-285}$ and Ankrd24x6$^{1-222}$. The quantitative analysis of Coomassie-stained SDS-gels demonstrated that the membrane binding ability of the N-Ank module was not diminished when the NaCl concentration was increased from 150 mM to 250 mM (Fig. 9A-D). For Ankrd24x6$^{1-285}$, a significant increase in liposome binding was observed when the salt concentration was increased to 250 mM (Fig. 9A-B). The binding of the N-Ank proteins of Ankrd24x6 with liposomes was not reduced with increased salt concentration, thus indicating that electrostatic interactions played no major role in binding to the membrane lipids. In conclusion, the salt-extraction assays showed that the binding of the N-Ank module of Ankrd24x6 to liposomes was completely salt-resistant.
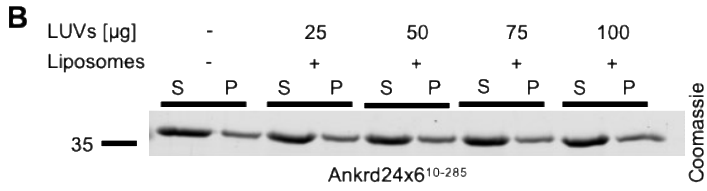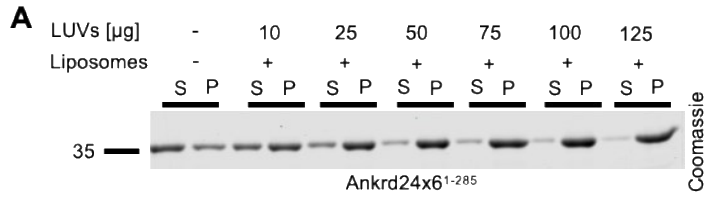


**Fig. 9**. **The N-Ank module of Ankrd24x6 binds to liposomes in a salt-resistant fashion.** Salt-extraction assays were performed with the wildtype N-Ank modules of Ankrd24x6 proteins, Ankrd24x6$^{1-285}$ and Ankrd24x6$^{1-222}$. Coomassie-stained SDS-gels of supernatant (S) and pellet (P) fractions of incubations of Ankrd24x6$^{1-285}$ with (+) or without liposomes (-), with increasing salt concentrations from 150 mM to 250 mM NaCl (A), and its bar blot representation of

quantitative analysis of liposome binding normalised to 150 mM NaCl (B), Coomassie-stained SDS-gels of supernatant (S) and pellet (P) fractions of Ankrd24x6[1-222] incubation with (+) or without liposomes (-) with increasing salt concentrations from 150 to 250 mM NaCl (C), and its bar blot representation of quantitative analysis of liposome binding normalised to 150 mM NaCl (D). The results showed that the N-Ank module of Ankrd24x6 remained strongly bound to liposomes with increasing salt concentration. Binding of protein to liposomes was quantified as liposome binding $[\%]=[((P/(S+P))_{Sample} - (P/(S+P))_{HN\ buffer\ control}) \times 100]$, where the sample included the protein and liposomes, and the HN buffer control comprised only of protein and it was then normalised to 150 mM $NaCl_{sample}$. Quantitative analyses included three independent liposome preparations with technical replicates, n=7-9 (sum of biological and technical replicates). Data represent mean ± sem. Kruskal-Wallis with Dunn's multiple comparison test. *$**p<0.01$* (B,D).

## 3.5 The N-Ank module of Ankrd24x6, Ankrd24x6[1-285], had a half-maximal binding concentration of 24.94 µg LUVs and 11.53 µg SUVs

As liposome pelleting (Fig. 6) and sensing assays (Fig. 7) demonstrated that the 4 µM N-Ank module of Ankrd24x6 bound partially to the 50 µg LUVs and SUVs offered, the next question considered was whether the 4 µM protein used in the assays might need more liposomes for complete precipitation. This question was answered by performing binding assays with the wildtype Ankrd24x6[1-285] and its mutant lacking the amphipathic helix, Ankrd24x6[10-285], and increasing amounts of LUVs and SUVs were offered up to 100 µg or 125 µg, respectively. Quantitative analysis of Coomassie-stained SDS-gels of binding assays disclosed that Ankrd24x6[1-285] bound to LUVs and SUVs with some affinity and reached half-maximal binding capacity at 24.94 µg LUVs (Fig. 10A,C) and 11.53 µg SUVs (Fig. 10D,F), respectively as determined by nonlinear regression model with Michaelis-Menten equation. In line with the experiments reported so far, the mutant lacking the amphipathic helix, Ankrd24x6[10-285], did not precipitate with either LUVs (Fig. 10B-C) or SUVs (Fig. 10E-F) and therefore, the half-maximal binding capacity could not be determined. Altogether, only Ankrd24x6[1-285] demonstrated a binding ability to liposomes with a half-maximal binding concentration of 24.94 µg LUVs and 11.53 µg SUVs, respectively.

**A**

| LUVs [µg] | - | | 10 | | 25 | | 50 | | 75 | | 100 | | 125 | |
| Liposomes | - | | + | | + | | + | | + | | + | | + | |
| | S | P | S | P | S | P | S | P | S | P | S | P | S | P |

Coomassie

35 —

Ankrd24x6$^{1-285}$

**B**

| LUVs [µg] | - | | 25 | | 50 | | 75 | | 100 | |
| Liposomes | - | | + | | + | | + | | + | |
| | S | P | S | P | S | P | S | P | S | P |

Coomassie

35 —

Ankrd24x6$^{10-285}$

**C**



**D**

| SUVs [µg] | - | | 10 | | 25 | | 50 | | 75 | | 100 | |
| Liposomes | - | | + | | + | | + | | + | | + | |
| | S | P | S | P | S | P | S | P | S | P | S | P |

Coomassie

35 —

Ankrd24x6$^{1-285}$

**E**

| SUVs [µg] | - | | 25 | | 50 | | 75 | | 100 | |
| Liposomes | - | | + | | + | | + | | + | |
| | S | P | S | P | S | P | S | P | S | P |

Coomassie

35 —

Ankrd24x6$^{10-285}$

**F**
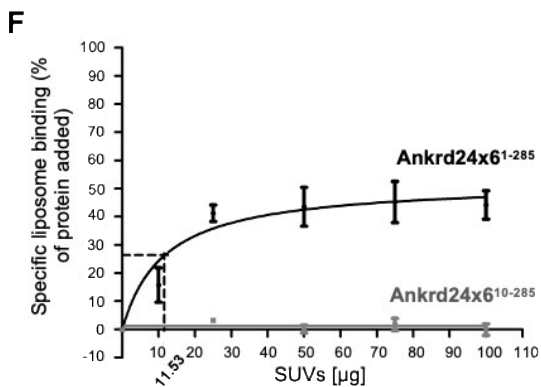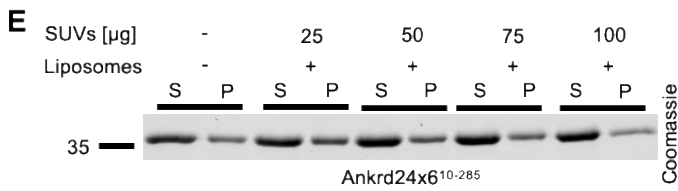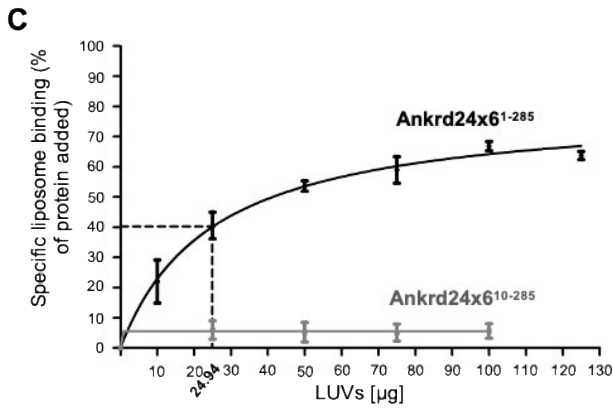
**Fig. 10**. **The N-Ank module of Ankrd24x6, Ankrd24x6$^{1-285}$, had a half-maximal binding concentration of 24.94 µg LUVs and 11.53 µg SUVs, respectively.** Binding assays were performed with the wildtype N-Ank module, Ankrd24x6$^{1-285}$ and its mutant lacking the amphipathic helix, Ankrd24x6$^{10-285}$. Coomassie-stained SDS-gels of supernatant (S) and pellet (P) fractions of Ankrd24x6$^{1-285}$ (A) and Ankrd24x6$^{10-285}$ (B) incubations with (+) or without liposomes (-) with increasing amounts of LUVs. Line graph representation of the quantitative analysis of Ankrd24x6$^{1-285}$ and Ankrd24x6$^{10-285}$ (C), Coomassie-stained SDS-gels of supernatant (S) and pellet (P) fractions of Ankrd24x6$^{1-285}$ (D) and Ankrd24x6$^{10-285}$ (E) incubations with (+) or without liposomes (-) with increasing amounts of SUVs. Line graph representation of quantitative analysis of Ankrd24x6$^{1-285}$ and Ankrd24x6$^{10-285}$ (F). Nonlinear regression model with Michaelis-Menten equation was used to calculate half-maximal binding of 24.94 µg LUVs (C) and 11.53 µg SUVs (F) for Ankrd24x6$^{1-285}$. Half-maximal binding of Ankrd24x6$^{10-285}$ remained non-determined as no binding to increasing amounts of LUVs or SUVs was observed. Binding of protein to liposomes was quantified as liposome binding $[\%]=[((P/(S+P))_{Sample} - (P/(S+P))_{HN\ buffer\ control})\times 100]$, where the sample included the protein and liposomes, and HN buffer comprised only of protein. Quantitative analyses included two to four independent liposome preparations with two technical replicates for each sample, making n=4 (2*2) or 8 (4*2). For LUVs, Ankrd24x6$^{1-285}$, n=4 for 10 µg and 125 µg, n= 8 for 25 µg, 50 µg, 75 µg and 100 µg, respectively and for Ankrd24x6$^{10-285}$, n=4 for 25 µg, 50 µg, 75 µg and 100 µg, respectively. For SUVs, Ankrd24x6$^{1-285}$, n=4 for 10 µg, n=8 for 25 µg, 50 µg, 75 µg and 100 µg, respectively and for Ankrd24x6$^{10-285}$, n=4 for 25 µg, 50 µg, 75 µg and 100 µg, respectively. Data represent mean ± sem.
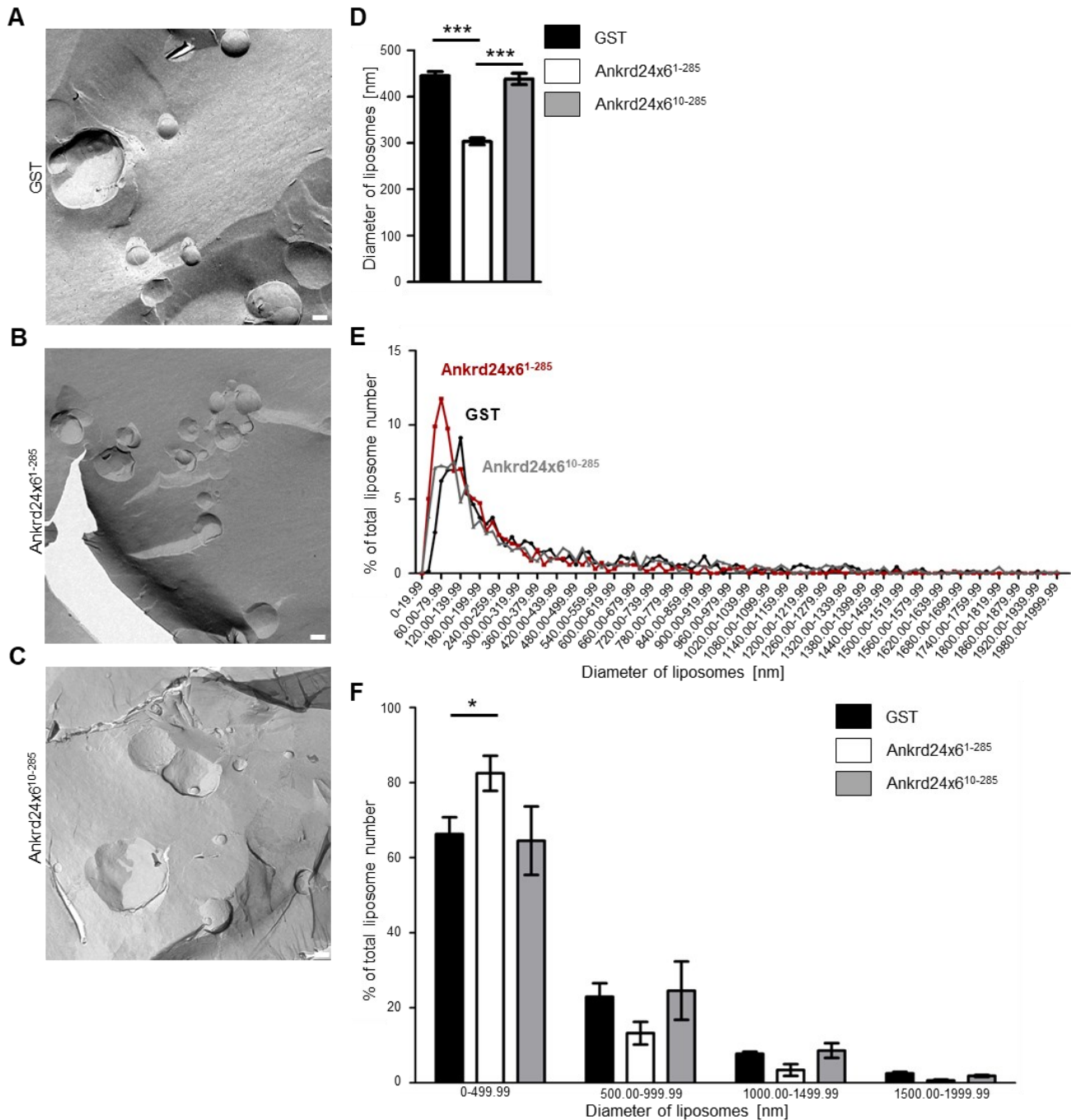
## 3.6 The N-Ank module of Ankrd24x6, Ankrd24x6$^{1-285}$, shaped liposomes

So far, the investigation of the N-Ank module of Ankrd24x6 showed that it bound partially to liposomes. Further experiments aimed at addressing whether it shaped the liposomes, i.e., if it changes big liposomes into smaller spheres, elongated tubule structures or any other shape. This hypothesis was tested by carrying out freeze-fracture experiments with liposomes, followed by TEM imaging. Freeze-fracturing was performed with liposomes incubated with Ankrd24x6$^{1-285}$, its mutant lacking amphipathic helix, Ankrd24x6$^{10-285}$, and GST protein as a control. The TEM images showed a higher percentage of large size liposomes with GST (Fig. 11A), smaller size liposomes with Ankrd24x6$^{1-285}$ (Fig. 11B) and similar sizes as GST with Ankrd24x6$^{10-285}$ (Fig. 11C).

The quantitative analysis of the diameter of liposomes demonstrated that indeed the average size of liposomes was significantly reduced by Ankrd24x6$^{1-285}$ when compared to GST or Ankrd24x6$^{10-285}$ (Fig. 11D). Deeper analysis into the distribution of the sizes of liposomes disclosed that the percentage of liposomes incubated with Ankrd24x6$^{1-285}$ was increased in the range of 60.00-79.99 nm (Fig. 11E). Ankrd24x6$^{1-285}$ reduced the average liposome diameter size to ~300 nm (Fig. 11D), which was contributed by the

significant increase in percentage of liposomes in the range of 0-499.99 nm when compared to GST (Fig. 11F). In addition, there was also a decrease in the percentage of liposomes incubated with Ankrd24x6$^{1\text{-}285}$ in the ranges of 500.00-999.99 nm, 1000.00-1499.99 nm and 1500.00-1999.99 nm, when compared to GST and Ankrd24x6$^{10\text{-}285}$, respectively (Fig. 11F). GST and Ankrd24x6$^{10\text{-}285}$ showed similar behavior in terms of average liposome diameter size (Fig. 11D) and in the size distribution (Fig. 11E-F).

Overall, the analysis of TEM images of freeze-fractured liposomes incubated with Ankrd24x6$^{1\text{-}285}$, Ankrd24x6$^{10\text{-}285}$ and GST unveiled that the N-Ank module, Ankrd24x6$^{1\text{-}285}$ shaped the liposomes by significantly reducing the average size of liposomes when compared to GST or Ankrd24x6$^{10\text{-}285}$. Furthermore, the investigation for the N-Ank properties of the N-Ank module of Ankrd24x6 revealed that it binds and shapes the lipid membrane.

**Fig. 11**. **The N-Ank module of Ankrd24x6, Ankrd24x6[1-285] shaped liposomes.** Representative TEM images of freeze-fractured liposomes after incubation with GST as a control (A), the N-Ank module, Ankrd24x6[1-285] (B), and its mutant lacking the amphipathic helix, Ankrd24x6[10-285] (C), scale bar 200 nm. Quantitative analysis of the diameter of liposomes demonstrated a significant reduction of the average size of liposomes by Ankrd24x6[1-285] when compared to GST and Ankrd24x6[10-285] (D), line graph representation of the size distribution of liposomes according to their diameter in percentage of the total liposome number, showing an increased peak in the range of 60-79.99 nm diameter by liposomes incubated with Ankrd24x6[1-285]. One of the two independent assays represented with n=692 for GST, n=699 for Ankrd24x6[1-285] and n=709 for Ankrd24x6[10-285], respectively, where n represents the number of liposomes

(E). (*See* Appendix 7.1, Fig. 22 for the cumulative size distribution of liposomes from both the assays). Quantitative analysis of the diameter size distribution of liposomes in percentage of the total liposome number, showing a significant increase in the range of 0-499.99 nm diameter and a decreasing trend in the range of 500.00-999.99, 1000.00-1499.99 and 1500.00-1999.99, respectively by liposomes incubated with Ankrd24x6$^{1\text{-}285}$ when compared to GST and Ankrd24x6$^{10\text{-}285}$ (F). Quantitative analyses included two independent liposome preparations: n=2165 for GST, n=1672 for Ankrd24x6$^{1\text{-}285}$ and n=1164 for Ankrd24x6$^{10\text{-}285}$, where n represents number of liposomes. Data represent mean ± sem (D,F). One-way ANOVA Kruskal-Wallis with Dunn's multiple comparison test. ****p<0.001* (D). Two-way ANOVA with Bonferroni post-hoc test. **p< 0.05* (F).

## 3.7   Ankrd24x6 oligomerised via its predicted coiled coil domains

*In silico* analysis of Ankrd24x6 secondary structure had predicted the presence of amphipathic helix, ankyrin repeats and coiled coil domains (Fig. 2). So far, the *in vitro* reconstitution assays with liposomes revealed that the N-Ank module of Ankrd24x6, Ankrd24x6$^{1\text{-}285}$ bound to liposomes via the putative amphipathic helix. Next, the coiled coil domains in Ankrd24x6 which were predicted by the bioinformatic tool, Marcoil (Delorenzi and Speed, 2002) were investigated for its putative oligomerisation function because coiled coil domains are known for their involvement in forming and/or stabilizing higher order protein structures (Lupas, 1996). Also, ankycorbin (Wolf et al., 2019) and Ankrd26 (Hofbrucker-MacKenzie, 2021), the N-Ank proteins were predicted to have coiled coil domains and they both demonstrated their ability to self-oligomerise. Therefore, Ankrd24x6 was also tested for its putative oligomerisation function by incubating lysates of Ankrd24x6$^{1\text{-}285}$-GFP, Ankrd24x6$^{283\text{-}1041}$-GFP or Ankrd24x6$^{1\text{-}1041}$-GFP transfected HEK293 cells with increasing EDC (cross-linker) concentration. Ankrd24x6 contained two coiled coil domains ranging from amino acid 289-490 and 746-1009 (Fig. 12A); predicted with a high probability by the bioinformatic tool, Marcoil (Delorenzi & Speed, 2002). Immunoblotting analysis showed that the N-Ank module, Ankrd24x6$^{1\text{-}285}$-GFP (Fig. 12B) remained monomerised and lacked the ability to oligomerise unlike Ankrd24x6$^{283\text{-}1041}$-GFP (Fig. 12C) and full-length Ankrd24x6$^{1\text{-}1041}$-GFP (Fig. 12D), both of which displayed their ability to form higher molecular weight complexes at more than 180 and 250 kDa, respectively. The experiment illustrated that the presence of the putative coiled coil domains in Ankrd24x6$^{283\text{-}1041}$-GFP and full-length Ankrd24x6$^{1\text{-}1041}$-GFP, is in line with an increase in oligomerisation with the increasing

concentration of the cross-linker, EDC, while subsequently reducing the monomer levels. Thus, the results indicated that the presence of the two putative coiled coil domains in Ankrd24x6 within the amino acid range of 283-1041, mediated oligomerisation in the presence of the cross-linker, EDC.
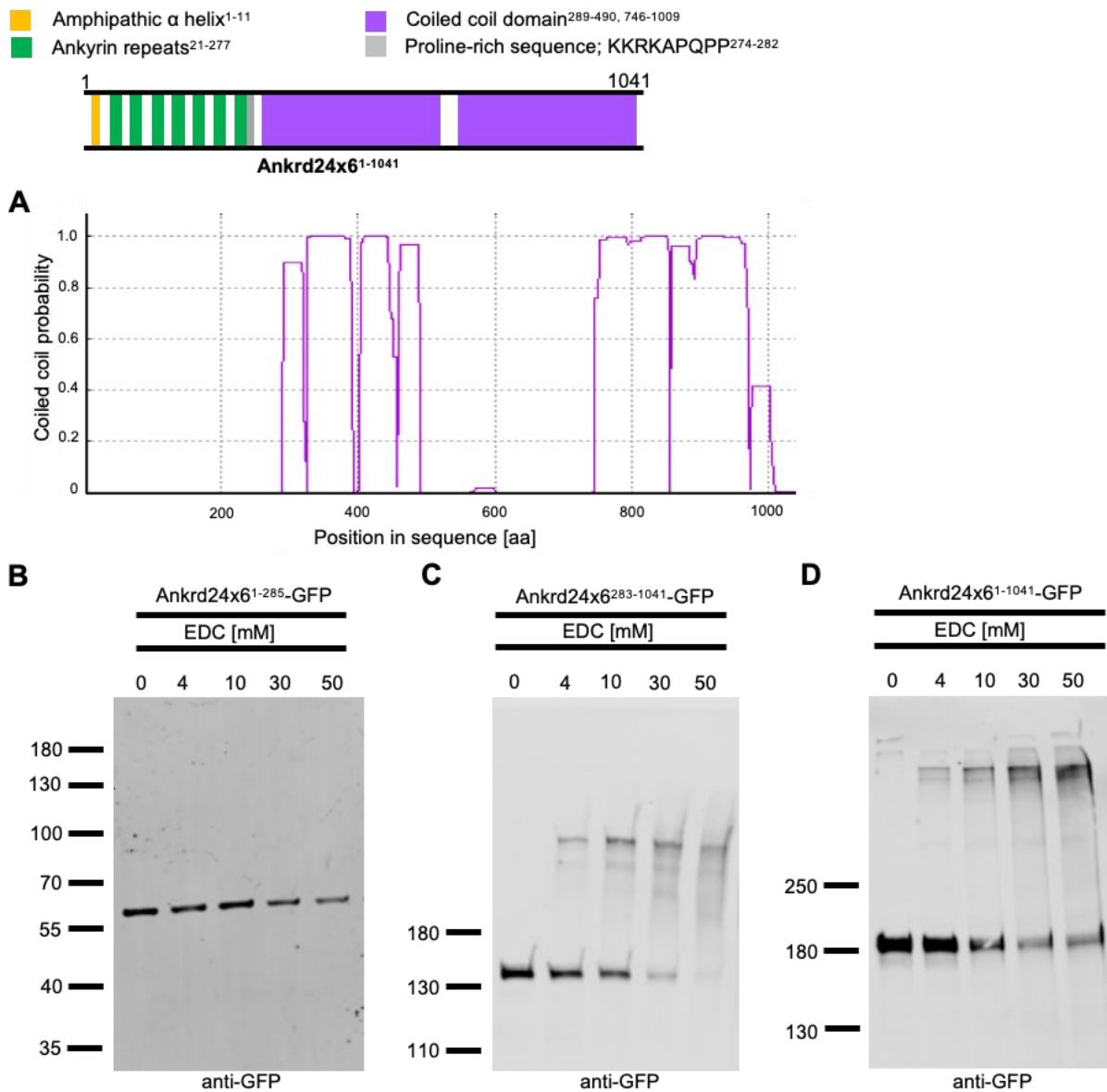


**Fig. 12. Self-association of Ankrd24x6 via its predicted coiled coil domains containing region.** Coiled coil domains prediction by the bioinformatic tool, Marcoil (Delorenzi and Speed, 2002) with high probabilities at the amino acid range of 289-490 and 746-1009 (A), immunoblot representation of the crosslinking experiments with increasing concentrations of EDC incubation with the lysates of HEK293 cells overexpressing Ankrd24x6[1-285]-GFP (B), Ankrd24x6[283-1041]-GFP (C), Ankrd24x6[1-1041]-GFP (D). The experiment demonstrated that in the presence of the cross-linker, EDC, the N-Ank module, Ankrd24x6[1-285]-GFP did not form higher molecular weight

complexes while both Ankrd24x6[283-1041]-GFP and Ankrd24x6[1-1041]-GFP, which contain the putative coiled coil domains, displayed their ability to form oligomers. Immunoblot as a representation of two independent experiments (B-D).

## 3.8  Ankrd24x6, an N-Ank protein, bound to family of syndapins, F-BAR domain-containing proteins

After investigating the domains in Ankrd24x6 (Fig. 2E) for their function as an N-Ank protein, the investigation was extended to a proline-rich motif PxxP with the sequence of KKRKAPQPP (Ankrd24x6[274-282]). Proline-rich motif PxxP, has been known to be involved in protein-protein interactions (Sparks et al., 1996; Tong et al., 2002). Proline-rich sequences have the capability of binding to the SH3 domains (Kaneko et al., 2008; Sparks et al., 1996; Tong et al., 2002) and 'KrrAPpPP' has been identified as the consensus belonging to class 1 PxxP motif, which can bind to the SH3 domain-containing syndapin proteins (Schwintzer, 2012; Schwintzer et al., 2011). Ankrd24 was also predicted to be a syndapin I-interacting partner (Schwintzer, 2012). In Wolf (2018), ankycorbin, an N-Ank protein which contains 'KrrAPpPP' was shown to bind to the SH3 domain-containing syndapin I protein. Thus, studies were performed to check if syndapin proteins bind to Ankrd24x6. The family of syndapins in *Rattus norvegicus* has three members and syndapin II is additionally alternatively spliced: brain enriched syndapin I, wide tissue distributed, syndapin II-s (small) and syndapinII-l (long) (Qualmann & Kelly, 2000) and muscle enriched syndapin III isoform (Kessels & Qualmann, 2004; Qualmann et al., 2011). Therefore, to address the hypothesis that Ankrd24x6 binds to members of the family of proteins called, syndapins, which contain the SH3 domain (Plomann et al., 1998), *in vitro* reconstitution coprecipitation assays were designed.

The assay investigated the binding of GST-tagged isoforms of syndapins or GST to lysates of HEK293 cells overexpressing GFP-fusion full-length Ankrd24x6[1-1041] and GFP. GST and GFP proteins were used as controls. Immunoblot analysis revealed that indeed Ankrd24x6 bound to all isoforms of syndapins (Fig. 13) as Ankrd24x6[1-1041]-GFP was detected in eluates with GST-tagged syndapins and the supernatants were depleted of Ankrd24x6[1-1041]-GFP. The same assay with GST alone showed that there was no unspecific binding mediated by the tag as Ankrd24x6[1-1041]-GFP was detected

alone in supernatant. Also, GFP was detected in supernatants with GST and GST-tagged syndapins, demonstrating again the specificity of the binding. Thus, the results unveiled that Ankrd24x6, an N-Ank protein binds specifically to syndapins, F-BAR domain containing membrane-shapers.
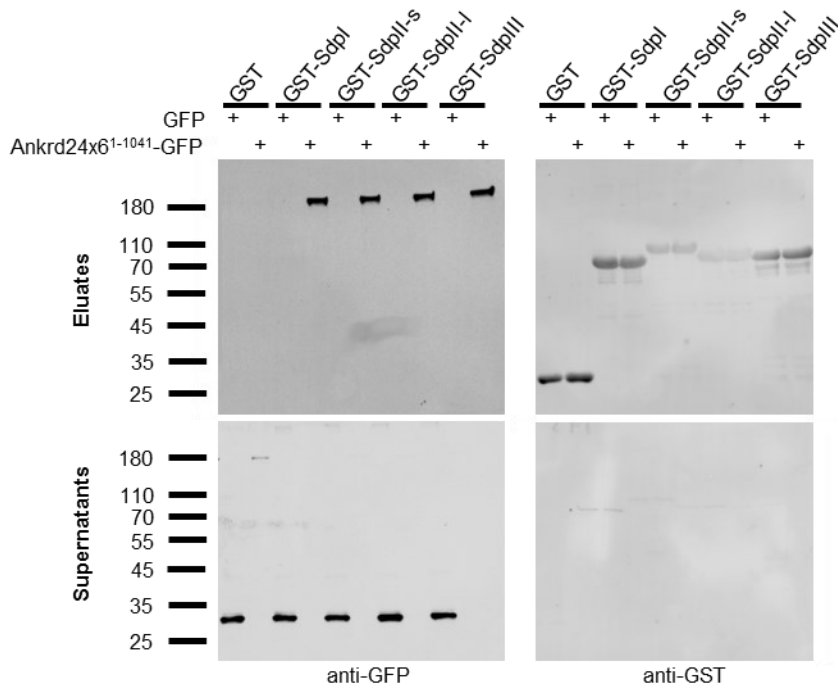


**Fig. 13. Ankrd24x6, an N-Ank protein binds to all isoforms of syndapin protein, F-BAR domain-containing membrane-shapers.** *In vitro* reconstitution coprecipitation assays were performed using GST-tagged full-length syndapin I, syndapin II-small, syndapin II-long, syndapin III or GST with lysates of HEK293 cells overexpressing Ankrd24x6$^{1-1041}$-GFP or GFP for 24 h. The immunoblot analysis demonstrated that Ankrd24x6$^{1-1041}$-GFP coprecipitated with GST-SdpI, GST-SdpII-s, GST-SdpII-l and GST-SdpIII, respectively. Immunoblot is a representation of two biological replicates.

## 3.9 Ankrd24x6 proline-rich sequence KKRKAPQPP binds specifically to the SH3 domain of syndapin I

As proline-rich sequence with consensus 'KrrAPpPP' and class 1 PxxP motif have been reported to bind to the SH3 domain of syndapin I (Schwintzer, 2012; Schwintzer et al., 2011; Wolf, 2013, 2018), the next question to be investigated was to find which domain of Ankrd24x6 specifically interacts with syndapin I. *In vitro* reconstitution coprecipitation assays were performed using GST-tagged SH3 domain from syndapin I or GST as a control with cell lysates of HEK293 cells overexpressing full-length or different domains

of Ankrd24x6 fusion proteins with GFP. Also, GFP alone was used as a control. The results demonstrated that the fusion proteins of the part of Ankrd24x6 containing the proline-rich sequence KKRKAPQPP, which was Ankrd24x6$^{1\text{-}285}$-GFP and Ankrd24x6$^{1\text{-}1041}$-GFP (Fig. 14A), coprecipitated with GST-SH3 of syndapin I as they were detected in eluates with anti-GFP immunostaining, whereas Ankrd24x6$^{1\text{-}222}$-GFP and Ankrd24x6$^{283\text{-}1041}$-GFP, which lacked the proline-rich sequence were detected in the supernatants along with GFP. GST alone did not coprecipitate with either GFP or GFP-fusion Ankrd24x6 proteins, indicating that the interaction of GST-tagged SH3 domain of syndapin I to Ankrd24x6$^{1\text{-}285}$-GFP and Ankrd24x6$^{1\text{-}1041}$-GFP was not mediated by the tag.

To explicitly show the importance of the proline-rich sequence and its interaction with the SH3 domain of syndapin I, additional set of *in vitro* reconstitution coprecipitation assays were performed with the lysates of HEK293 cells overexpressing Ankrd24x6$^{1\text{-}1041\Delta273\text{-}286}$-GFP, a mutant lacking KKRKAPQPP, and the wildtype Ankrd24x6$^{1\text{-}1041}$-GFP with GST-tagged SH3 of syndapin I or GST alone (Fig. 14B). The results showed that the mutant lacking KKRKAPQPP could not bind to the SH3 domain of syndapin I as the mutant was detected in the supernatant, compared to the wildtype fusion protein, which was rather observed in the eluates with anti-GFP detection. The specificity of the binding was demonstrated by the lack of coprecipitation of GFP and the GFP-fusion proteins of Ankrd24x6 with GST. Taken together, the results showed that Ankrd24x6 specifically binds to the SH3 domain of syndapin I via KKRKAPQPP, a proline-rich sequence with consensus 'KrrAPpPP'.
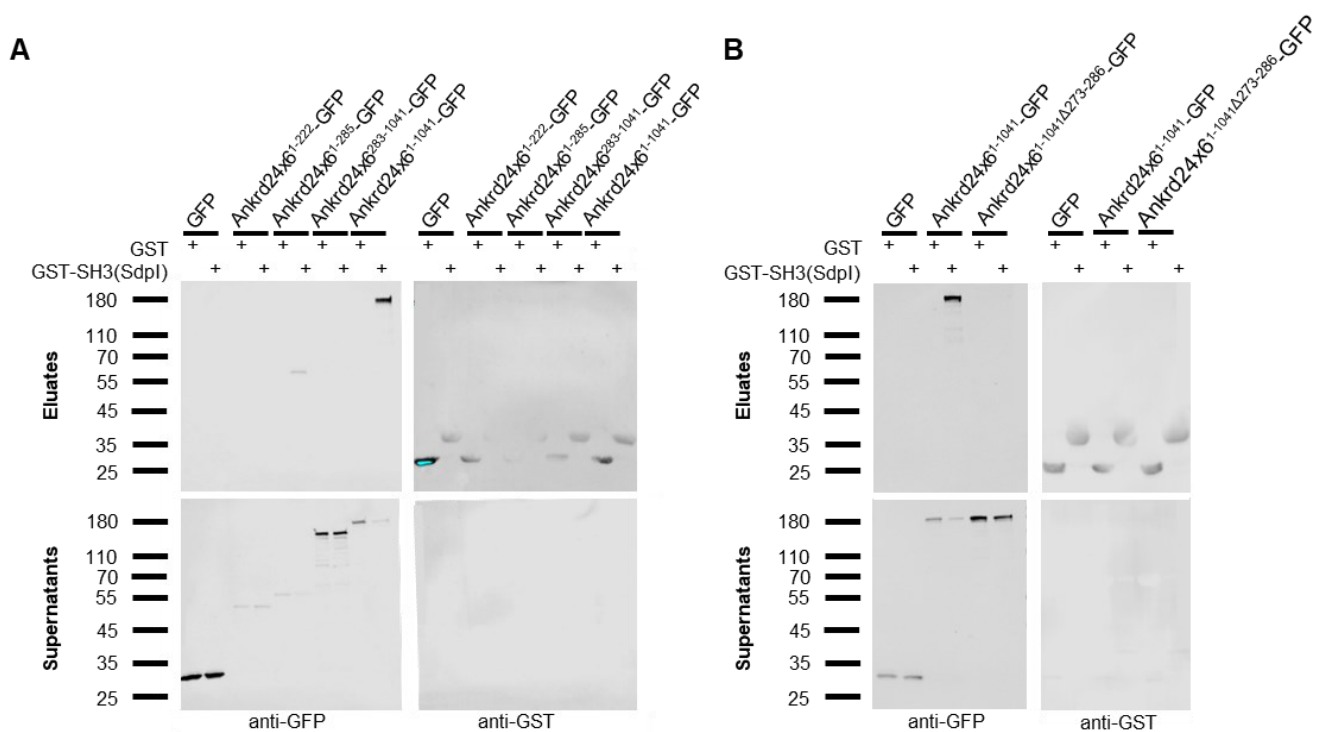
**Fig. 14. Ankrd24x6 proline-rich sequence KKRKAPQPP binds to the SH3 domain of syndapin I.** *In vitro* reconstitution coprecipitation assays were performed using GST-SH3 (syndapin I) or GST with lysates of HEK293 cells overexpressing GFP-fusion proteins of wildtype Ankrd24x6, its mutant, or GFP for 24 h. Experiment showed specific binding of Ankrd24x6$^{1-285}$-GFP and Ankrd24x6$^{1-1041}$-GFP (A) and lack of binding of Ankrd24x6$^{1-1041\Delta273-286}$-GFP (B) to GST-SH3 (syndapin I). Immunoblots are representation of two biological replicates. (*See* Appendix 7.1, Fig. 23 for an immunoblot, which is a technical replicate of an *in vitro* reconstitution coprecipitation assays showing lack of binding of Ankrd24x6$^{1-222}$-GFP and binding of Ankrd24x6$^{1-285}$-GFP to GST-SH3 (syndapin I), respectively).

## 3.10 Ankrd24x6$^{1-285}$ interacts with syndapin I in lysates of an adult rat brain

Binding of SH3 domains to proline-rich domains are known to be promiscuous in nature with low affinity and specificity (Castagnoli et al., 2004; Viguera et al., 1994), therefore, to be sure that Ankrd24x6 binds to syndapin I in rat brain, endogenous coprecipitation assays were performed. Brain tissue lysate of a 21-week-old adult rat was used since syndapin I expression is known to increase with age (Plomann et al., 1998; Qualmann et al., 1999). The lysate was offered to GST-Ankrd24x6$^{1-285}$, which includes the KKRKAPQPP sequence and was coupled to GSH-sepharose. The results demonstrated that syndapin I in adult rat brain tissue lysate coprecipitated with GST-

Ankrd24x6$^{1-285}$ which was detected in the eluates, via anti-syndapin I immunoblot analysis (Fig. 15). Lysates incubated with GST immbobilized on GSH-sepharose did not detect syndapin I in the eluate, although a weak band of GST was detected which was stronger in the supernatant. Either the excess of the GST protein got leaked from the supernatant to eluate and/or anti-syndapin I detected GST as the antibody was raised against GST-syndapin I$^{1-382}$ as an antigen (Qualmann et al., 1999), which could explain detection of GST by anti-syndapin I. Immunoblot analysis by anti-GST showed a stronger band of GST in eluate than what got detected by anti-syndapin I in the sample where GST was offered to the lysate. Anti-GST detected two bands in the eluate of sample where lysates were incubated with GST-Ankrd24x6$^{1-285}$, a weaker band of syndapin I (~52 kDa) and a strong band of GST-Ankrd24x6$^{1-285}$ (~57 kDa). Both anti-GST and anti-syndapin I were raised against rabbit, therefore, syndapin I got detected in the supernatant of the sample which contains GST and lysate. Thus, the results indicated that the N-Ank module of Ankrd24x6, Ankrd24x6$^{1-285}$ containing the proline-rich sequence binds specifically to syndapin I in 21-week-old adult rat brain.
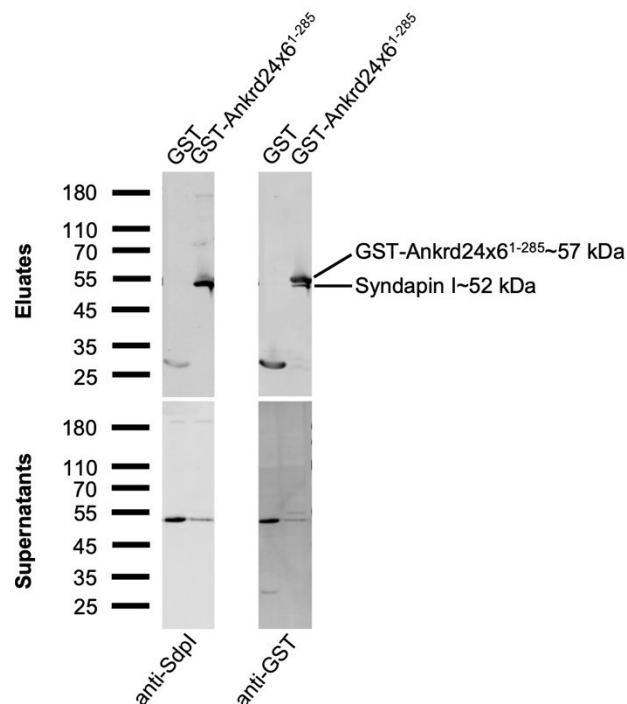


**Fig. 15. Ankrd24x6$^{1-285}$ interacts with syndapin I in adult rat brain tissue lysate.** Immunoblot analysis of endogenous coprecipitation experiment with lysates from the brain of 21-week-old adult rat and GST-Ankrd24x6$^{1-285}$ or GST, used as a control. The results showed

that GST-Ankrd24x6$^{1-285}$ coprecipitated with syndapin I in adult rat brain tissue lysate. Immunoblot is a representation of two biological replicates.

## 3.11 The gain-of-function phenotype of *Mus musculus* Ankrd24x6 in primary rat hippocampal neurons led to a significant increase of primary dendrites

Thus far, the investigation on Ankrd24x6 had demonstrated that it has the ability of binding to membranes and forming higher molecular weight complexes in the presence of a cross-linker. Ankrd24x6 also displayed that it is capable of associating with all members of syndapin family; a family of F-BAR domain-containing proteins and especially with the isoform syndapin I, which has been reported for its vital role in neuromorphogenesis (Dharmalingam et al., 2009). Ankrd24x6$^{1-285}$ shaped liposomes which indicated that it has the potential of shaping membranes and it also showed interaction with syndapin I in adult brain. All these features of Ankrd24x6 of membrane binding and shaping, and oligomerising have also been observed with proteins like syndapin I (Dharmalingam et al., 2009; Kessels & Qualmann, 2006; Koch et al., 2020; Qualmann et al., 2011) and ankycorbin (Wolf et al., 2019), both of which have been shown to be crucial for dendritic arbor development. Thus, the next step of investigating the function of Ankrd24 was carried out by analysing the dendritic arbor of primary rat hippocampal neurons by overexpressing Ankrd24x6. According to the NCBI database, three isoforms of Ankrd24 were predicted in *Rattus norvegicus* (19 May 2021), out of which x2 isoform (XM_039078672.1) showed 90.28% percent identity to *Mus musculus* Ankrd24x6 mRNA transcript and therefore, x2 isoform was used as a reference to observe differences in exons from the other two isoforms (Fig. 16A). While x2 isoform started at gene locus position of 703 (exon 1), NM_001106771.1 started at gene locus position of 1 (see Appendix 7.1, table 14 for the gene locus position of all exons and Ankrd24 isoforms in *Rattus norvegicus*) and interesting, they both translate to the same amino acid sequence from 1-261, indicating that while the transcription start site is different, their translation start site is the same. The translated amino acid sequence of *Rattus norvegicus* x2 isoform (XP_038934600.1) showed 85.39% percent identity to the translated amino acid sequence of *Mus musculus* Ankrd24x6 (XP_006514159.1), represented by a dot plot in Fig. 16B, where the lines represented alignments between

the two protein sequences. There was 85% percent identity of amino acid sequences observed between *Rattus norvegicus* x2 isoform (XP_038934600.1) and *Mus musculus* Ankrd24x6 (XP_006514159.1) from amino acid 1-930 and 1-925, respectively. The C-terminus region from amino acid 795 to 988 of *Rattus norvegicus* x2 isoform showed 32% percent identity to 933 to 1041 of *Mus musculus* Ankrd24x6. *Rattus norvegicus* x2 isoform was also one of the only isoforms of Ankrd24 with a proline-rich motif PxxP and sequence of KKRKAPQPP. The PxxP motif has been known to interact with proteins containing SH3 domains (Schwintzer et al., 2011; Sparks et al., 1996; Tong et al., 2002; Zarrinpar et al., 2003). Therefore, the gain-of-function studies were conducted with *Mus musculus* Ankrd24x6$^{1-1041}$ overexpression in primary rat hippocampal neurons.
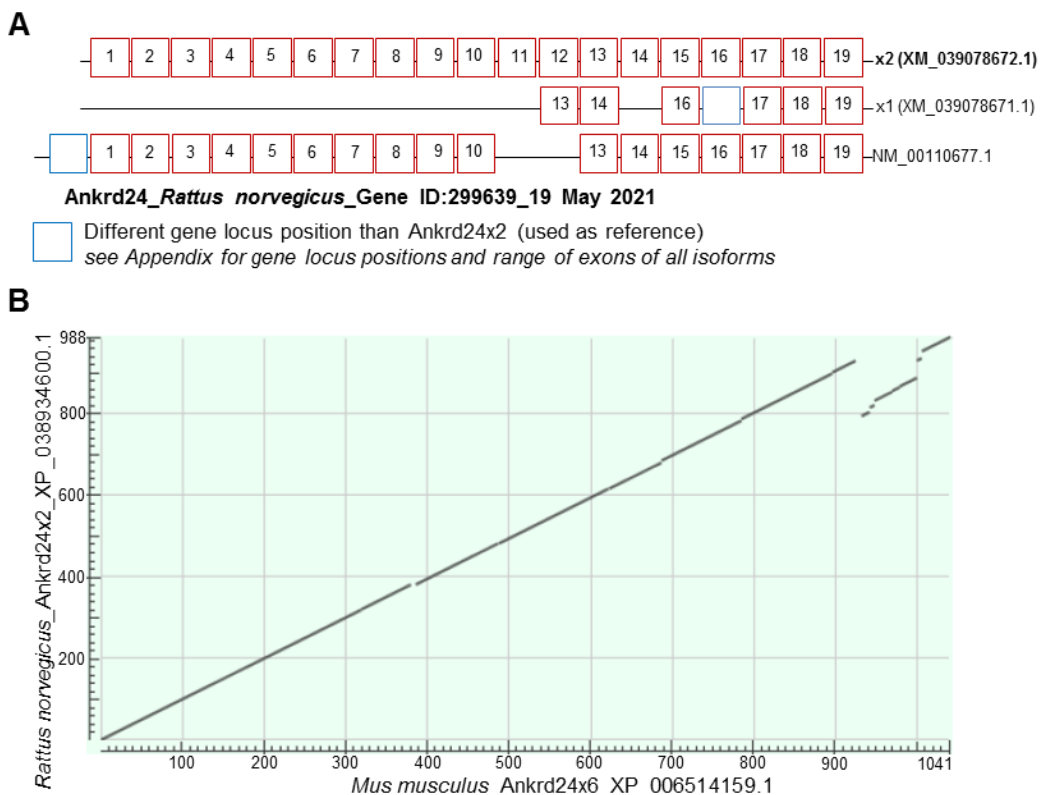


Fig. 16. Schematic representation of exons present in Ankrd24 isoforms with their respective nucleotide accession number in *Rattus norvegicus* according to the NCBI database on 19 May 2021, *Rattus norvegicus* x2 (XM_039078672.1) was used as a reference (A) and a dot plot representation of the alignment of amino acid sequence between *Rattus norvegicus* x2 isoform (XP_038934600.1) and *Mus musculus* Ankrd24x6 (XP_006514159.1), where the number of lines in the plot represent the number of alignments using alignment feature of BLAST (B).

The neurons were transfected at DIV4 for 30 h with *Mus musculus* Ankrd24x6$^{1-1041}$-GFP or GFP and thus, were analysed at DIV6 (DIV4+2). The analysis of the dendritic arbor of DIV6 primary rat hippocampal neurons was initiated by quantifying the parameter total number of points (Fig. 17A), which showed no significant difference between the overexpressed Ankrd24x6$^{1-1041}$-GFP and the GFP. The comparison of the dendritic terminal points (Fig. 17B) and the total dendritic tree length (Fig. 17C) between the primary rat hippocampal neurons expressing Ankrd24x6$^{1-1041}$-GFP and GFP displayed no variation too. Further analysis of the dendritic branch points (Fig. 17D) and dendritic segments (Fig. 17D) revealed no differences too but the profile of Sholl intersections unveiled an increasing trend in the number of points from 5 to 35 µm distance from soma (Fig. 17F) in Ankrd24x6$^{1-1041}$-GFP expressing primary rat hippocampal neurons. Since the increase in the number of points were at shorter distance from the soma center, deeper analysis of dendritic arbor was performed by quantifying dendritic branch depth to know the number of primary and higher degree dendrites (*see* section 2.2.6, Fig. 1). Indeed, a significant increase of dendritic segments of dendritic branch depth '1' was observed, which indicated that the number of primary dendrites were significantly increased (Fig. 17G). Example of neurons expressing GFP and Ankrd24x6$^{1-1041}$-GFP with their reconstructed dendritic arbor using Imaris 8.4.0 is represented in Fig. 17H.

Thus, the analyses demonstrated that *Mus musculus* Ankrd24x6$^{1-1041}$ induced the formation of primary dendrites in DIV6 primary rat hippocampal neurons.
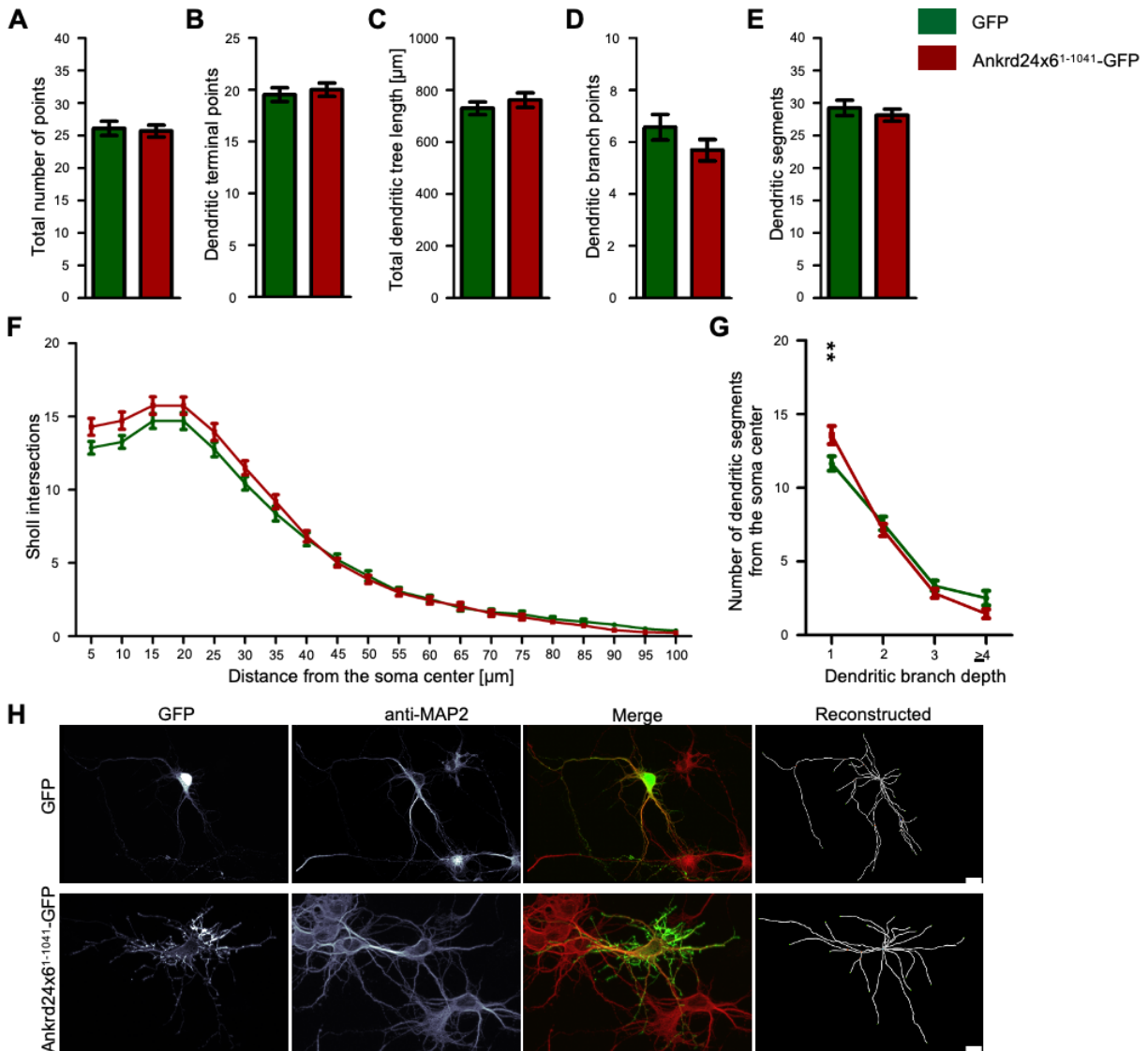
**Fig. 17. The gain-of-function phenotype of *Mus musculus* Ankrd24x6 in primary rat hippocampal neurons led to a significant increase of primary dendrites.** Quantitative analysis of dendritic arborization of primary rat hippocampal neurons at DIV6 (DIV4+2). The cells were transfected at DIV4 with GFP or Ankrd24x6$^{1-1041}$-GFP for 30 h, followed by 4% PFA fixation and immunostaining with anti-MAP2. Total number of points (A), dendritic terminal points (B), total dendritic tree length (C), dendritic branch points (D), dendritic segments (E), Sholl intersections (F), dendritic branch depth (G). Representative images of DIV6 primary rat hippocampal neurons transfected with GFP or Ankrd24x6$^{1-1041}$-GFP (H). The analysis indicated that the putative function of Ankrd24 is in primary dendrites of DIV6 primary rat hippocampal neurons as Ankrd24x6$^{1-1041}$-GFP gain-of-function led to significant increase in the number of dendritic segments from the soma center at dendritic branch depth '1' compared to GFP. Dendrites were considered as MAP2-positive structures ≥ 10 μm in length. Analyses included 3 independent primary rat hippocampal neuron preparations: n=65 for GFP and n=62 for Ankrd24x6$^{1-1041}$-GFP, where n represents the number of cells. Data represent mean ± sem. Unpaired t-test (A-E). Two-way-ANOVA with Bonferroni post-hoc test (F-G). ***p<0.01*. Scale bar, 10 μm (H).

## 3.12 The loss-of-function phenotype of Ankrd24 in primary rat hippocampal neurons resulted in a significantly reduced dendritogenesis and dendritic arborization

Functional studies were continued with the loss-of-function analyses. Thus, four potential shRNAs (RNAi$^{160-166}$, RNAi$^{231-237}$, RNAi$^{352-359}$ and RNAi$^{130-136}$) were designed to knockdown endogenous Ankrd24 in *Rattus norvegicus*. RNAi superscript represents the target amino acid sequence number of *Rattus norvegicus* x2 isoform of Ankrd24 (XP_038934600.1). RNAi$^{352-359}$ targets all isoforms of Ankrd24 in *Rattus norvegicus* and *Mus musculus* while RNAi$^{160-166}$, RNAi$^{231-237}$ and RNAi$^{130-136}$ targets only isoform x2 (XM_039078672.1) and NM_001106771.1 in *Rattus norvegicus* and all isoforms in *Mus musculus* except Ankrd24x21 and Ankrd24x22 (*see* table 4).

The first test of finding the most potent shRNAi against Ankrd24 was performed by co-expressing *Mus musculus* Ankrd24x6$^{1-1041}$-GFP sequence containing the RNAi target sequence and mcherry. This technique of having a plasmid coexpressing the RNAi, GFP-fusion full-length *Mus musculus* Ankrd24x6 and mcherry, from independent promoters had the advantage of accurately calculating RNAi efficiency by normalizing GFP signal against the mcherry signal. The lysates of HEK293 cells transfected with the above plasmids or scrambled/Ankrd24x6$^{1-1041}$-GFP/mcherry as a control were analysed by running SDS-PAGE, WB, followed by detection and quantification of GFP to mcherry signal (Fig. 18A). The results indicated that both RNAi$^{160-166}$ (Ankrd24 RNAi) and RNAi$^{130-136}$ were effective in reducing Ankrd24x6$^{1-1041}$ expression, while the other two candidates, i.e., RNAi$^{231-237}$ and RNAi$^{352-359}$ showed no reduction in Ankrd24x6$^{1-1041}$ expression, thus, indicating their ineffectiveness in targeting the coexpressed Ankrd24x6$^{1-1041}$ (Fig. 18B). Since both Ankrd24 RNAi and RNAi$^{130-136}$ demonstrated a lower expression of Ankrd24x6$^{1-1041}$-GFP, the loss-of-function investigation in primary rat hippocampal neurons were commenced with both. The quantitative analysis of dendritic arborisation showed that both Ankrd24 RNAi and RNAi$^{130-136}$ resulted in a smaller dendritic arbor when compared to scrambled RNAi/GFP. The two RNAis (Ankrd24 RNAi and RNAi$^{130-136}$) caused significant reduction of the total number of points (Fig. 19A) and the dendritic terminal points (Fig. 19B).
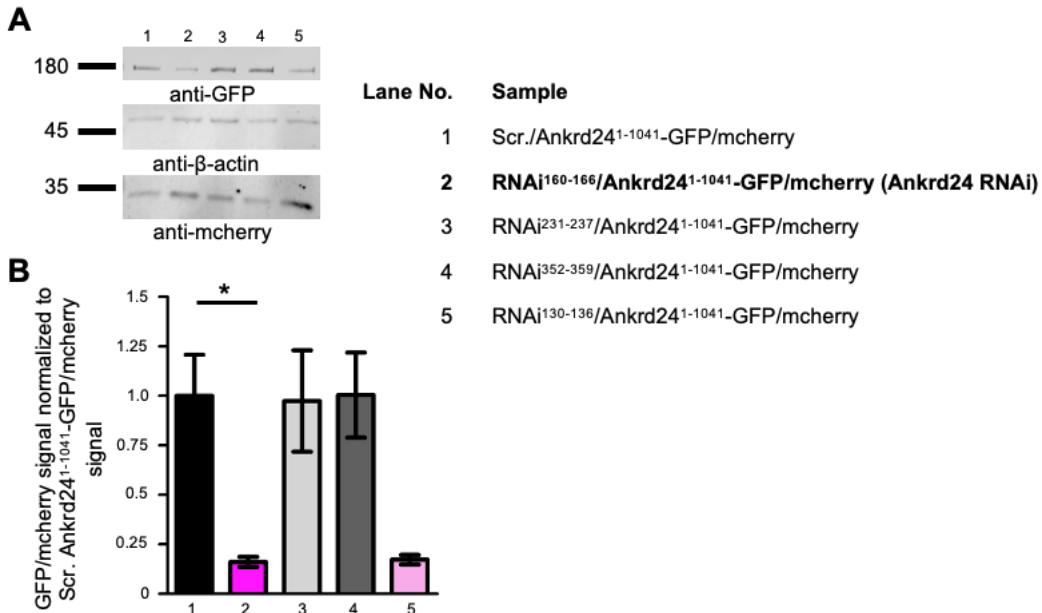
**Fig. 18. Both Ankrd24 RNAi and RNAi$^{207\text{-}214}$/Ankrd24x6$^{1\text{-}1041}$-GFP/mcherry showed reduced levels of coexpressed Ankrd24x6$^{1\text{-}1041}$-GFP in HEK293 cells.** The lysates of HEK293 cells transfected with plasmids expressing shRNAs (RNAi$^{160\text{-}166}$, RNAi$^{231\text{-}237}$, RNAi$^{352\text{-}359}$, RNAi$^{130\text{-}136}$)/Ankrd24x6$^{1\text{-}1041}$-GFP/mcherry or Scr./Ankrd24x6$^{1\text{-}1041}$-GFP/mcherry for 24 h were subjected to immunoblotting. Ankrd24x6$^{1\text{-}1041}$ included all the RNAi target sequences. Immunoblot is a representation of 6 biological replicates (A), Ankrd24x6$^{1\text{-}1041}$-GFP expression levels were quantified by normalising the GFP/mcherry signal to Scr./Ankrd24x6$^{1\text{-}1041}$-GFP/mcherry (B). The results demonstrated that both Ankrd24 RNAi and RNAi$^{130\text{-}136}$/Ankrd24x6$^{1\text{-}1041}$-GFP/mcherry reduced the expression of Ankrd24x6$^{1\text{-}1041}$. The analysis included 6 biological replicates: n=6. Data represent mean ± sem. Statistical significances were tested using Kruskal-Wallis with Dunn's multiple comparison test. *p<0.05.

They also shortened the length of the dendrites, which when quantified resulted in a significantly reduced parameter of the total dendritic tree length (Fig. 19C). Analysis of the dendritic branches showed that both the RNAis caused reduced number of dendritic branch points but only RNAi$^{130\text{-}136}$ showed a statistical significance (Fig. 19D). Also, the dendritic segments were significantly reduced by both the RNAis (Fig. 19E). Sholl intersections of primary rat hippocampal neurons were significantly reduced from 5-25 µm in case of Ankrd24 RNAi/GFP and from 5-40 µm in case of RNAi$^{130\text{-}136}$/GFP (Fig. 19F). The analysis and quantification of the parameter dendritic branch depth unveiled that both the RNAis significantly reduced the number of dendritic segments at dendritic branch depth '1'. Thus, indicating that the primary dendrites were significantly reduced by both Ankrd24 RNAi and RNAi$^{130\text{-}136}$ (Fig. 19G). As the number of neuronal cells

investigated for RNAi[130-136]/GFP were less than scrambled RNAi/GFP and Ankrd24 RNAi, the statistical analysis could have been influenced (Fig. 19).

Taken together, the result suggested that both Ankrd24 RNAi/GFP and RNAi[130-136]/GFP caused significant reductions of the dendritic tree in DIV6 primary rat hippocampal neurons. It was interesting to discover that while the gain-of-function phenotype of Ankrd24x6[1-1041] resulted in increased number of primary dendrites, the loss-of-function phenotype of Ankrd24 caused a significant reduction in dendritogenesis and dendritic arborisation in DIV6 primary rat hippocampal neurons.
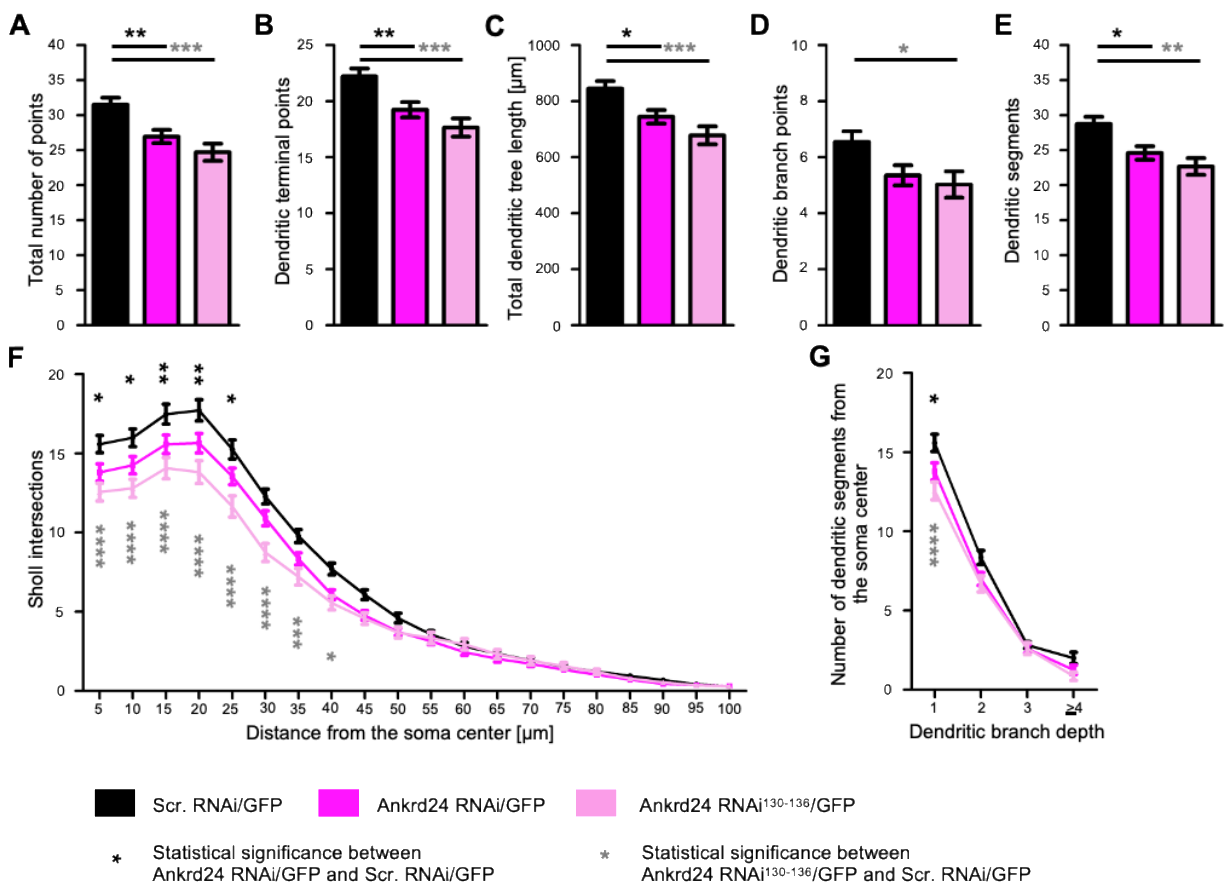


**Fig. 19. The loss-of-function phenotype of Ankrd24 in primary rat hippocampal neurons resulted in a significantly reduced dendritogenesis and dendritic arborization.** Quantitative analysis of dendritic arborization of primary rat hippocampal neurons at DIV6 (DIV4+2). The cells were transfected at DIV4 with Scr.RNAi/GFP, Ankrd24 RNAi/GFP or Ankrd24 RNAi[130-136]/GFP for 30 h, followed by 4% PFA fixation and immunostaining with anti-MAP2. Total number of points (A), dendritic terminal points (B), total dendritic tree length (C), dendritic branch points (D), dendritic segments (E), Sholl intersections (F), dendritic branch depth (G). The analysis showed that both Ankrd24 RNAi and Ankrd24 RNAi[130-136] led to a significant reduction in the total number of points, dendritic terminal points, total dendritic tree

length, dendritic segments, Sholl intersections (5-25 μm) and the number of dendritic branch segments from the soma center at dendritic branch depth '1', thus, leading to reduced dendritogenesis and dendritic arborization when compared to scrambled (Scr.) RNAi/GFP. Dendrites were considered as MAP2-positive structures ≥ 10 μm in length.  Analyses included 3 to 5 independent primary rat hippocampal neuron preparations: n=91 for Scr. RNAi/GFP, n=87 for Ankrd24 RNAi/GFP and n=47 for Ankrd24 RNAi[130-136]/GFP, where n represents number of cells. Data represent mean ± sem. One-way ANOVA with Tukey's test (A-E). Two-way-ANOVA with Bonferroni post-hoc test (F-G). *p < 0.05; **p < 0.01; ***p < 0.001; ****p < 0.0001.*

## 3.13 Incomplete rescue of Ankrd24 loss-of-function phenotype by the mutant lacking proline-rich sequence KKRKAPQPP

To further investigate whether the function of Ankrd24 in DIV6 primary rat hippocampal neurons was dependent on the interaction of its proline-rich motif, functional assays were extended by rescue attempts with Ankrd24 RNAi insensitive rescue mutants, Ankrd24 RNAi/Ankrd24x6$^{1-1041}$-GFP* (wildtype rescue mutant) and Ankrd24 RNAi/Ankrd24x6$^{1-1041\Delta273-286}$-GFP* (deletion rescue mutant), lacking KKRKAPQPP, respectively.

The quantitative neuromorphogenic analysis validated that the Ankrd24 loss-of-function phenotype was specifically due to the reduced levels of Ankrd24 as the Ankrd24 RNAi wildtype rescue mutant recovered the Ankrd24 knockdown-induced phenotype of reduced dendritic arborization completely. The phenotype of significantly reduced number of the total number of points and dendritic terminal points by Ankrd24 RNAi were rescued by Ankrd24 RNAi/Ankrd24$^{1-1041}$-GFP* as latter behaved similar to scrambled RNAi/GFP (Fig. 20A-B). Also, the feature of smaller dendritic tree length by Ankrd24 RNAi/GFP was recovered by Ankrd24 RNAi/Ankrd24$^{1-1041}$-GFP* with significant difference between Ankrd24 RNAi/GFP and Ankrd24 RNAi/Ankrd24$^{1-1041}$-GFP* (Fig. 20C). Dendritic branch points of the wildtype rescue mutant displayed a slight increase and a decrease in the number of points compared to Ankrd24 RNAi/GFP and scrambled RNAi/GFP, respectively (Fig. 20D). The significantly reduced dendritic segments by Ankrd24 RNAi/GFP was also recovered by Ankrd24 RNAi/Ankrd24$^{1-1041}$-GFP* as latter showed more dendritic segments than Ankrd24 RNAi/GFP (Fig. 20E). Analysis of Sholl intersections explicitly showed that the significantly reduced intersections by Ankrd24 RNAi at 5 μm, 15 μm and 20 μm distance from the soma

center were significantly increased by Ankrd24 RNAi/Ankrd24$^{1-1041}$-GFP* (Fig. 20F). Furthermore, the analysis of dendritic branch depth showed that the significantly reduced number of primary dendrites was rescued by Ankrd24 RNAi/Ankrd24$^{1-1041}$-GFP* with a significant difference between the Ankrd24 RNAi/GFP and Ankrd24 RNAi/Ankrd24$^{1-1041}$-GFP* (Fig. 20G). Altogether, the analysis confirmed that the morphological changes caused by Ankrd24 RNAi/GFP in the dendritic tree were indeed due to the knockdown of Ankrd24 as the wildtype rescue mutant was able to recover the same, displaying similar values as scrambled RNAi/GFP in the various parameters quantified and analysed.

Next, deletion rescue mutant lacking the proline-rich sequence KKRKAPQPP was investigated. The analysis demonstrated that the Ankrd24 RNAi/Ankrd24x6$^{1-1041\Delta273-286}$-GFP* showed significant reduction of the total number of points, similar to the number obtained by Ankrd24 RNAi/GFP (Fig. 20A). The number of dendritic terminal points observed by the deletion rescue mutant were also in similar range as Ankrd24 RNAi/GFP (Fig. 20B). So far, no rescue with these two parameters was observed by the deletion rescue mutant. Next, the parameter of the total dendritic tree length was analysed which showed a slight increase by the deletion rescue mutant compared to the Ankrd24 RNAi/GFP but with no statistical significance (Fig. 20C). However, dendritic branch points were significantly reduced by the deletion rescue mutant when compared to scrambled RNAi/GFP, and the reduced numbers were slightly lower than Ankrd24 RNAi/GFP (Fig. 20D). Furthermore, the deletion rescue mutant showed similar number of dendritic segments as Ankrd24 RNAi/GFP (Fig. 20E). Analysis of Sholl intersections revealed that the number of intersections by the deletion rescue mutant displayed an increasing and a decreasing trend when compared to Ankrd24 RNAi/GFP and wildtype rescue mutant, respectively (Fig. 20F) and this was consistent with the parameter dendritic branch depth '1' (Fig. 20G). While the parameters like total number of points and dendritic branch points were not recovered by the deletion rescue mutant, Sholl intersections and dendritic branch depth '1' showed a partial rescue by the same. It is important to note that the statistical analysis might have been affected by the lower number of neuronal cells analysed for deletion rescue mutant compared to the other conditions. Example of neurons with scrambled RNAi/GFP, Ankrd24 RNAi/GFP,

Ankrd24 RNAi/Ankrd24x6$^{1\text{-}1041}$-GFP* and Ankrd24 RNAi/Ankrd24x6$^{1\text{-}1041\Delta273\text{-}286}$-GFP* with their reconstructed dendritic arbor using Imaris 8.4.0 is represented in Fig. 20H.

Altogether, neuromorphogenic analysis with the rescue mutants demonstrated that the specific Ankrd24 knockdown effects could not be completely rescued by the deletion rescue mutant lacking the proline-rich sequence, Ankrd24 RNAi/Ankrd24x6$^{1\text{-}1041\Delta273\text{-}286}$-GFP*, thus, indicating the importance of KKRKAPQPP in the function of Ankrd24 in DIV6 primary rat hippocampal neurons.
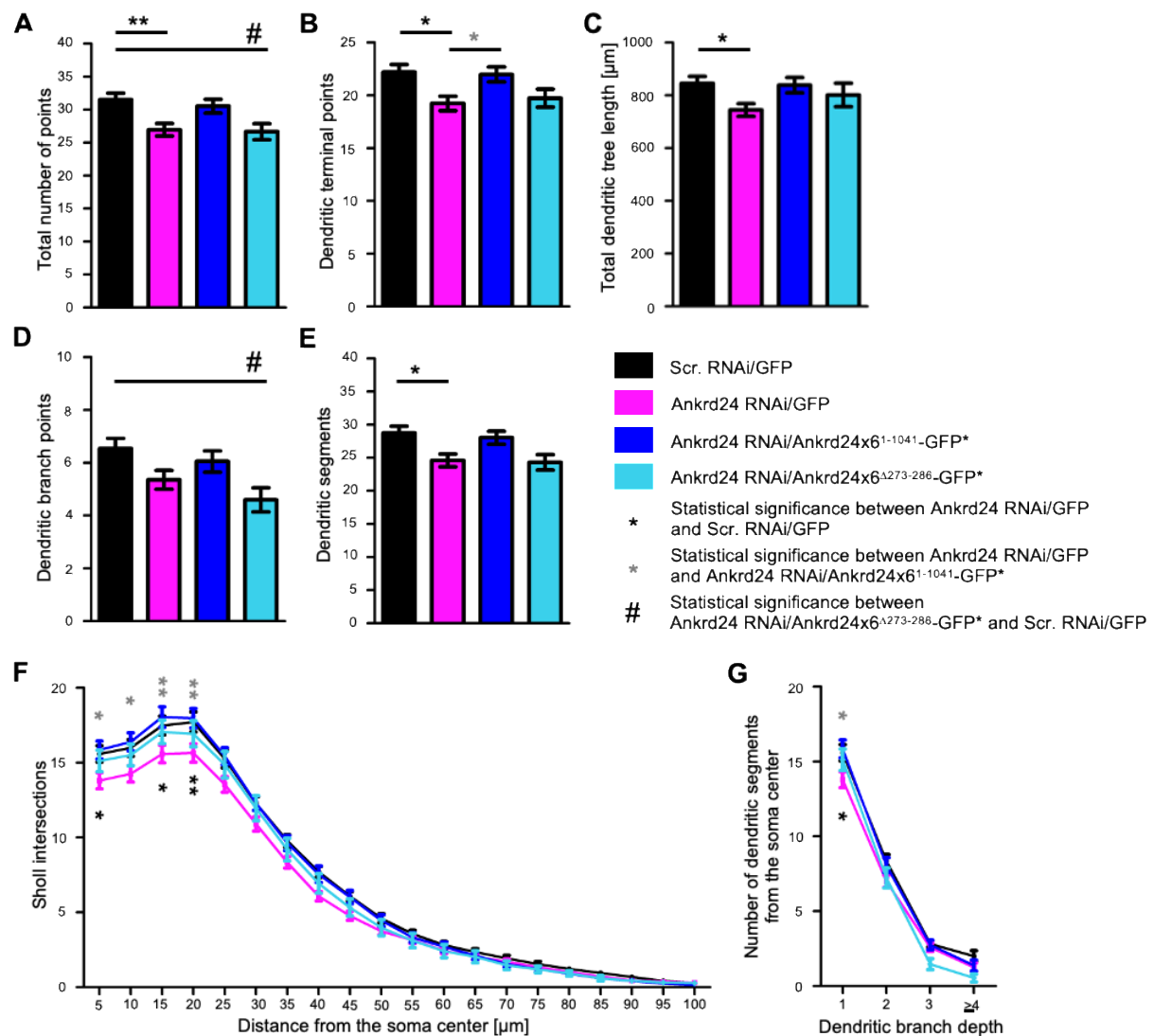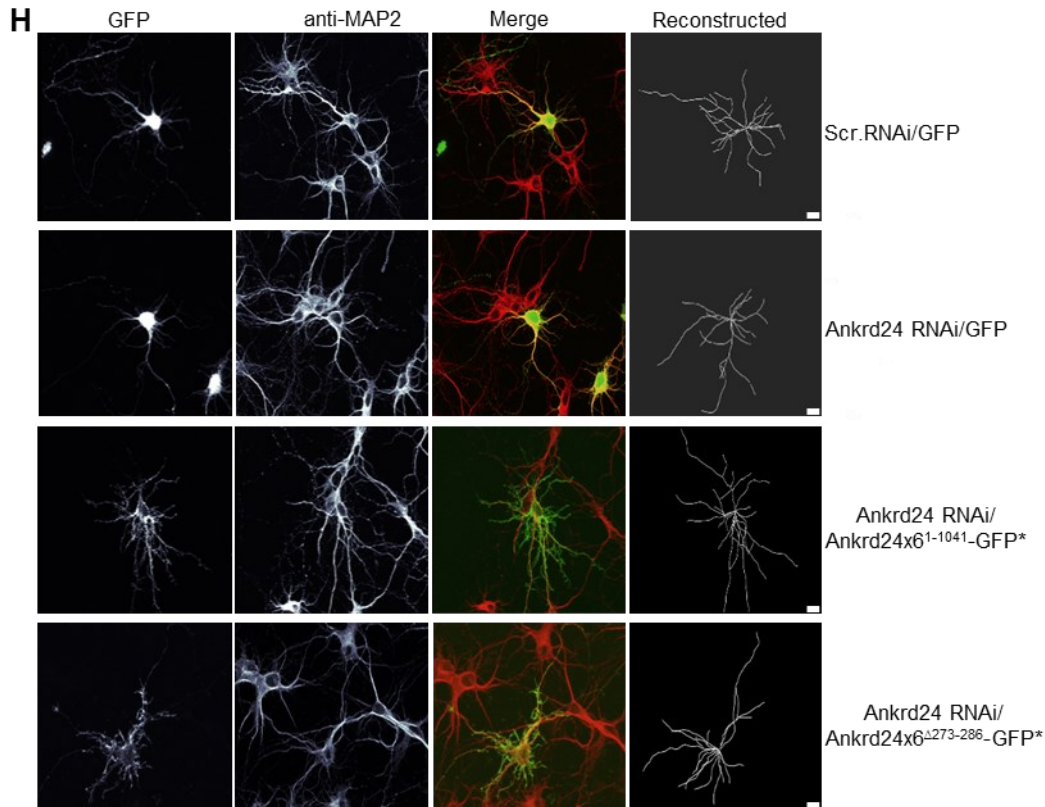
**Fig 20. The loss-of-function phenotype of Ankrd24 was only partially rescued by the mutant lacking the proline-rich sequence**. Quantitative analysis of dendritic arborization of primary rat hippocampal neurons at DIV6 (DIV4+2) was performed. The cells were transfected at DIV4 with Scr. RNAi/GFP, Ankrd24 RNAi/GFP, Ankrd24 RNAi/Ankrd24x6$^{1-1041}$-GFP* or Ankrd24 RNAi/Ankrd24x6$^{1-1041\Delta273-286}$-GFP* for 30 h, followed by 4% PFA fixation and immunostaining with anti-MAP2. Total number of points (A), dendritic terminal points (B), total dendritic tree length (C), dendritic branch points (D), dendritic segments (E), Sholl intersections (F), dendritic branch depth (G), representative images of DIV6 primary rat hippocampal neurons transfected with Scr. RNAi/GFP, Ankrd24 RNAi/GFP, Ankrd24 RNAi/Ankrd24x6$^{1-1041}$-GFP* or Ankrd24 RNAi/Ankrd24x6$^{1-1041\Delta273-286}$-GFP* (H). The analysis demonstrated that the significantly reduced Sholl intersections (5, 15, 20 μm) and the number of dendritic segments from the soma center at dendritic branch depth '1' by Ankrd24 RNAi/GFP were partially rescued by the deletion rescue mutant lacking the proline-rich sequence, Ankrd24 RNAi/Ankrd24x6$^{1-1041\Delta273-286}$-GFP*. Dendrites were considered as MAP2-positive structures ≥ 10 μm in length. Analyses included 3 to 5 independent primary rat hippocampal neuron preparations: n=91 for Scr. RNAi/GFP, n=87 for Ankrd24 RNAi/GFP, n=56 for Ankrd24 RNAi/Ankrd24x6$^{1-1041}$-GFP* and n=37 for Ankrd24 RNAi/Ankrd24x6$^{1-1041\Delta273-286}$-GFP*, where n represents number of cells. Cells for Scr. RNAi/GFP and Ankrd24 RNAi/GFP are same as in Fig. 19. Data represent mean ± sem. One-way ANOVA with Tukey's test (A-E). Two-way-ANOVA with Bonferroni post-hoc test (F-G). *p < 0.05; **p < 0.01. Scale bar, 10 μm (H).

# 4   Discussion

The N-Ank superfamily is a new class of membrane shaping proteins defined by their ability to bind and bend the lipid bilayer by incorporating their N-terminal amphipathic helix and ankyrin repeats (Wolf et al., 2019). N-Ank proteins are phylogenetically classified into two subfamilies, out of which Ankrd24 belongs to the smaller sub-family (Wolf et al., 2019). Ankrd24 had been an uncharacterised protein as no data were available on its membrane-binding abilities or its biological function. Therefore, this study investigated putative N-Ank properties of the Ankrd24 protein.

Dr. Wolf had described that ankycorbin's physiological function in primary rat hippocampal neurons was dependent on its domains (amphipathic helix, ankyrin repeat and coiled coil) and hypothesised that there might be other proteins which might have similar arrangement of domains which could explain an evolutionarily conserved mechanism behind bending and shaping of biomembranes (Wolf, 2018). Thus, Dr. Wolf performed domain-enhanced BLAST searches based on ankycorbin (UniProtKB Q9EP71) and was able to identify UACA (UniProtKB Q8CGB3), Ankrd24_2 (UniProtKB-Q80VM7, NCBI Reference Sequence NM_027480.3) along with 13 other proteins which comprised of the same specific arrangement of domains as ankycorbin (Wolf, 2018; Wolf et al., 2019).

## 4.1   The many isoforms of Ankrd24

The primers designed to obtain full-length Ankrd24_2 (UniProtKB Q80VM7) amplified nucleotide sequence corresponding to Ankrd24x6. *In silico* structure predicted Ankrd24x6 to have an N-terminal amphipathic helix, followed by an ankyrin repeat domain consisting of seven ankyrin repeats and a coiled coil domain, respectively. Ankrd24x6 also contained a proline-rich amino acid sequence (Fig. 2) belonging to the consensus 'KrrAPpPP'. Ankrd24x6 has a longer C-terminus than Ankrd24_2 due to the presence of exon 20 (Appendix 7.1). According to the NCBI data, several isoforms of Ankrd24 are predicted and Dr. Wolf was able to obtain partial sequences of Ankrd24x11 and Ankrd24x12 from the cDNA of 8-week-old mice brain (Wolf, 2018). *In vitro* reconstitution assays with liposomes demonstrated that unlike Ankrd24x11, Ankrd24x12

bound to the liposomes (Wolf, 2018) because of the presence of an N-terminal putative amphipathic helix corresponding to the amino acid sequence MKTLRARFKKT (same as Ankrd24x6). On the other hand, Ankrd24x11 has an amino acid sequence of MKQLCLCAAAS which does not form a putative amphipathic helix and thus, did not show binding to liposomes (Wolf, 2018). Both Ankrd24x12 and Ankrd24x6 comprise of exon 3 (Ankrd24x3 as a reference) while Ankrd24x11 has an alternative transcription start site (Fig. 3, Appendix 7.1). Ankrd24x6 consists of exon five-seven (Ankrd24x3 as a reference), which was absent in Ankrd24x12 and therefore, Ankrd24x6 has more nucleotides than Ankrd24x12. (PS)2-v2 prediction suggested three and seven ankyrin repeats in Ankrdx12 (data not shown) and Ankrd24x6, respectively. Ankrd24x21 and Ankrd24x22 are the only two isoforms which have truncated N-terminus and lack the proline-rich motif too. *Ankrd24* has predicted isoforms constituting putative amphipathic α helix and non-putative amphipathic helix like Ankrd24x12 and Ankrd24x11 or isoforms which differ in the number of ankyrin repeats like Ankrdx12 and Ankrd24x6 and there are also predicted isoforms which lack the proline-rich sequence like Ankrd24x21 and Ankrd24x22. Since partial nucleotide sequences of Ankrd24x11 and Ankrd24x12 were obtained from the cDNA of 8-week-old mice brain (Wolf, 2018), it will be interesting to investigate their full forms for their membrane-shaping abilities and physiological function. It could also be that isoforms of *Ankrd24* are expressed specific to a developmental stage or cell-type like family of neurexins as latter has several isoforms expressed in different types of neurons, which participate in diverse functions for neural connectivity (Missler & Südhof, 1998; Scheiffele et al., 2000; Ullrich et al., 1995). Taken together, an mRNA and protein expression profile of Ankrd24 in a development-stage and cell-type specific manner will help to understand the physiological relevance of Ankrd24 isoforms.

## 4.2   Ankrd24x6 and the smaller sub-family of the N-Ank superfamily

The smaller sub-family of the N-Ank superfamily comprise of ankycorbin, UACA, Ankrd35 and Ankrd24 (Wolf et al., 2019). Ankrd24x6 protein (XP_006514159.1) showed 50.63% percent identity with ankycorbin (UniProtKB Q9EP71) when the protein sequences were aligned using BLAST, while showing 43.91% percent identity with

Ankrd35 (UniProtKB E9Q9D8) and 37.22% percent identity with UACA (UniProtKB Q8CGB3), respectively. All the above aligned proteins belong to *Mus musculus* species. While all the four members of this smaller sub-family share the similarity of domains arrangement, only ankycorbin and Ankrd24x6 proteins share the presence of the proline-rich consensus. Both Ankrd35 and UACA comprise of five ankyrin repeats (Wolf et al., 2019), while both ankycorbin (Wolf et al., 2019) and Ankrd24x6 have seven.

## 4.3 Ankrd24x6, an N-Ank protein with distinct properties

Ankrd24x6 is a membrane-associating protein as shown by immunofluorescence microscopy analysis of HeLa cells (Fig. 4), along with the subcellular fractionation of HEK293 cells (Fig. 5). Although both full-length Ankrd24x6, Ankrd24x6$^{1-1041}$-GFP and the N-Ank module of Ankrd24x6, Ankrd24x6$^{1-285}$-GFP were colocalised with the membrane marker, mcherryF on the same filopodia-like membrane structures in HeLa cells (Fig. 4), there were fewer of such structures observed with the N-Ank module than with the full length. The subcellular fractionations of Ankrd24x6$^{1-1041}$-GFP and Ankrd24x6$^{1-285}$-GFP were detected in the membrane protein containing fractions (P2, P2') of HEK293 cells along with mcherryF (Fig. 5), however, relatively high amount of Ankrd24x6$^{1-285}$-GFP was observed in S2 fraction compared to its P2, P2' fraction and to the subcellular fractionations of the full-length. These results of observing fewer protrusive membrane structures colocalized with the N-Ank module and mcherryF are similar to ankycorbin's N-Ank module ankycorbin$^{1-252}$ when compared to the full-length GFP-fusion proteins (Wolf, 2018). The subcellular fractionations of ankycorbin$^{1-252}$ was observed more in S2 than the membrane protein containing fractions (Wolf, 2018). These results suggest that the N-Ank module of both ankycorbin and Ankrd24x6 has a weaker binding to the membrane compared to their full-length. The N-Ank module of other members of the N-Ank superfamily, UACA$^{1-263}$-GFP (Wolf, 2018), Ankrd20A1$^{1-227}$-GFP, mouse Ankrd26$^{1-208}$-GFP (Hofbrucker-MacKenzie, 2021) also showed colocalisation with mCherryF in the apical protrusions of HeLa cells. Altogether, the results indicated that the N-Ank module of the N-Ank proteins associate with the membrane while suggesting that other domains in the protein aid in stronger association

as the full-length N-Ank proteins showed better colocalisation with the membrane marker mcherryF.

Furthermore, *in vitro* reconstitution experiments of the N-Ank module of Ankrd24x6 with liposomes showed its direct lipid association. It was demonstrated that the putative amphipathic helix is crucial for the binding of the N-Ank module of Ankrd24x6 (Fig. 6) as the mutant lacking it significantly reduced the liposome binding ability from ~40% to ~2% as observed in liposome copelleting assays. This property of Ankrd24x6 is similar to mouse Ankrd26 (Hofbrucker-MacKenzie, 2021) where Ankrd26$^{1-208}$ showed ~73.5% binding to liposomes which was significantly reduced to ~1.3% with Ankrd26$^{11-208}$. The N-Ank module of ankycorbin, ankycorbin$^{1-252}$ had shown ~80% binding to liposomes which was significantly reduced to ~8% by the amphipathic helix-disrupting mutant, ankycorbin$^{1-252\ K2A,K5A,K7A,R9A,K10A}$ (Wolf et al., 2019). Also, UACA$^{1-263}$ demonstrated ~90% binding to liposomes which was diminished by the mutant lacking the putative amphipathic helix, UACA$^{41-263}$ (Wolf et al., 2019). Dr. Hofbrucker-MacKenzie showed that the N-Ank module of human Ankrd26, Ankrd26$^{1-217}$ had a liposome binding of ~90% which was significantly reduced to ~50% by Ankrd26$^{45-217}$ (Hofbrucker-MacKenzie, 2021). Similar behaviour was also observed with Ankrd20A1$^{1-227}$, where liposome binding ability of ~80% was significantly reduced to ~55% by Ankrd20A1$^{23-227}$ (Hofbrucker-MacKenzie, 2021). Additionally, Ankrd24x6$^{1-285}$ achieved half-maximal binding concentration at 24.94 µg LUVs (Fig. 10) while ankycorbin$^{1-400}$ achieved the same at 3.2 µg LUVs (Wolf et al., 2019). Both Ankrd24x6$^{10-285}$ (Fig. 10) and ankycorbin$^{17-400}$ (Wolf et al., 2019), the mutants lacking the amphipathic helix, did not show any binding to the increasing amounts of LUVs. As these studies have not been performed with other members of N-Ank family, it is difficult to conclude on the property of binding affinity of the N-Ank superfamily, however, results do indicate that members of N-Ank superfamily bind to membrane with different affinity and that the presence of the putative amphipathic helix significantly increases the binding ability of the N-Ank proteins.

The predicted amphipathic $\alpha$ helix in Ankrd24x6 is followed by the predicted seven ankyrin repeats which form the ankyrin repeat domain. Based on the experimental evidence of the N-Ank proteins ankycorbin, UACA and Ankrd20A1, it was postulated that the ankyrin repeat domain in N-Ank proteins prefer higher membrane curvatures (Wolf et al., 2019). As the number of repeats and the repeats at the terminal end might influence protein's folding and thus its binding ability to the membrane (Barrick, 2009; Ferreiro et al., 2005; Li et al., 2006), wildtype Ankrd24x6 containing seven (Ankrd24x6[1-285]) and the first five (Ankrd24x6[1-222]) ankyrin repeats along with their respective mutants lacking the amphipathic helix were checked for their liposome binding ability. Both Ankrd24x6[1-285] and Ankrd24x6[1-222] showed ~40% binding to the LUVs (Fig. 6). Ankrd24x6[1-285] demonstrated ~55% and Ankrd24x6[1-222] showed ~30% binding to both LUVs and SUVs, respectively (Fig. 7). However, Ankrd24x6[1-285] demonstrated ~50% and ~40% binding to 50 µg LUVs and SUVs, respectively when increasing amounts of liposomes were offered (Fig. 10). The apparent inconsistency of the liposome binding ability of proteins could be due to the difference in the batch of protein purification, liposome preparation or the difference in the volume of the supernatant and the pellet analysed as SUVs have a lose pellet (*see* section 2.2.16). Also, the change in RT could have influenced the binding ability of liposomes and proteins as during *in vitro* reconstitution assays with liposomes, the proteins and liposomes were incubated at RT (*see* section 2.2.16) and it has been reported that the membrane properties of liposomes are sensitive to the temperature (Sułkowski et al., 2005; Wu et al., 2014). Thus, it is difficult to conclude whether the N-Ank module of Ankrd24x6 with difference in the number and lack of terminal ankyrin repeats (Ankrd24x6[1-285] and Ankrd24x6[1-222]) effected the binding ability to liposomes. Additionally, the ankyrin repeats of Ankrd24x6, Ankrd24x6[10-285] and Ankrd24x6[10-222] demonstrated binding to neither LUVs or SUVs (Fig. 6, 8, 10). Ankrd24x6[10-285], the mutant lacking the amphipathic helix did not show any binding to increasing amounts of LUVs or SUVs (Fig. 10), highlighting the importance of amphipathic helix. This behaviour of the mutant was similar to ankycorbin[17-400] with LUVs i.e., the values remained not determined, however, ankycorbin[17-400] did achieve half-maximal binding at 5.6 µg SUVs (Wolf et al., 2019).

The peculiar feature of the Ankrd24x6 mutants, which lack the putative amphipathic helix and thus contain only the ankyrin repeats and showing no preference towards higher curvature SUVs is strikingly different to other N-Ank proteins like UACA[41–263] which showed a significant increase in liposome binding to SUVs when compared to LUVs (Wolf et al., 2019). Similarly, Ankrd20A1[23-227], mouse Ankrd26[11-208], human Ankrd26[45-217] (Hofbrucker-MacKenzie, 2021) also demonstrated their preference to SUVs by showing a significant increase in binding to SUVs than LUVs. The mutant of ankycorbin which lacked the amphipathic helix, Ankycorbin[17-400] also showed significant increase in binding to SUVs when compared to LUVs (Wolf et al., 2019). This indicates that the property of ankyrin repeats sensing and binding to membranes is not unanimous in the N-Ank family of proteins and that Ankrd24x6 might just be one of members displaying the property of ankyrin repeats showing no preference towards SUVs. It is quite plausible that perhaps other isoform of Ankrd24 display the property of ankyrin repeats in sensing and binding to the membranes. Predicted isoforms like Ankrd24x5 (XP_006514158.1) and Ankrd24x11 (XP_006514164.1), which lack the putative amphipathic helix and also differ in the number of ankyrin repeats as Ankrd24x5 has seven ankyrin repeats while Ankrd24x11 has five, predicted by (PS)2-v2 (data not shown) could demonstrate its association with liposomes via their ankyrin repeats. It could be a compensation mechanism for associating with the membrane as the above mentioned isoforms lack the amphipathic helix. Another set of ankyrin repeats and amphipathic helix containing proteins has been reported (Kitamata et al., 2019), where it was demonstrated that ANKHD1, a protein containing N-terminal 15 ankyrin repeats, could dimerise and latter 10 repeats along with an adjacent C-terminal amphipathic helix could bind and vesiculate lipid membrane. Ankyrin repeats were also reported for their interaction with other proteins and sugar (Islam et al., 2018), which has not been analysed for Ankrd24 yet.

Taken together, the *in vitro* analysis of the N-Ank properties of Ankrd24x6 suggest that the function of the amphipathic helix is similar to other members of the family while the feature of ankyrin repeats, which do not demonstrate any binding to the liposome membrane is an exception. As the structure of a protein is the key to its biological

function (Martin et al., 1998; Yon, 2001), it will be interesting to perform X-ray crystallography to confirm if the predicted secondary structure of Ankrd24x6 indeed comprises of amphipathic $\alpha$ helix, seven ankyrin repeats and two coiled-coil domains. Furthermore, simulation studies with models like $C^{\alpha}$-based Gō (Takada, 2019; Taketomi et al., 1975) can help understand the mechanism of Ankrd24x6 protein folding. In addition, simulation studies could also be performed with only ankyrin repeats to understand the coupling mechanism between the repeats which results in their successful folding.

Moreover, Ankrd24x6 binds to the membrane via hydrophobic interaction and lack any electrostatic interaction for the same (Fig. 9). This feature is similar to other N-Ank members like Ankycorbin[1-252] and UACA[1–263] (Wolf et al., 2019), mouse Ankrd26[1-208], human Ankrd26[1-217] and Ankrd20A1[1-227] (Hofbrucker-MacKenzie, 2021). Ankrd24x6[1-285] (Fig. 9) showed significant increase in binding to the membrane at 250 mM NaCl concentration while mouse Ankrd26[1-208] showed significant increase at 200 mM and 250 mM NaCl concentration (Hofbrucker-MacKenzie, 2021). These results indicate that the N-Ank proteins Ankrd24x6 and mouse Ankrd26 might have a different mechanism of action as electrostatic interactions play critical role in protein folding, binding and its physiological function (Zhou & Pang, 2018). Therefore, to better understand the behaviour of Ankrd24x6 and mouse Ankrd26, it would be necessary to perform salt-extraction assay by diluting the proteins in HN buffer containing 250 mM NaCl instead of 150 mM and then to further increase the concentration to 300 mM, so that it can be concluded whether it is the increased binding or the precipitation of the protein due to Hofmeister effect (Zhou & Pang, 2018).

A sophisticated technique of freeze-fracture electron microscopy was used to visualize and analyse the shape of liposomes incubated with proteins. Liposomes incubated with Ankrd24x6[1-285] were shaped to an average diameter of ~300 nm, unlike its mutant, Ankrd24x6[10-285] or GST which shaped the liposomes to an average diameter of ~430 nm and ~450 nm, respectively (Fig. 11). The reduced average diameter of Ankrd24x6[1-285] was attributed by the increase in the percentage of total number of 60.00-79.99 nm

diameter liposomes and a significant increase of 0-499.99 nm diameter liposomes when compared to GST (Fig. 11). Ankycorbin[1–252] shaped the liposomes to an average diameter of ~220 nm which was smaller than the control (liposomes with no protein), which had an average diameter size of ~400 nm (Wolf et al., 2019). The decrease in the size of liposomes incubated with Ankycorbin[1–252] was contributed by the accumulation of 20.00-50.00 nm diameter liposomes (Wolf et al., 2019). Other N-Ank members like UACA[1–263] also reduced the average diameter size of liposomes from ~300 nm (liposomes with no protein) to ~150 nm which was due to the increase in the percentage of total number of liposomes in the range of 30.00-50.00 nm (Wolf et al., 2019). Mouse Ankrd26[1-208] shaped the liposomes to an average diameter size of ~300 nm with accumulation of 10.00-200.00 nm diameter liposomes compared to the control (liposomes with no protein) which had an average diameter of 600 nm (Hofbrucker-MacKenzie, 2021). The diameter of liposomes incubated with human Ankrd20A1[1-227] displayed an average diameter size of ~300 nm, while liposomes with no protein had an average diameter of ~530 nm. Human Ankrd20A1[1-227] showed an increase in the percentage of total number of 60.00-80.00 nm diameter liposomes (Hofbrucker-MacKenzie, 2021). These studies highlight the diversity of N-Ank membrane shapers in shaping the membrane to different curvature sizes, thus indicating their respective relevance in *in vivo* functions.

Ankrd24x6 had furthermore demonstrated to have the ability to self-oligomerise via its putative two coiled coil domains from aa 289-490 and 746-1009, respectively (Fig. 12). To further understand if either of the two coiled coil domain is sufficient for self assembly or if both are necessary, cross-linking experiments could be performed with the respective deletion mutants. The property of Ankrd24 of oligomerisation is similar to other N-Ank members like ankycorbin (Wolf et al., 2019) and human Ankrd26 (Hofbrucker-MacKenzie, 2021). Endogenous ankycorbin (Wolf et al., 2019) and Ankrd26 (Hofbrucker-MacKenzie, 2021) were also detected as clusters in nanodomains at the membrane of primary rat hippocampal neurons, when the ultrastructure was observed with high-resolution technique of FRIL and TEM. The observation of ankycorbin and Ankrd26 in clusters indicated their respective potential of self-

association. These studies with N-Ank members characterised so far, indicate that oligomerisation is also one of their common properties. It will be fascinating to test whether members of N-Ank family could oligomerise with each other to maybe act as a molecular scaffold as coiled coil domains in proteins enable both intra- and inter-molecular interactions which are important for diverse biological function (Truebestein & Leonard, 2016). Coiled coil domains can act as molecular spacers as in Giantin (Lesa et al., 2000), molecular rulers like in ROCK2 (Truebestein et al., 2015) or as molecular scaffolds in tropomyosin (Truebestein & Leonard, 2016). Giantin is a 250 nm long protein, belonging to the family of tethering proteins called Golgins (Lesa et al., 2000; Witkos & Lowe, 2016). C-terminus of Giantin binds to the Golgi membrane and the other end tethers vesicle in the cytoplasm, thus, acting as a molecular spacer (Lesa et al., 2000; Truebestein & Leonard, 2016). ROCK2 is a 120 nm long protein with 107 nm coiled coil domain which acts as a molecular ruler by precisely localising the kinase domain of ROCK2 from the plasma membrane to its substrate in the actin cytoskeleton (Truebestein et al., 2015). Tropomyosin, a coiled coil domain containing protein in isolated state is ~40 nm long and has a dynamic persistence length of ~460 nm (Li et al., 2010). In skeletal muscle, tropomyosin acts as a molecular scaffold by exposing myosin-binding sites on tropomyosin-decorated actin filament (Behrmann et al., 2012; Truebestein et al., 2015).

Ankrd24x6 via its proline-rich sequence KKRKAPQPP binds to the SH3 domain of brain enriched syndapin I (Fig. 14), which is involved in diverse processes like in actin remodelling (Qualmann et al., 1999; Qualmann & Kelly, 2000), or in vesicle trafficking in neuronal and non-neuronal cells (Braun et al., 2005; Kessels & Qualmann, 2004). The interaction between Ankrd24 and syndapin I was also observed in 21-week-old-rat brain tissue lysates (Fig. 15). Interaction with syndapin I had also been observed with the N-Ank protein ankycorbin which has a proline-rich sequence KKRKAPPPP (Wolf, 2018). These findings supports Schwintzer (2012) that a proline-rich motif with consensus 'KrrAPpPP' can bind to the SH3 domain of syndapin I (Schwintzer, 2012). Cobl was identified as the syndapin I interacting partner in a yeast two-hybrid analysis and was shown to be a powerful novel actin nucleator which controlled the development and

morphology of the dendritic tree (Ahuja et al., 2007). Both Cobl and its relative Cobl-like via their proline-rich motif with consensus 'KrRAPpPP' were shown to bind to the SH3 domain of syndapin I (Schwintzer, 2012) and thus, *in silico* analysis was performed using the consensus of 'KrRAPpPP' motifs from Cobl and Cobl-like, K-[RAGS]-[RKQ]-A-P-[PLAS]-P-P to identify the potential interacting partners of syndapin I. The results revealed 201 sequences from vertebrates, out of which 190 sequences aligned to proteins Ankrd24, ankycorbin, Cobl, Cobl-like, Eps15 homology domain-binding protein 1 and Rhotekin 2 as the putative syndapin I-interacting partners (Schwintzer, 2012). Cobl-like demonstrated formation of the dendritic branches in primary rat hippocampal neurons (Izadi et al., 2017) while Rhotekin 2, which is highly expressed in brain was reported to be localised at the synapses of primary rat hippocampal neurons (Ito et al., 2006).

## 4.4 The N-Ank protein Ankrd24 plays role in dendritogenesis of primary rat hippocampal neurons

Since the mRNA expression of Ankrd24 is high in human and mouse brain (Uhlén et al., 2015) and as the sequence of full-length Ankrd24x6 was obtained from the cDNA of 8-week-old mice brain, Ankrd24 was investigated for its function in primary rat hippocampal neurons. Overexpression of Ankrd24x6 led to a significant increase of primary dendrites in DIV6 primary rat hippocampal neurons (Fig. 17) whereas ankycorbin in similar conditions led to a significant increase in dendritic arborization (Wolf et al., 2019). The increase in dendritic arborization was contributed by the significant increase in dendritic branch and terminal points, and Sholl intersections (5-30 µm) when compared to the GFP, used as a control (Wolf et al., 2019). Interestingly, knocking down of Ankrd24 by Ankrd24 RNAi/GFP in primary rat hippocampal neurons led to a significant reduction of the total number of points, dendritic terminal points, total dendritic tree length, dendritic segments, Sholl intersections (5-25 µm) and primary dendrites, which all contributed in a smaller dendritic arbor when compared to scrambled RNAi/GFP (Fig. 19). It is difficult to compare literature on primary dendrites of rat hippocampal neurons as the method of analysis or the age are different (Chen et al., 2010). Loss-of-function phenotype of the

N-Ank protein ankycorbin included significantly reduced dendritic branch and terminal points, and fewer Sholl intersections (Wolf et al., 2019). Both Ankrd24 (Fig. 20) and ankycorbin (Wolf et al., 2019) loss-of-function phenotypes were specific, as they were completely rescued by the re-expression of their respective RNAi insensitive wildtype rescue mutants. Ankrd24 overexpression phenotype was mild, which might postulate to Ankrd24 having an autoinhibition mechanism or the fact that due to membrane trafficking, overexpression phenotype was difficult. Also, Ankrd24 RNAi targeted all Ankrd24 isoforms in rat except the predicted isoform 1, which if it exists can affect the knockdown effects. Other N-Ank proteins like Ankrd26 and Ankrd20A1, which are both expressed in rat brain (Hofbrucker-MacKenzie, 2021) are yet to be functionally characterized.

The knockdown effect of Ankrd24 (Fig. 20) and ankycorbin (Wolf, 2018) in primary rat hippocampal neurons at DIV6 were rescued incompletely by the deletion rescue mutants lacking proline-rich motif of consensus 'KrrAPpPP'. Ankrd24 deletion rescue mutant failed to completely rescue the Ankrd24 loss-of-function phenotype of reduced number of the total number of points, dendritic terminal points and segments. Parameters like Sholl intersections and the number of primary dendrites showed an increasing trend by Ankrd24 deletion rescue mutant when compared to Ankrd24 RNAi/GFP (Fig. 20). Additionally, significant reduction of dendritic branch points was observed with this deletion rescue mutant in comparison to scrambled RNAi/GFP. The statistical analysis could have been influenced by the fewer number of neuronal cells investigated for the Ankrd24 deletion rescue mutant compared to the other conditions (Fig. 20), therefore, it will be important to analyse more number of cells to be sure for the phenotype. Ankycorbin showed partial compensation of the loss-of-function phenotype of dendritic branch and terminal points, and Sholl intersections by the deletion rescue mutant lacking the proline-rich motif (Wolf, 2018). These functional studies highlight the importance of the proline-rich motif in the physiological function of both Ankrd24 and ankycorbin in early dendritogenesis of primary rat hippocampal neurons.

Syndapin I, a brain enriched protein which shows increase in its expression with age (Plomann et al., 1998; Qualmann et al., 1999), has been shown to be crucial for axon and dendritic arbor development (Dharmalingam et al., 2009). F-BAR domain of syndapin I binds to the membrane (Dharmalingam et al., 2009) and its SH3 domain binds to the proline-rich motif of consensus 'KrrAPpPP' of N-Ank proteins (Ankrd24x6 and ankycorbin (Wolf, 2018)), Cobl and Cobl-like (Schwintzer, 2012). Syndapin I loss-of-function in primary rat hippocampal neurons resulted in increased length of axon and branching while gain-of-function induced formation and branching of dendrites (Dharmalingam et al., 2009). SH3 domain of syndapin I binds to proline-rich motif RRQAPPPP of dynamin I and thus regulate the process of synaptic vesicle endocytosis (Anggono & Robinson, 2007) while associates with proline-rich motif RKKAPPPP of ProSAP1/SHANK2 in the postsynapse. Neurons of syndapin I knockout mice displayed reduced density of dendritic spines and synapse formation (Schneider et al., 2014). Syndapins also self-associates and form dimers (Kessels & Qualmann, 2006) and additionally, syndapin I was also observed in nanoclusters at the spines of hippocampal neurons by high-resolution TEM (Schneider et al., 2014). Syndapin I knockout mice showed defects in synaptic plasticity with absence of long term potentiation and impaired long term depression, leading to schizophrenia-like symptoms (Koch et al., 2020). Both Cobl and Cobl-like associate with each other only in the presence of syndapin I, which acts as a bridging component between them and thus, all three acts in a coordinated manner to induce dendritic branches in developing neurons (Izadi et al., 2021).

Taken together, these studies with syndapin I indicate that it probably acts like a scaffold by F-BAR domain mediated oligomerisation and binding to the membrane while associating with different proteins via its SH3 domain, thus, regulating diverse biological processes (Qualmann et al., 2011). Since N-Ank proteins Ankrd24 and ankycorbin demonstrated binding to the SH3 domain of syndapin I and as the deletion rescue mutant (lacking the proline-rich motif) of both Ankrd24 and ankycorbin failed to completely rescue their loss-of-function phenotype, it will be interesting to test the hypothesis whether syndapin I interaction with Ankrd24 is important for the formation of

primary dendrites. To test the hypothesis, Ankrd24 could be overexpressed in the neurons of syndapin I knockout mice and if the phenotype is an increase in primary dendrites with reduced dendritic branches, it will indicate that Ankrd24 functions independent of syndapin I interaction. Additionally, a phenotype of reduced primary dendrites and increased dendritic branches in cells which have reduced Ankrd24 expression and overexpressed syndapin I would indicate and verify the same. N-Ank proteins Ankrd24 and ankycorbin (Wolf et al., 2019) induce the formation of primary dendrites and dendritic branches, respectively while syndapin I not only regulate synaptic vesicle endocytosis but is also involved in the axonogenesis, dendritogenesis and formation of spines (Dharmalingam et al., 2009; Qualmann et al., 1999; Schneider et al., 2014). Ankycorbin's (Wolf et al., 2019) and syndapin's expression (Plomann et al., 1998; Qualmann et al., 1999) in mice brain reduces and increases with age, respectively and both Ankrd24x6 and ankycorbin can interact with syndapin I. Therefore, it will be interesting to know the protein expression profile of Ankrd24 in the mice brain as the age advances to know if Ankrd24 has any other potential function in mature neurons.

*In vitro* assays with the N-Ank module and full-length of Ankrd24x6 have thus far shown that amphipathic helix is important for binding to the membrane and coiled coil domains mediate self-association but the physiological relevance of these domains in Ankrd24's function in hippocampal neurons is still unknown. Therefore, functional assays with hippocampal neurons can be performed by investigating if the rescue mutants lacking either amphipathic helix, ankyrin repeats, one or both coiled coil domain are still able to retain the phenotype. Furthermore, hydrophobic amino acids in the predicted amphipathic helix of Ankrd24x6 could be mutated to alanine to check if the N-Ank module still retains the binding to the membrane. This will affirmatively infer that it is indeed the interaction of the hydrophobic amino acids into one of the leaflets of the membrane that enables the binding. Thereafter, a conclusion could be made of their physiological relevenace by testing if the knockdown phenotype of Ankrd24 is still rescued. None of the rescue mutants of ankycorbin lacking either amphipathic helix, ankyrin repeats or coiled coil domain were able to show ankycorbin-mediated dendrite

branching in primary rat hippocampal neurons, thus demonstrating that each domain is quinessential for ankycorbin's function in the development of dendritic arbor (Wolf et al., 2019).

Since RNA transcriptomics studies have been vastly increased in recent years, *Ankrd24* has been reported to be regulated in several diseases like progeria (Sola-Carvajal et al., 2019), cancer (Dausinas et al., 2020; Giraldi et al., 2020; Liu et al., 2021; Wang et al., 2019), congenital heart disease (Matos-Nieves et al., 2021) and in endoplasmic reticulum stress (Bartoszewski et al., 2020). It will be interesting to investigate whether Ankrd24's membrane association and membrane-shaping abilities are important for any of these above pathological diseases. Also, defects in ankyrin repeats of a protein can lead to diseases like cancer (Tang et al., 2003; Löw et al., 2007; Mosavi et al., 2004).

So far, no data has been reported on biochemistry or functional analysis of Ankrd24 in *Rattus norvegicus* or *Mus musculus* and this is the first study to characterise Ankrd24 via biochemistry and neurofunctional analysis.

# 5 Conclusion

In conclusion, this study confirms the postulation of phylogenetic relationship that Ankrd24 is indeed an N-Ank protein with distinct characteristics. Ankrd24x6 is expressed in the brains of 8-week-old mice and could be found membrane-associated by subcellular fractionation and colocalisation studies. Biochemical analysis and ultrastructure investigations of the N-Ank module of Ankrd24x6 like those of other members of the N-Ank superfamily was shown to bind and shape the liposomes membrane with amphipathic helix being crucial for binding to the membrane. However, unlike other members of the N-Ank superfamily ankycorbin (Wolf et al., 2019), UACA (Wolf et al., 2019), Mus musculus Ankrd26, human Ankrd26 and Ankrd20A1 (Hofbrucker-MacKenzie, 2021), the ankyrin repeats of Ankrd24x6 alone neither displayed binding to the liposome's membrane nor any potential involvement of electrostatic interaction. The two putative coiled coil domains at the C-terminus of Ankrd24x6 demonstrated the ability to self-associate. These findings indicate that perhaps, in addition to the N Ank module sensing, binding, and shaping the membrane, oligomerisation is also one of the common features of the N-Ank proteins. Additonally, it was revealed that Ankrd24x6 via its consensus of proline-rich motif 'KrrAPpPP' binds to the SH3 domain of syndapin I, another membrane shaping protein which is vital for brain development.

Investigation of Ankrd24 function in primary rat hippocampal neurons at DIV6 unveiled that overexpression of Ankrd24x6 induced formation of primary dendrites while loss-of-function caused reduced dendritogenesis with less primary dendrites. The loss-of-function was precisely due to the knockdown of Ankrd24 as the re expression of silently mutated, RNAi insensitive wildtype Ankrd24x6 mutant completely rescued the loss-of-functions phenotype in the cultured neurons. Furthermore, the rescue mutant lacking the 'KrrAPpPP' motif showed an incomplete rescue of the Ankrd24 knockdown phenotype, indicating the importance of proline-rich motif in Ankrd24's function in developing neurons.

# 6 References

Ahuja, R., Pinyol, R., Reichenbach, N., Custer, L., Klingensmith, J., Kessels, M., & Qualmann, B. (2007). Cordon-Bleu Is an Actin Nucleation Factor and Controls Neuronal Morphology. *Cell*, 131(2), 337-350.

Akbarzadeh, A., Rezaei-Sadabady, R., Davaran, S., Joo, S., Zarghami, N., Hanifehpour, Y., Samiei, M., Kouhi, M., & Nejati-Koshki, K (2013). Liposome: classification, preparation, and applications. *Nanoscale Research Letters*, 8(1).

Anantharamaiah, G. (1986). [36] Synthetic peptide analogs of apolipoproteins. *Methods In Enzymology*, 627-647.

Anggono, V., & Robinson, P. (2007). Syndapin I and endophilin I bind overlapping proline-rich regions of dynamin I: role in synaptic vesicle endocytosis. *Journal of Neurochemistry*, 102(3), 931-943.

Bai, X., Meng, G., Luo, M., & Zheng, X. (2012). Rigidity of Wedge Loop in PACSIN 3 Protein Is a Key Factor in Dictating Diameters of Tubules. *Journal of Biological Chemistry*, 287(26), 22387-22396.

Barrick, D. (2009). Biological Regulation via Ankyrin Repeat Folding. *ACS Chemical Biology*, 4(1), 19-22.

Bartoszewski, R., Gebert, M., Janaszak-Jasiecka, A., Cabaj, A., Króliczewski, J., Bartoszewska, S., Sobolewska, A., Crossman, D., Ochocka, R., Kamysz, W., Kalinowski, L., Dąbrowski, M., & Collawn, J. (2020). Genome-wide mRNA profiling identifies RCAN1 and GADD45A as regulators of the transitional switch from survival to apoptosis during ER stress. *The FEBS Journal*, 287(14), 2923-2947.

Behrmann, E., Müller, M., Penczek, P., Mannherz, H., Manstein, D., & Raunser, S. (2012). Structure of the Rigor Actin-Tropomyosin-Myosin Complex. *Cell*, 150(2), 327-338.

BLAST: Basic Local Alignment Search Tool. Blast.ncbi.nlm.nih.gov. (2021). Retrieved 19 May 2021, from https://blast.ncbi.nlm.nih.gov/.

Bradford, M. (1976). A rapid and sensitive method for the quantitation of microgram quantities of protein utilizing the principle of protein-dye binding. *Analytical Biochemistry*, Volume 72(Issues 1–2), 248-254.

Bradke, F., & Dotti, C. (2000). Establishment of neuronal polarity: lessons from cultured hippocampal neurons. *Current Opinion in Neurobiology*, 10(5), 574-581.

Braun, A., Lacy, M., Ducas, V., Rhoades, E., & Sachs, J. (2017). α-Synuclein's Uniquely Long Amphipathic Helix Enhances its Membrane Binding and Remodeling Capacity. *The Journal of Membrane Biology*, 250(2), 183-193.

Braun, A., Pinyol, R., Dahlhaus, R., Koch, D., Fonarev, P., Grant, B., Kessels, M., & Qualmann, B. (2005). EHD Proteins Associate with Syndapin I and II and Such Interactions Play a Crucial Role in Endosomal Recycling. *Molecular Biology of The Cell*, 16(8), 3642-3658.

Brewer, G., Torricelli, J., Evege, E., & Price, P. (1993). Optimized survival of hippocampal neurons in B27-supplemented neurobasal, a new serum-free medium combination. *Journal of Neuroscience Research*, 35(5), 567-576.

Castagnoli, L., Costantini, A., Dall'Armi, C., Gonfloni, S., Montecchi-Palazzi, L., Panni, S., Paoluzi, S., Santonico, E., & Cesareni, G. (2004). Selectivity and promiscuity in the interaction network mediated by protein recognition modules. *FEBS Letters*, 567(1), 74-79.

Chen, C., Hwang, J., & Yang, J. (2009). (PS)2-v2: template-based protein structure prediction server. *BMC Bioinformatics*, 10(1).

Chen, N., Newcomb, J., Garbuzova-Davis, S., Sanberg, C., Sanberg, P., & Willing, A. (2010). Human Umbilical Cord Blood Cells Have Trophic Effects on Young and Aging Hippocampal Neurons in Vitro. *Aging And Disease*, 1(3), 173-190.

Chen, Z., Zhu, C., Kuo, C., Robustelli, J., & Baumgart, T. (2016). The N-Terminal Amphipathic Helix of Endophilin Does Not Contribute to Its Molecular Curvature Generation Capacity. *Journal of the American Chemical Society*, 138(44), 14616-14622.

Choi, B., Choi, M., Kim, J., Yang, Y., Lai, Y., Kweon, D., Lee, N., & Shin, Y. (2013). Large -synuclein oligomers inhibit neuronal SNARE-mediated vesicle docking. *Proceedings of the National Academy of Sciences*, 110(10), 4087-4092.

Church, D., Goodstadt, L., Hillier, L., Zody, M., Goldstein, S., She, X., Bult, C., Agarwala, R., Cherry, J., DiCuccio, M., Hlavina, W., Kapustin, Y., Meric, P., Maglott, D., Birtle, Z., Marques, A., Graves, T., Zhou, S., Teague, Potamousis, K., Churas, C., Place, M., Herschleb, J., Runnheim, R., Forrest, D., Amos-Landgraf, J., Schwartz, D., Cheng, Z., LindbladToh, K., Eichler, E., & Ponting, C. (2009). Lineage-Specific Biology Revealed by a Finished Genome Assembly of the Mouse. *Plos Biology*, 7(5), e1000112.

Church, D., Schneider, V., Graves, T., Auger, K., Cunningham, F., Bouk, N., Chen, H., Agarwala, R., McLaren, W., Ritchie, G., Albracht, D., Kremitzki, M., Rock, S., Kotkiewicz, H., Kremitzki, C., Wollam, A., Trani, L., Fulton, L., Fulton, R., Matthews, L., Whitehead, S., Chow, W., Torrance, J., Dunn, M., Harden,G., Threadgold, G., Wood, J., Collins, J., Heath, P., Griffiths, G., Pelan, S., Grafham, D., Eichler, E., Weinstock, G., Mardis, E., Wilson,R., Howe, K., Flicek, P., & Hubbard, T. (2011). Modernizing Reference Genome Assemblies. *Plos Biology*, 9(7), e1001091.

Daraee, H., Etemadi, A., Kouhi, M., Alimirzalu, S., & Akbarzadeh, A. (2016). Application of liposomes in medicine and drug delivery. *Artificial Cells, Nanomedicine, And Biotechnology*, 44(1), 381-391.

Dausinas, P., Pulakanti, K., Rao, S., Cole, J., Dahl, R., & Cowden Dahl, K. (2020). ARID3A and ARID3B induce stem promoting pathways in ovarian cancer cells. *Gene,* 738, 144458.

David, C., Solimena, M., & de Camilli, P. (1994). Autoimmunity in Stiff-Man Syndrome with breast cancer is targeted to the C-terminal region of human amphiphysin, a protein similar to the yeast proteins, Rvs167 and Rvs161. *FEBS Letters*, 351(1), 73–79.

Delorenzi, M., & Speed, T. (2002). An HMM model for coiled-coil domains and a comparison with PSSM-based predictions. *Bioinformatics*, 18(4), 617-625.

Dharmalingam, E., Haeckel, A., Pinyol, R., Schwintzer, L., Koch, D., Kessels, M., & Qualmann, B. (2009). F-BAR proteins of the syndapin family shape the plasma membrane and are crucial for neuromorphogenesis. *Journal of Neuroscience*, 29(42), 13315–13327.

Dotti, C., Sullivan, C., & Banker, G. (1988). The establishment of polarity by hippocampal neurons in culture. *The Journal of Neuroscience*, 8(4), 1454-1468.

Drin, G., & Antonny, B. (2009). Amphipathic helices and membrane curvature. *FEBS Letters*, 584(9), 1840-1847.

Drin, G., Casella, J. F., Gautier, R., Boehmer, T., Schwartz, T. U., & Antonny, B. (2007). A general amphipathic α-helical motif for sensing membrane curvature. Nature Structural and Molecular Biology, 14(2), 138–146.

Engelman, D. (2005). Membranes are more mosaic than fluid. *Nature*, 438(7068), 578-580.

Fassler, J., & Cooper, P. (2021). BLAST Glossary. Ncbi.nlm.nih.gov. Retrieved 24 October 2021, from https://www.ncbi.nlm.nih.gov/books/NBK62051.

Feng, S., Chen, J., Yu, H., Simon, J., & Schreiber, S. (1994). Two Binding Orientations for Peptides to the Src SH3 Domain: Development of a General Model for SH3-Ligand Interactions. *Science,* 266(5188), 1241-1247.

Ferreiro, D., Cho, S., Komives, E., & Wolynes, P. (2005). The Energy Landscape of Modular Repeat Proteins: Topology Determines Folding Mechanism in the Ankyrin Family. *Journal of Molecular Biology*, 354(3), 679-692.

Frost, A., Perera, R., Roux, A., Spasov, K., Destaing, O., Egelman, E., de Camilli, P., & Unger, V. M. (2008). Structural Basis of Membrane Invagination by F-BAR Domains. *Cell*, 132(5), 807-817.

Frost, A., Unger, V., & De Camilli, P. (2009). The BAR Domain Superfamily: Membrane-Molding Macromolecules. *Cell*, 137(2), 191-196.

Gautier, R., Douguet, D., Antonny, B., & Drin, G. (2008). HELIQUEST: A web server to screen sequences with specific α-helical properties. *Bioinformatics*, 24(18), 2101–2102.

Giménez-Andrés, M., Čopič, A., & Antonny, B. (2018). The Many Faces of Amphipathic Helices. *Biomolecules*, 8(3), 45.

Giraldi, F., Cassarino, M., Sesta, A., Terreni, M., Lasio, G., & Losa, M. (2020). Sexual Dimorphism in Cellular and Molecular Features in Human ACTH-Secreting Pituitary Adenomas. *Cancers*, 12(3), 669.

Goñi, F. (2014). The basic structure and dynamics of cell membranes: An update of the Singer–Nicolson model. *Biochimica Et Biophysica Acta (BBA) - Biomembranes*, 1838(6), 1467-1476.

Graham, F., Russell, W., Smiley, J., & Nairn, R. (1977). Characteristics of a Human Cell Line Transformed by DNA from Human Adenovirus Type 5. *Journal of General Virology*, 36(1), 59-72.

Gruber, M., Söding, J., & Lupas, A. (2006). Comparative analysis of coiled-coil prediction methods. *Journal of Structural Biology*, 155(2), 140–145.

Hansen, C., Howard, G., & Nichols, B. (2011). Pacsin 2 is recruited to caveolae and functions in caveolar biogenesis. *Journal of Cell Science*, 124(16), 2777–2785.

Henne, W. M., Kent, H., Ford, M., Hegde, B., Daumke, O., Butler, P., Mittal, R., Langen, R., Evans, P., & McMahon, H. (2007). Structure and Analysis of FCHo2 F-BAR Domain: A Dimerizing and Membrane Recruitment Module that Effects Membrane Curvature. *Structure*, 15(7), 839–852.

Hofbrucker-MacKenzie, S. (2021). Membrane shaping by members of the N-Ank superfamily and membrane-associated signalling in synaptic plasticity [Dissertation]. Jena: Friedrich-Schiller-Universität Jena.

Hofbrucker-MacKenzie, S., Sivaprakasam, I., Ji, Y., Kessels, M., & Qualmann, B. (2019). Neuronal stress and its hormetic aspects. The Science of Hormesis in Health and Longevity (pp. 171-180). Academic Press.

Horton, A., & Ehlers, M. (2003). Dual Modes of Endoplasmic Reticulum-to-Golgi Transport in Dendrites Revealed by Live-Cell Imaging. *The Journal of Neuroscience*, 23(15), 6188-6199.

Inoue, H., Nojima, H., & Okayama, H. (1990). High efficiency transformation of Escherichia coli with plasmids. *Gene*, 96(1), 23-28.

Insinna, C., Lu, Q., Teixeira, I., Harned, A., Semler, E., Stauffer, J., Magidson, V., Tiwari, A., Kenworthy, A. K., Narayan, K., & Westlake, C. (2019). Investigation of F-BAR domain PACSIN proteins uncovers membrane tubulation function in cilia assembly and transport. *Nature Communications*, 10(1).

Islam, Z., Nagampalli, R., Fatima, M., & Ashraf, G. (2018). New paradigm in ankyrin repeats: Beyond protein-protein interaction module. *International Journal of Biological Macromolecules*, 109, 1164-1173.

Ito, H., Iwamoto, I., Mizutani, K., Morishita, R., Deguchi, T., Nozawa, Y., Asano, T., & Nagata, K. I. (2006). Possible interaction of a Rho effector, Rhotekin, with a PDZ-protein, PIST, at synapses of hippocampal neurons. *Neuroscience Research*, 56(2), 165–171.

Izadi, M., Schlobinski, D., Lahr, M., Schwintzer, L., Qualmann, B., & Kessels, M. (2017). Cobl-like promotes actin filament formation and dendritic branching using only a single WH2 domain. *Journal of Cell Biology*, 217(1), 211-230.

Izadi, M., Seemann, E., Schlobinski, D., Schwintzer, L., Qualmann, B., & Kessels, M. (2021). Functional interdependence of the actin nucleator Cobl and Cobl-like in dendritic arbor development. *Elife*, 10.

Kaksonen, M., & Roux, A. (2018). Mechanisms of clathrin-mediated endocytosis. *Nature Reviews Molecular Cell Biology*, 19(5), 313-326.

Kaneko, T., Li, L., & Li, S. (2008). The SH3 domain- a family of versatile peptide- and protein-recognition module. *Frontiers In Bioscience*, Volume(13), 4938.

Kessels, M., & Qualmann, B. (2002). Syndapins integrate N-WASP in receptor-mediated endocytosis. *The EMBO Journal*, 21(22), 6083-6094.

Kessels, M., & Qualmann, B. (2004). The syndapin protein family: linking membrane trafficking with the cytoskeleton. *Journal of Cell Science*, 117(15), 3077-3086.

Kessels, M., & Qualmann, B. (2006). Syndapin oligomers interconnect the machineries for endocytic vesicle formation and actin polymerization. *Journal of Biological Chemistry*, 281(19), 13285–13299.

Kessels, M., Schwintzer, L., Schlobinski, D., & Qualmann, B. (2011). Controlling actin cytoskeletal organization and dynamics during neuronal morphogenesis. *European Journal of Cell Biology,* 90(11), 926–933.

Kim, D., Park, M., Gwon, G., Silkov, A., Xu, Z., Yang, E., Song, S., Song, K., Kim, Y., Yoon, H., Honig, B., Cho, W., Cho, Y., & Hwang, I. (2014). An ankyrin repeat domain of AKR2 drives chloroplast targeting through coincident binding of two chloroplast lipids. *Developmental Cell*, 30(5), 598–609.

Kitamata, M., Hanawa-Suetsugu, K., Maruyama, K., & Suetsugu, S. (2019). Membrane-Deformation Ability of ANKHD1 Is Involved in the Early Endosome Enlargement. *IScience*, 17, 101–118.

Koch, D., Spiwoks-Becker, I., Sabanov, V., Sinning, A., Dugladze, T., Stellmacher, A., Ahuja, R., Grimm, J., Schüler, S., Müller, A., Angenstein, F., Ahmed, T., Diesler, A., Moser, M., Tom Dieck, S., Spessert, R., Boeckers, T., Fässler, R., Hübner, C., Balschun, D., Gloveli, T., Kessels, M., & Qualmann, B. (2011). Proper synaptic vesicle formation and neuronal network activity critically rely on syndapin I. *EMBO Journal*, 30(24), 4955–4969.

Koch, N., Koch, D., Krueger, S., Tröger, J., Sabanov, V., Ahmed, T., McMillan, L. E., Wolf, D., Montag, D., Kessels, M., Balschun, D., & Qualmann, B. (2020). Syndapin I Loss-of-Function in Mice Leads to Schizophrenia-Like Symptoms. *Cerebral Cortex*, 30(8), 4306–4324.

Kunimoto, M., Otto, E., & Bennett, V. (1991). A new 440-kD isoform is the major ankyrin in neonatal rat brain. *The Journal of Cell Biology*, 115(5), 1319-1331.

Lesa, G., Seemann, J., Shorter, J., Vandekerckhove, J., & Warren, G. (2000). The amino-terminal domain of the Golgi protein giantin interacts directly with the vesicle-tethering protein p115. *Journal of Biological Chemistry*, 275(4), 2831-2836.

Leuner, B., & Gould, E. (2010). Structural Plasticity and Hippocampal Function. *Annual Review of Psychology*, 61(1), 111-140.

Li, J., Mahajan, A., & Tsai, M. (2006). Ankyrin Repeat:  A Unique Motif Mediating Protein−Protein Interactions. *Biochemistry*, 45(51), 15168-15178.

Li, X., Lehman, W., & Fischer, S. (2010). The relationship between curvature, flexibility and persistence length in the tropomyosin coiled coil. *Journal of Structural Biology*, 170(2), 313–318.

Lim, S., Sala, C., Yoon, J., Park, S., Kuroda, S., Sheng, M., & Kim, E. (2001). Sharpin, a Novel Postsynaptic Density Protein That Directly Interacts with the Shank Family of Proteins. *Molecular And Cellular Neuroscience*, 17(2), 385-397.

Liu, B., Liu, Z., Wang, Y., Lian, X., Han, Z., Cheng, X., Zhu, Y., Liu, R., Zhao, Y., & Gao, Y. (2021). Overexpression of GINS4 is associated with poor prognosis and survival in glioma patients. *Molecular Medicine*, 27(1).

Löw, C., Weininger, U., Zeeb, M., Zhang, W., Laue, E., Schmid, F., & Balbach, J. (2007). Folding Mechanism of an Ankyrin Repeat Protein: Scaffold and Active Site Formation of Human CDK Inhibitor p19INK4d. *Journal of Molecular Biology*, 373(1), 219-231.

Lupas, A. (1996). Coiled coils: new structures and new functions. *Trends In Biochemical Sciences*, 21(10), 375-382.

Lupas, A., Bassler, J., & Dunin-Horkawicz, S. (2017). The Structure and Topology of α-Helical Coiled Coils. *Subcellular Biochemistry*, 95-129.

MacArthur, M., & Thornton, J. (1991). Influence of proline residues on protein conformation. *Journal of Molecular Biology*, 218(2), 397-412.

Martin, A. C., Orengo, C. A., Gail Hutchinson, E., Jones, S., Karmirantzou, M., Laskowski, R. A., Mitchell, J. B., Taroni, C., & Thornton, J. M. (1998). Protein folds and functions. *Structure*, 6(7), 875-884.

Mason, J., & Arndt, K. (2004). Coiled coil domains: Stability, specificity, and biological implications. *ChemBioChem*, 5(2), 170–176.

Matos-Nieves, A., Manivannan, S., Majumdar, U., McBride, K., White, P., & Garg, V. (2021). A Multi-Omics Approach Using a Mouse Model of Cardiac Malformations for Prioritization of Human Congenital Heart Disease Contributing Genes. *Frontiers In Cardiovascular Medicine*, 8.

Mattila, P., & Lappalainen, P. (2008). Filopodia: molecular architecture and cellular functions. *Nature Reviews Molecular Cell Biology*, 9(6), 446-454.

Mayer, B. (2001). SH3 domains: complexity in moderation. *Journal of Cell Science*, 114(7), 1253-1263.

McMahon, H., & Gallop, J. (2005). Membrane curvature and mechanisms of dynamic cell membrane remodelling. *Nature*, 438(7068), 590-596.

Meirson, T., Bomze, D., Kahlon, L., Gil-Henn, H., & Samson, A. (2019). A helical lock and key model of polyproline II conformation with SH3. *Bioinformatics*, 36(1), 154-159.

Merrifield, C., Feldman, M., Wan, L., & Almers, W. (2002). Imaging actin and dynamin recruitment during invagination of single clathrin-coated pits. *Nature Cell Biology*, 4(9), 691–698.

Merrifield, C., Qualmann, B., Kessels, M., & Almers, W. (2004). Neural Wiskott Aldrich Syndrome Protein (N-WASP) and the Arp2/3 complex are recruited to sites of clathrin-mediated endocytosis in cultured fibroblasts. *European Journal of Cell Biology*, 83(1), 13-18.

Missler, M., & Südhof, T. (1998). Neurexins: Three genes and 1001 products. *Trends In Genetics*, 14(1), 20-26.

Mosavi, L., Cammett, T., Desrosiers, D., & Peng, Z. (2004). The ankyrin repeat as molecular architecture for protein recognition. *Protein Science*, 13(6), 1435-1448.

Musacchio, A. (2002). How SH3 domains recognize proline. *Advances In Protein Chemistry*, 211-268.

Parry, D., Fraser, R., & Squire, J. (2008). Fifty years of coiled-coils and α-helical bundles: A close relationship between sequence and structure. *Journal Of Structural Biology*, 163(3), 258-269.

Peter, B., Kent, H., Mills, I., Vallis, Y., Butler, P., Evans, P., & McMahon, H. (2004). BAR Domains as Sensors of Membrane Curvature: The Amphiphysin BAR Structure. *Science*, 303(5657), 495–499.

Plomann, M., Lange, R., Vopper, G., Cremer, H., Heinlein, U., Scheff, S., Baldwin, S., Leitges, M., Cramer, M., Paulsson, M., & Barthels, D. (1998). PACSIN, a brain protein that is upregulated upon differentiation into neuronal cells. *European Journal of Biochemistry*, 256(1), 201-211.

Pruitt, K., Brown, G., Tatusova, T. and Maglott, D. (2002). Reference Sequence (RefSeq) Database. In J. McEntyre and J. Ostell (eds.), The NCBI Handbook the [Internet]. Bethesda, MD: National Center for Biotechnology Information (US).

Pruitt, K., Tatusova, T., Brown, G.R. and Maglott, D.R. (2012). NCBI Reference Sequences (RefSeq): current status, new features and genome annotation policy. *Nucleic Acids Research*, 40(Database), pp. D130–D135.

Qualmann, B., & Kelly, R. (2000). Syndapin Isoforms Participate in Receptor-Mediated Endocytosis and Actin Organization. *Journal of Cell Biology*, 148(5), 1047-1062.

Qualmann, B., Koch, D., & Kessels, M. (2011). Let's go bananas: revisiting the endocytic BAR code. *The EMBO Journal*, 30(17), 3501-3515.

Qualmann, B., Roos, J., DiGregorio, P., & Kelly, R. (1999). Syndapin I, a Synaptic Dynamin-binding Protein that Associates with the Neural Wiskott-Aldrich Syndrome Protein. *Molecular Biology of The Cell*, 10(2), 501-513.

Rao, Y., Ma, Q., Vahedi-Faridi, A., Sundborger, A., Pechstein, A., Puchkov, D., Luo, L., Shupliakov, O., Saenger, W., & Haucke, V. (2010). Molecular basis for SH3 domain regulation of F-BAR-mediated membrane deformation. *Proceedings of the National Academy of Sciences*, 107(18), 8213-8218.

Reeves, J., & Dowben, R. (1969). Formation and properties of thin-walled phospholipid vesicles. *Journal of Cellular Physiology*, 73(1), 49-60.

Ritter, B., Modregger, J., Paulsson, M., & Plomann, M. (1999). PACSIN 2, a novel member of the PACSIN family of cytoplasmic adapter proteins. *FEBS Letters*, 454(3), 356-362.

Scheiffele, P., Fan, J., Choih, J., Fetter, R., & Serafini, T. (2000). Neuroligin Expressed in Nonneuronal Cells Triggers Presynaptic Development in Contacting Axons. *Cell*, 101(6), 657-669.

Scherer, W., Syverton, J., & Gey, G. (1953). Studies On the Propagation In Vitro of Poliomyelitis Viruses. Iv. Viral multiplication in a stable strain of human malignant epithelial cells (strain HeLa) derived from an epidermoid carcinoma of the cervix. *Journal of Experimental Medicine*, 97(5), 695-710.

Schneider, K., Seemann, E., Liebmann, L., Ahuja, R., Koch, D., Westermann, M., Hübner, C. A., Kessels, M., & Qualmann, B. (2014). ProSAP1 and membrane nanodomain-associated syndapin I promote postsynapse formation and function. *Journal of Cell Biology*, 205(2), 197–215.

Schüler, S., Hauptmann, J., Perner, B., Kessels, M., Englert, C., & Qualmann, B. (2013). Ciliated sensory hair cell formation and function require the F-BAR protein syndapin I and the WH2 domain-based actin nucleator Cobl. *Journal of Cell Science*, 126(17), 4059-4059.

Schwintzer, L. (2012). Analyse der molekularen Mechanismen und zellbiologischen Funktionen des auf WH2-Domänen basierenden Aktinnukleationsfaktors Cordon-bleu. [Dissertation]. Jena: Friedrich-Schiller-Universität Jena.

Schwintzer, L., Koch, N., Ahuja, R., Grimm, J., Kessels, M., & Qualmann, B. (2011). The functions of the actin nucleator Cobl in cellular morphogenesis critically depend on syndapin I. *EMBO Journal*, 30(15), 3147–3159.

Sedgwick, S., & Smerdon, S. (1999). The ankyrin repeat: a diversity of interactions on a common structural framework. *Trends In Biochemical Sciences*, 24(8), 311-316.

Seelig, J. (2004). Thermodynamics of lipid–peptide interactions. *Biochimica Et Biophysica Acta (BBA) - Biomembranes*, 1666(1-2), 40-50.

Seemann, E., Sun, M., Krueger, S., Trö ger, J., Hou, W., Haag, N., Schüler, S., Westermann, M., Huebner, C., Romeike, B., Kessels, M., & Qualmann, B. (2017). Deciphering caveolar functions by syndapin III KO-mediated impairment of caveolar invagination. *Elife,* 6.

Segrest, J., De Loof, H., Dohlman, J., Brouillette, C., & Anantharamaiah, G. (1990). Amphipathic helix motif: Classes and properties. *Proteins: Structure, Function, And Genetics*, 8(2), 103-117.

Senju, Y., Itoh, Y., Takano, K., Hamada, S., & Suetsugu, S. (2011). Essential role of PACSIN2/syndapin-II in caveolae membrane sculpting. *Journal of Cell Science*, 124(12), 2032–2040.

Shimada, A., Niwa, H., Tsujita, K., Suetsugu, S., Nitta, K., Hanawa-Suetsugu, K., Akasaka, R., Nishino, Y., Toyama, M., Chen, L., Liu, Z. J., Wang, B. C., Yamamoto, M., Terada, T., Miyazawa, A., Tanaka, A., Sugano, S., Shirouzu, M., Nagayama, K., Takenawa, T., & Yokoyama, S. (2007). Curved EFC/F-BAR-Domain Dimers Are Joined End to End into a Filament for Membrane Invagination in Endocytosis. *Cell,* 129(4), 761–772.

Simunovic, M., Voth, G., Callan-Jones, A., & Bassereau, P. (2015). When Physics Takes Over: BAR Proteins and Membrane Curvature. *Trends In Cell Biology*, 25(12), 780-792.

Singer, S., & Nicolson, G. (1972). The Fluid Mosaic Model of the Structure of Cell Membranes. *Science*, 175(4023), 720-731.

Sjöstedt, E., Zhong, W., Fagerberg, L., Karlsson, M., Mitsios, N., & Adori, C. et al. (2020). An atlas of the protein-coding genes in the human, pig, and mouse brain. *Science*, 367(6482).

Sola-Carvajal, A., Revêchon, G., Helgadottir, H. T., Whisenant, D., Hagblom, R., Döhla, J., Katajisto, P., Brodin, D., Fagerström-Billai, F., Viceconte, N., & Eriksson, M. (2019). Accumulation of Progerin Affects the Symmetry of Cell Division and Is Associated with Impaired Wnt Signaling and the Mislocalization of Nuclear Envelope Proteins. *Journal of Investigative Dermatology*, 139(11), 2272-2280.e12.

Sparks, A., Rider, J., Hoffman, N., Fowlkes, D., Quillam, L., & Kay, B. (1996). Distinct ligand preferences of Src homology 3 domains from Src, Yes, Abl, Cortactin, p53bp2, PLC gamma, Crk, and Grb2. *Proceedings of the National Academy of Sciences*, 93(4), 1540-1544.

Sue, S. C., Cervantes, C., Komives, E., & Dyson, H. (2008). Transfer of Flexibility between Ankyrin Repeats in IκBα upon Formation of the NF-κB Complex. *Journal of Molecular Biology*, 380(5), 917–931.

Suetsugu, S. (2016). Higher-order assemblies of BAR domain proteins for shaping membranes. *Microscopy*, 65(3), 201-210.

Suetsugu, S., Kurisu, S., & Takenawa, T. (2014). Dynamic Shaping of Cellular Membranes by Phospholipids and Membrane-Deforming Proteins. *Physiological Reviews*, 94(4), 1219-1248.

Suetsugu, S., Toyooka, K., & Senju, Y. (2010). Subcellular membrane curvature mediated by the BAR domain superfamily proteins. *Seminars In Cell & Developmental Biology*, 21(4), 340-349.

Sułkowski, W. W., Pentak, D., Korus, W., & Sułkowska, A. (2005). Effect of temperature on liposome structures studied using EPR spectroscopy. *Spectroscopy*, 19(1), 37–42.

Takada, S. (2019). Gō model revisited. *Biophysics and Physicobiology*, 16(0), 248–255.

Takahashi, N., Hamada-Nakahara, S., Itoh, Y., Takemura, K., Shimada, A., Ueda, Y., Kitamata, M., Matsuoka, R., Hanawa-Suetsugu, K., Senju, Y., Mori, M. X., Kiyonaka, S., Kohda, D., Kitao, A., Mori, Y., & Suetsugu, S. (2014). TRPV4 channel activity is modulated by direct interaction of the ankyrin domain to PI(4,5)P2. *Nature Communications*, 5(1).

Taketomi, H., Ueda, Y., & Gō, N. (1975). Studies on protein folding, unfolding and fluctuations by computer simulation. *International Journal of Peptide Protein Research*, 7(6), 445-459.

Tan, I., Ng, C., Lim, L., & Leung, T. (2001). Phosphorylation of a Novel Myosin Binding Subunit of Protein Phosphatase 1 Reveals a Conserved Mechanism in the Regulation of Actin Cytoskeleton. *Journal of Biological Chemistry*, 276(24), 21209–21216.

Tang, K., Fersht, A., & Itzhaki, L. (2003). Sequential Unfolding of Ankyrin Repeats in Tumor Suppressor p16. *Structure*, 11(1), 67-73.

Tavosanis, G. (2011). Dendritic structural plasticity. *Developmental Neurobiology*, 72(1), 73-86.

Tong Yan Amy Hin, Drees, B., Nardelli, G., Bader, G. D., Brannetti, B., Castagnoli, L., Evangelista, M., Ferracuti, S., Nelson, B., Paoluzi, S., Quondam, M., Zucconi, A., Hogue, C. W. v, Fields, S., Boone, C., & Cesareni, G. (2002). A combined experimental and computational strategy to define protein interaction networks for peptide recognition modules. *Science*, 295(5553), 321-324.

Truebestein, L., Elsner, D., Fuchs, E., & Leonard, T. (2015). A molecular ruler regulates cytoskeletal remodelling by the Rho kinases. *Nature Communications*, 6(1).

Truebestein, L., & Leonard, T. A. (2016). Coiled coils: The long and short of it. *BioEssays*, 38(9), 903–916.

Uhlén, M., Fagerberg, L., Hallström, B. M., Lindskog, C., Oksvold, P., Mardinoglu, A., Sivertsson, Å., Kampf, C., Sjöstedt, E., Asplund, A., Olsson, I. M., Edlund, K., Lundberg, E., Navani, S., Szigyarto, C. A. K., Odeberg, J., Djureinovic, D., Takanen, J. O., Hober, S., … Pontén, F. (2015). Tissue-based map of the human proteome. *Science*, 347(6220).

Ullrich, B., Ushkaryov, Y., & Südhof, T. (1995). Cartography of neurexins: More than 1000 isoforms generated by alternative splicing and expressed in distinct subsets of neurons. *Neuron*, 14(3), 497-507.

UniProt: the universal protein knowledgebase. (2016). *Nucleic Acids Research*, 45(D1), D158-D169.

Viguera, A., Arrondo, J., Musacchio, A., Saraste, M., & Serrano, L. (1994). Characterization of the Interaction of Natural Proline-Rich Peptides with Five Different SH3 Domains. *Biochemistry*, 33(36), 10925-10933.

Wang, Q., Navarro, M., Peng, G., Molinelli, E., Lin Goh, S., & Judson, B. Rajashankar, K., & Sondermann, H. (2009). Molecular mechanism of membrane constriction and tubulation mediated by the F-BAR protein Pacsin/Syndapin. *Proceedings of the National Academy of Sciences*, 106(31), 12700-12705.

Wang, Y., Cheng, T., Lu, M., Mu, Y., Li, B., Li, X., & Zhan, X. (2019). TMT-based quantitative proteomics revealed follicle-stimulating hormone (FSH)-related molecular characterizations for potentially prognostic assessment and personalized treatment of FSH-positive non-functional pituitary adenomas. *EPMA Journal*, 10(4), 395-414.

Williamson, M. (1994). The structure and function of proline-rich regions in proteins. *Biochemical Journal*, 297(2), 249-260.

Witkos, T., & Lowe, M. (2016). The Golgin Family of Coiled-Coil Tethering Proteins. *Frontiers In Cell and Developmental Biology*, 3.

Wolf, D. (2013). Untersuchungen der in-vivo-Relevanz einer mittels in-silico-Suche gefundenen Interaktion des F-BAR Proteins Syndapin [Masterarbeit]. Jena: Friedrich-Schiller-Universität Jena.

Wolf, D. (2018). Funktionelle und phänotypische Analyse eines neuartigen Membrantopologie-beeinflussenden Proteins [Dissertation]. Jena: Friedrich-Schiller-Universität Jena.

Wolf, D., Hofbrucker-MacKenzie, S., Izadi, M., Seemann, E., Steiniger, F., Schwintzer, L., Koch, D., Kessels, M. M., & Qualmann, B. (2019). Ankyrin repeat-containing N-Ank proteins shape cellular membranes. *Nature Cell Biology*, 21(10), 1191–1205.

Wu, H., Sheng, Y., & Tsao, H. (2014). Phase behaviors and membrane properties of model liposomes: Temperature effect. *The Journal of Chemical Physics*, 141(12), 124906.

Yon, J. (2001). Protein folding: a perspective for biology, medicine and biotechnology. *Brazilian Journal of Medical and Biological Research*, 34(4), 419-435.

Yoshida, Y., Kinuta, M., Abe, T., Liang, S., Araki, K., Cremona, O., di Paolo, G., Moriyama, Y., Yasuda, T., de Camilli, P., & Takei, K. (2004). The stimulatory action of amphiphysin on dynamin function is dependent on lipid bilayer curvature. *The EMBO Journal*, 23(17), 3483-3491.

Zarrinpar, A., Bhattacharyya, R., & Lim, W. (2003). The Structure and Function of Proline Recognition Domains. *Science Signaling*, 2003(179), re8.

Zhou, H., & Pang, X. (2018). Electrostatic Interactions in Protein Structure, Folding, Binding, and Condensation. *Chemical Reviews*, 118(4), 1691-1741.

Zimmerberg, J., & Kozlov, M. (2005). How proteins produce cellular membrane curvature. *Nature Reviews Molecular Cell Biology*, 7(1), 9-19.

# 7 Appendix

## 7.1 Supplementary data

**Table 13: Ankrd24 isoforms with gene locus positions of exons with their respective range in different isoforms of Ankrd24 in Mus musculus, according to the NCBI database; gene ID 70615 as of 19 May 2021.** Ankrd24x3 (XM_006514093.5) was used as a reference

| exons | x3 (XM_006514093.5) | x23 (XM_030245274.2) | x6 (XM_006514096.5) | x8 (XM_006514098.5) | x12 (XM_006514102.5) | x4 (XM_006514094.5) | x10 (XM_036156008.1) | x20 (XM_036156013.1) | x13 (XM_006514103.5) | 2 (NM_027480.3) |
|---|---|---|---|---|---|---|---|---|---|---|
| 1 | 1..123 | 1..123 | 1..123 | 1..123 | 1..123 | 1..123 | 1..123 | 1..123 | 1..123 | 23..123 |
| 2 | 223..408 | 223..408 | 223..408 | 223..408 | 223..408 | | | | | |
| 3 | 1032..1231 | 1032..1231 | 1032..1231 | 1032..1231 | 1032..1231 | 1032..1231 | 1032..1231 | 1032..1231 | 1032..1231 | 1032..1231 |
| 4 | 6150..6236 | | | | | 6150..6236 | | | | |
| 5 | 6348..6478 | 6348..6478 | 6348..6478 | 6348..6478 | | 6348..6478 | | | | 6348..6478 |
| 6 | 6553..6641 | 6553..6641 | 6553..6641 | 6553..6641 | | 6553..6641 | 6553..6641 | | | 6553..6641 |
| 7 | 7171..7235 | 7171..7909 | 7171..7235 | 7171..7235 | | 7171..7235 | 7171..7235 | 7171..7235 | | 7171..7235 |
| 8 | 7852..7909 | | 7852..7909 | 7852..7909 | 7852..7909 | 7852..7909 | 7852..7909 | 7852..7909 | 7852..7909 | 7852..7909 |
| 9 | 9552..9622 | 9552..9622 | 9552..9622 | 9552..9622 | 9552..9622 | 9552..9622 | 9552..9622 | 9552..9622 | 9552..9622 | 9552..9622 |
| 10 | 9754..9860 | 9754..9860 | 9754..9860 | 9754..9860 | 9754..9860 | 9754..9860 | 9754..9860 | 9754..9860 | 9754..9860 | 9754..9860 |
| 11 | 10044..10231 | 10044..10231 | 10044..10231 | 10044..10231 | 10044..10231 | 10044..10231 | 10044..10231 | 10044..10231 | 10044..10231 | 10044..10231 |
| 12 | 10790..10827 | 10790..10827 | 10790..10827 | 10790..10827 | 10790..10827 | 10790..10827 | 10790..10827 | 10790..10827 | 10790..10827 | 10790..10827 |
| 13 | 11339..11419 | 11339..11419 | 11339..11419 | 11339..11419 | 11339..11419 | 11339..11419 | 11339..11419 | 11339..11419 | 11339..11419 | 11339..11419 |
| 14 | 11511..11618 | 11511..12295 | 11511..11618 | 11511..11618 | 11511..11618 | 11511..11618 | 11511..11618 | 11511..11618 | 11511..11618 | 11511..11618 |
| 15 | 12251..12295 | | 12251..12295 | 12251..12295 | 12251..12295 | 12251..12295 | 12251..12295 | 12251..12295 | 12251..12295 | 12251..12295 |
| 16 | 12375..12473 | 12375..12473 | 12375..12473 | 12375..12473 | 12375..12473 | 12375..12473 | 12375..12473 | 12375..12473 | 12375..12473 | 12375..12473 |
| 17 | 13459..13531 | | 13459..13531 | 13459..13531 | 13459..13531 | 13459..13531 | 13459..13531 | 13459..13531 | 13459..13531 | 13459..13531 |
| 18 | 13784..13902 | 13784..13902 | 13784..13902 | 13784..13902 | 13784..13902 | 13784..13902 | 13784..13902 | 13784..13902 | 13784..13902 | 13784..13902 |
| 19 | 14000..15376 | 14000..15376 | 14000..15376 | 14000..15376 | 14000..15376 | 14000..15376 | 14000..15376 | 14000..15376 | 14000..15376 | 14000..15376 |
| 20 | 16459..16626 | 16459..16626 | 16459..16626 | | 16459..16626 | 16459..16626 | 16459..16626 | 16459..16626 | 16459..16626 | |
| 21 | 17788..17916 | 17788..17916 | 17788..17916 | 17788..17916 | 17788..17916 | 17788..17916 | 17788..17916 | 17788..17916 | 17788..17916 | 17788..17916 |
| 22 | 18276..18341 | 18276..18341 | 18276..18341 | 18276..18341 | 18276..18341 | 18276..18341 | 18276..18341 | 18276..18341 | 18276..18341 | 18276..18341 |
| 23 | 18583..19093 | 18583..19093 | 18583..19093 | 18583..19093 | 18583..19093 | 18583..19093 | 18583..19093 | 18583..19093 | 18583..19093 | 18583..19095 |

| exons | x3 (XM_006514093.5) | x1 (XM_006514091.5) | x7 (XM_006514097.5) | x2 (XM_006514092.5) | x5 (XM_006514095.5) | x9 (XM_006514099.5) | x11 (XM_006514101.5) | x15 (XM_036156009.1) | x16 (XM_036156010.1) | x17 (XM_036156011.1) |
|---|---|---|---|---|---|---|---|---|---|---|
| 1 | 1..123 | | | | | | | | | |
| 2 | 223..408 | | | | | | | | | |
| 3 | 1032..1231 | 3803..5238 | 3805..5238 | 3806..5238 | 3807..5238 | 3810..5238 | 3811..5238 | 3812..5238 | 3813..5238 | 3813..5238 |
| 4 | 6150..6236 | 6099..6236 | 6099..6236 | 6150..6236 | | | | | | |
| 5 | 6348..6478 | 6348..6478 | 6348..6478 | 6348..6478 | 6348..6478 | | | | 6348..6478 | |
| 6 | 6553..6641 | 6553..6641 | 6553..6641 | 6553..6641 | 6553..6641 | 6553..6641 | | 6553..6641 | 6553..6641 | 6553..6641 |
| 7 | 7171..7235 | 7171..7235 | 7171..7235 | 7171..7235 | 7171..7235 | 7171..7235 | | | 7171..7235 | 7171..7235 |
| 8 | 7852..7909 | 7852..7909 | 7852..7909 | 7852..7909 | 7852..7909 | 7852..7909 | 7852..7909 | 7852..7909 | 7852..7909 | 7852..7909 |
| 9 | 9552..9622 | 9552..9622 | 9552..9622 | 9552..9622 | 9552..9622 | 9552..9622 | 9552..9622 | 9552..9622 | 9552..9622 | 9552..9622 |
| 10 | 9754..9860 | 9754..9860 | 9754..9860 | 9754..9860 | 9754..9860 | 9754..9860 | 9754..9860 | 9754..9860 | 9754..9860 | 9754..9860 |
| 11 | 10044..10231 | 10044..10231 | 10044..10231 | 10044..10231 | 10044..10231 | 10044..10231 | 10044..10231 | 10044..10231 | 10044..10231 | 10044..10231 |
| 12 | 10790..10827 | 10790..10827 | 10790..10827 | 10790..10827 | 10790..10827 | 10790..10827 | 10790..10827 | 10790..10827 | 10790..10827 | 10790..10827 |
| 13 | 11339..11419 | 11339..11419 | 11339..11419 | 11339..11419 | 11339..11419 | 11339..11419 | 11339..11419 | 11339..11419 | 11339..11419 | 11339..11419 |
| 14 | 11511..11618 | 11511..11618 | 11511..11618 | 11511..11618 | 11511..11618 | 11511..11618 | 11511..11618 | 11511..11618 | 11511..11618 | 11511..11618 |
| 15 | 12251..12295 | 12251..12295 | 12251..12295 | 12251..12295 | 12251..12295 | 12251..12295 | 12251..12295 | 12251..12295 | 12251..12295 | 12251..12295 |
| 16 | 12375..12473 | 12375..12473 | 12375..12473 | 12375..12473 | 12375..12473 | 12375..12473 | 12375..12473 | 12375..12473 | 12375..12473 | 12375..12473 |
| 17 | 13459..13531 | 13459..13531 | 13459..13531 | 13459..13531 | 13459..13531 | 13459..13531 | 13459..13531 | 13459..13531 | 13459..13531 | 13459..13531 |
| 18 | 13784..13902 | 13784..13902 | 13784..13902 | 13784..13902 | 13784..13902 | 13784..13902 | 13784..13902 | 13784..13902 | 13784..13902 | 13784..13902 |
| 19 | 14000..15376 | 14000..15376 | 14000..15376 | 14000..15376 | 14000..15376 | 14000..15376 | 14000..15376 | 14000..15376 | 14000..15376 | 14000..15376 |
| 20 | 16459..16626 | 16459..16626 | | 16459..16626 | 16459..16626 | 16459..16626 | 16459..16626 | 16459..16626 | 16459..16626 | 16459..16626 |
| 21 | 17788..17916 | 17788..17916 | 17788..17916 | 17788..17916 | 17788..17916 | 17788..17916 | 17788..17916 | 17788..17916 | 17788..17916 | 17788..17916 |
| 22 | 18276..18341 | 18276..18341 | 18276..18341 | 18276..18341 | 18276..18341 | 18276..18341 | 18276..18341 | 18276..18341 | 18276..18341 | 18276..18341 |
| 23 | 18583..19093 | 18583..19093 | 18583..19093 | 18583..19093 | 18583..19093 | 18583..19093 | 18583..19093 | 18583..19093 | 18583..19093 | 18583..19093 |

| exons | x3 (XM_006514093.5) | x19 (XM_036156012.1) | x18 (XM_006514104.5) | x24 (XM_030245275.1) | 1 (NM_001374016.1) | x14 (XM_011243569.1) | x21 (XM_017314088.1) | x22 (XM_030245273.1) |
|---|---|---|---|---|---|---|---|---|
| 1 | 1..123 | | | | | | | |
| 2 | 223..408 | | | | | | | |
| 3 | 1032..1231 | 3813..5238 | 3813..5238 | 3854..5238 | 5182..5238 | 5186..5298 | | |
| 4 | 6150..6236 | | | | 6150..6236 | 6150..6236 | | |
| 5 | 6348..6478 | | | | 6348..6478 | 6348..6478 | | |
| 6 | 6553..6641 | | | | 6553..6641 | 6553..6641 | | |
| 7 | 7171..7235 | 7171..7235 | 7171..7235 | 7171..7235 | | | | |
| 8 | 7852..7909 | 7852..7909 | 7852..7909 | 7852..7909 | 7852..7909 | 7852..7909 | | |
| 9 | 9552..9622 | 9552..9622 | 9552..9622 | 9552..9622 | 9552..9622 | 9552..9622 | | |
| 10 | 9754..9860 | 9754..9860 | 9754..9860 | 9754..9860 | 9754..9860 | 9754..9860 | | |
| 11 | 10044..10231 | 10044..10231 | 10044..10231 | 10044..10231 | 10044..10231 | 10044..10231 | | |
| 12 | 10790..10827 | 10790..10827 | 10790..10827 | 10790..10827 | 10790..10827 | 10790..10827 | 10845..11195 | |
| 13 | 11339..11419 | 11339..11419 | 11339..11419 | 11339..11419 | 11339..11419 | 11339..11419 | 11339..11419 | |
| 14 | 11511..11618 | 11511..11618 | 11511..11618 | 11511..12295 | 11511..11618 | 11511..11618 | 11511..11618 | 11504..12295 |
| 15 | 12251..12295 | 12251..12295 | 12251..12295 | | 12251..12295 | 12251..12295 | 12251..12295 | |
| 16 | 12375..12473 | 12375..12473 | 12375..12473 | 12375..12473 | 12375..12473 | 12375..12473 | 12375..12473 | 12375..12473 |
| 17 | 13459..13531 | 13459..13531 | 13459..13531 | | 13459..13531 | 13459..13531 | 13459..13531 | 13459..13531 |
| 18 | 13784..13902 | 13784..13902 | 13784..13902 | 13784..13902 | 13784..13902 | 13784..13902 | 13784..13902 | 13784..13902 |
| 19 | 14000..15376 | 14000..15376 | 14000..15376 | 14000..15376 | 14000..15376 | 14000..15376 | 14000..15376 | 14000..15376 |
| 20 | 16459..16626 | 16459..16626 | 16459..16626 | 16459..16626 | 16459..16626 | 16459..16626 | 16459..16626 | 16459..16626 |
| 21 | 17788..17916 | 17788..17916 | 17788..17916 | 17788..17916 | 17788..17916 | 17788..17916 | 17788..17916 | 17788..17916 |
| 22 | 18276..18341 | 18276..18341 | 18276..18341 | 18276..18341 | 18276..18341 | 18276..18341 | 18276..18341 | 18276..18341 |
| 23 | 18583..19093 | 18583..19093 | 18583..19093 | 18583..19093 | 18583..19093 | 18583..19093 | 18583..19093 | 18583..19093 |

```
Ankrd24x6^841-900   VDAAREELERMRGASVPADEHEHALSALRDHVTRLQAQLADLARRHEKTSAEVFQVQREA

                    VDAAREELERMRGASVPADEHEHALSALRDHVTRLQAQLADLARRHEKTSAEVFQ+   +

Ankrd24_2^841-900   VDAAREELERMRGASVPADEHEHALSALRDHVTRLQAQLADLARRHEKTSAEVFQITDLS


Ankrd24x6^901-960   LFMKSERHAAEAQLATAEQQLRGLRTEAERARQAQSRAQEALDKAKEKDKKITDLSKEVF

                      + + + A + Q +T                 A S+ +EAL        ++T L +++

Ankrd24_2^901-937   KEVFTLKEALKVQQSTP---------------ASSKEEEAL------RGQVTALQQQI-


Ankrd24x6^961-1020  TLKEALKVQQSTPASSKEEEALRGQVTALQQQIQEEAREHGAVVALYRTHLLYAIQGQMD

                                                    QEEAREHGAVVALYRTHLLYAIQGQMD

Ankrd24_2^938-964   ------------------------------QEEAREHGAVVALYRTHLLYAIQGQMD
```

**Fig. 21. Alignment of amino acid sequence between Mus musculus Ankrd24x6841-1020 and Ankrd24_2841-964, showing the presence of additional sequence at C-terminus of Ankrd24x6.**
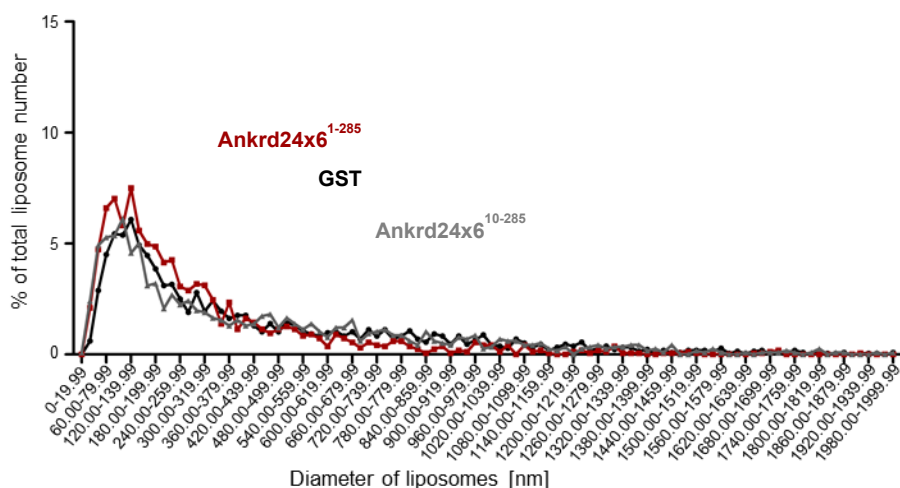
**Fig. 22: Size distribution of liposomes.** Line graph representation of the size distribution of the liposomes according to their diameter in percentage of the total liposome number, showing an increased peak in the percentage in the range of 60-79.99 nm and 120-139.99 nm diameter by liposomes incubated with the N-Ank module, Ankrd24x6$^{1-285}$ compared to Ankrd24x6$^{10-285}$ or GST. Quantitative analyses included two independent liposome preparations: n=2165 for GST, n=1672 for Ankrd24x6$^{1-285}$ and n=1164 for Ankrd24x6$^{10-285}$, where n represents the number of liposomes.

**Table 14: Gene locus positions of exons with their respective range in different isoforms of *Ankrd24* in *Rattus norvegicus*, according to the NCBI database; gene ID 299639 as of 19 May 2021.** Ankrd24x2 (XM_039078672.1) was used as a reference.

| exons | x2 (XM_039078672.1) | x1 (XM_039078671.1) | NM_001106771.1 |
|---|---|---|---|
|  |  |  | 1..196 |
| 1 | 703..972 |  | 773..972 |
| 2 | 6123..6253 |  | 6123..6253 |
| 3 | 6328..6416 |  | 6328..6416 |
| 4 | 7055..7119 |  | 7055..7119 |
| 5 | 7789..7846 |  | 7789..7846 |
| 6 | 9853..9923 |  | 9853..9923 |
| 7 | 10052..10158 |  | 10052..10158 |
| 8 | 10305..10492 |  | 10305..10492 |
| 9 | 10984..11021 |  | 10984..11021 |
| 10 | 11840..11920 |  |  |
| 11 | 12011..12121 |  |  |
| 12 | 12749..12793 |  |  |
| 13 | 12873..12971 | 12898..12971 | 12873..12971 |
| 14 | 13945..13999 | 13945..14366 | 13945..13999 |
| 15 | 14248..14366 |  | 14248..14366, |
| 16 | 14468..15865 | 14468..15865 | 14468..15865 |
|  |  | 16677..16844 |  |
| 17 | 17953..18084 | 17953..18084 | 17971..18084 |
| 18 | 18429..18494 | 18429..18494 | 18429..18494 |
| 19 | 18713..19509 | 18713..19509 | 18713..19190 |
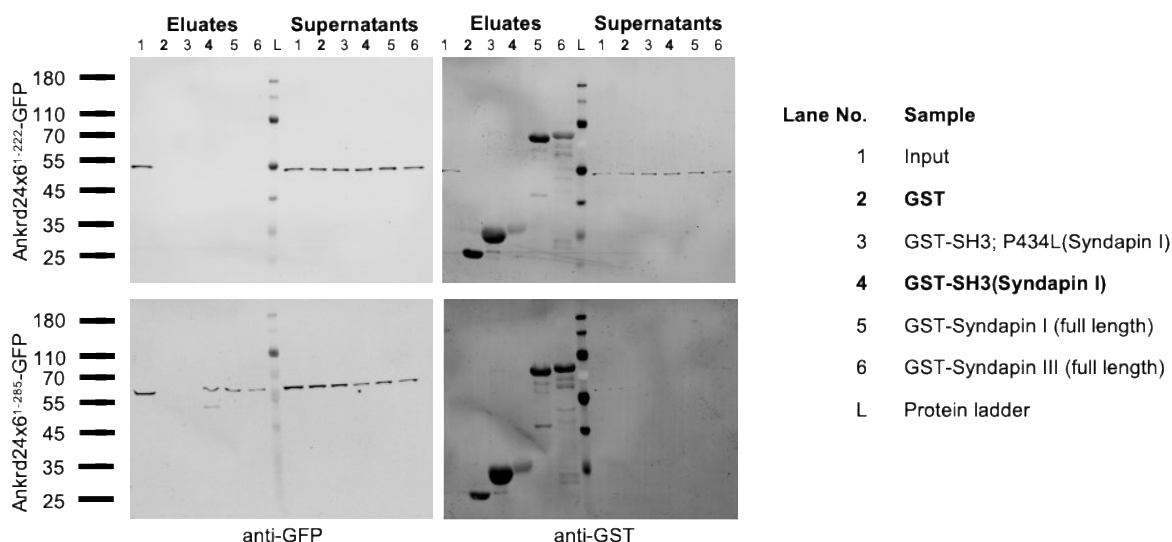
**Fig. 23. Ankrd24x6 proline-rich sequence KKRKAPQPP containing Ankrd24x6$^{1-285}$-GFP binds to the SH3 domain of syndapin I.** *In vitro* reconstitution coprecipitation assays were performed using GST-SH3 (syndapin I) or its mutant, GST-syndapin I (full-length), GST-Syndapin III (full-length) or GST with lysates of HEK293 cells overexpressing GFP-fusion proteins of Ankrd24x6$^{1-222}$-GFP and Ankrd24x6$^{1-285}$-GFP for 24 h. Experiment showed specific binding of Ankrd24x6$^{1-285}$-GFP, which contains the proline-rich sequence to GST-SH3 (syndapin I), GST-syndapin I (full-length) and GST-Syndapin III (full-length).

## 7.2  Tables

## 7.3 Figures

## 7.4  Acknowledgments

## 7.5 Ehrenwörtliche Erklärung

Hiermit erkläre ich, dass mir die Promotionsordnung der Medizinischen Fakultät der Friedrich-Schiller-Universität bekannt ist, ich die Dissertation selbst angefertigt habe und alle von mir benutzten Hilfsmittel, persönlichen Mitteilungen und Quellen in meiner Arbeit angegeben sind, mich folgende Personen bei der Auswahl und Auswertung des Materials sowie bei der Herstellung des Manuskripts unterstützt haben: Prof. Dr. Britta Qualmann & PD Dr. Michael M. Kessels, die Hilfe eines Promotionsberaters nicht in Anspruch genommen wurde und dass Dritte weder unmittelbar noch mittelbar geldwerte Leistungen von mir für Arbeiten erhalten haben, die im Zusammenhang mit dem Inhalt der vorgelegten Dissertation stehen, dass ich die Dissertation noch nicht als Prüfungsarbeit für eine staatliche oder andere wissenschaftliche Prüfung eingereicht habe und dass ich die gleiche, eine in wesentlichen Teilen ähnliche oder eine andere Abhandlung nicht bei einer anderen Hochschule als Dissertation eingereicht habe.


Jena, 28 Oct 2021                                                       Astha Jain

Ort, Datum                                                      Unterschrift des Verfassers